INTERACTION NOTES

Note 181

1970

BASIS TRANSFORMATION, LEAST SQUARE, AND CHARACTERISTIC MODE TECHNIQUES FOR THIN-WIRE SCATTERING ANALYSIS

by

Richard Harold Turpin

Ohio State University

This treatise is divided into three distinct parts.

(1) A numerical basis transformation technique is described which may be applied, in conjunction with point-matching methods (e.g., piecewise uniform or piecewise linear methods), to obtain least square solutions of electromagnetic scattering by thin wires. It is shown that reductions in both computer solution time and computer storage requirements result. The technique is demonstrated by its application, along with piecewise uniform methods, to the solution of scattering by circular and elliptical loops, straight wires and open circular arcs.

(2) A computational technique is developed for determining certain modes (termed characteristic modes in the literature) which are useful for the solution of scattering and radiation problems.

(3) The basis transformation, least square, and mode-finding techniques are combined to compute characteristic mode current distributions of circular and elliptical loops, straight wires, circular arcs, and helices.

In addition to the above topics, expressions are derived, in terms of the characteristic mode pattern functions, for the back-scattering and

tumble average backscattering cross sections of an object for arbitrary transmitter and receiver polarizations. Data are given in graphical form for the aforementioned objects for the backscattering cross section averaged over all possible tumble aspects as well as for various fixed orientations. Also given are characteristic mode solutions for the input admittance of circular loops.

ACKNOWLEDGEMENT

The author is pleased to acknowledge the guidance and encouragement given so unselfishly by his advisor, Professor J. H. Richmond, and by colleague Dr. R. J. Garbacz. Also deserving of recognition are Professors W. H. Peake, D. B. Hodge, and L. Peters,Jr., and Dr. G. A. Thiele for their critical reading of the manuscript as well as for earlier suggestions and assistance. The assistance and cooperation of all his associates at the ElectroScience Laboratory are greatly appreciated.

The support of the Ohio State University Computer Center, which provided computer time for portions of this work, is also gratefully acknowledged.

CONTENTS

CONTENTS (con't)

TABLES

ILLUSTRATIONS

Figure Page

CHAPTER I
INTRODUCTION

Computer solutions to scattering by straight or continuously curved, perfectly conducting wires (without generators or lumped loads) often are obtained by point-matching techniques whereby the boundary condition of zero total tangential electric field everywhere along the wire surface is approximated by enforcing this condition at, say, N points along the wire, where N is finite. The point-matching problem is represented by a set of N linear equations expressed in matrix notation as

$$[Z]\ (I) + (E) = (0), \tag{1}$$

where the N-dimensional column vector (E) is the tangential component of the incident electric field and the components I_n of the current vector (I) are coefficients of an expansion of the current induced on the wire in terms of a set of orthonormal basis functions $i_1, i_2, \cdots, i_N$. The mn^{th} element of the N x N impedance matrix [Z] gives the tangential component of the electric field at the m^{th} point on the wire due to the n^{th} basis function of current distributed over the wire length.

Selection of the basis functions is an important part of the point-matching methods. For the familiar piecewise uniform methods,[1-8]

the basis functions are unit pulses of width L/N, so that a step approximation is obtained for the induced current. Other segmental techniques include the piecewise linear[5,6] and the piecewise sinusoidal[8-11] methods.

A somewhat different class of point-matching methods, which will be called "modal methods", assumes a set of continuously differentiable, "modal" basis functions.[12-14] Unlike the segmental basis functions which are nonzero over only a small portion of the wire, the modal basis functions generally extend over the wire length. The cosine and sine functions $\cos(2n\pi\ell)/L$ and $\sin(2n\pi\ell)/L$, for example, where ℓ, $-L/2 \leq \ell \leq L/2$, is measured along the wire center-line, form a set of continuous basis functions well suited to certain shapes, such as closed wire loops.

These two classes of point-matching methods, i.e., the segmental and the modal methods, are further distinguished by certain characteristics encountered upon application. The segmental approaches usually afford efficient derivation of the set of linear equations for wires of arbitrary shape. The number of equations needed for good solution accuracy can become great, however, and since the time required to solve a set of N linear equations is proportional to N^3, computer time can become restrictive. Likewise, computer storage soon limits the size of the scatterer to which these methods can be applied.

On the other hand, sufficient solution accuracy often can be achieved with a relatively small number of linear equations when modal functions form the basis. The derivation of the linear

equations, is, except in the case of straight wires,[14] generally not efficient, however, usually requiring considerable numerical integration resulting in substantial computer time.[15]

Having derived a set of linear equations relative to a certain basis, it is possible to make a linear transformation to a new basis. This basis transformation is discussed in Chapter II. It is shown that a least square solution may be extracted from the new set of equations. Specific application of the basis transformation and least square techniques is made to a set of equations derived assuming the piecewise uniform basis where the transformation matrix has a very simple form. It is also shown that as a result of this transformation the number of linear equations required for good solution accuracy can be reduced considerably with consequent reductions in computer time and storage requirements. As examples of the basis transformation method, backscattering cross sections are computed for circular and elliptical loops, straight wires and open circular arcs.

To the author's knowledge, the basis transformation, although a familiar mathematical tool, has not previously been applied to the numerical solution of scattering problems in the manner discussed here. The least square method, however, has been applied to various problems including the following. Kennaugh[16] obtained a least square solution by a field-matching technique in which multipole expansions were used to represent electromagnetic fields. Successful calculations were carried out for prolate and oblate

spheroids illuminated by a plane wave incident along the axis of symmetry. Fenlon[17] obtained least square solutions for the acoustic radiation field at the surface of a finite cylinder. Hildebrand and Crout[18] have treated the least square solution of integral equations and Crout[19] has described a least square procedure for solving homogeneous integral equations.

The determination of "characteristic mode" currents,[20,21] particular modal currents which are characteristic of a given scatterer and which satisfy certain requirements, is another application of point-matching methods which is greatly facilitated by the basis transformation and least square techniques. The concept of characteristic modes was formulated by Garbacz,[20] who gave examples of such modes associated with several geometries including the infinite circular cylinder, the sphere, infinitely long, thin parallel wires arrayed arbitrarily in space, two coaxial circular loops of thin wire, and a single circular loop scatterer. Consideration of thin finite wires of arbitrary shape awaited the development of a mode-determining technique such as the one described in Chapter III of the present work. Included is the derivation, in terms of the characteristic mode pattern functions, of expressions for the tumble average backscattering cross section of a scatterer for arbitrary transmitter and receiver polarizations. Results are given in graphical form for the backscattering and tumble average cross sections of circular and elliptical loops, straight wires, circular arcs, and helices.

Considerable scattering data have been calculated for objects such as straight wires, circular loops and open circular arcs. Relatively little effort, however, has been directed toward the determination of the tumble average cross section as discussed in Chapter III. Curtis[22] has computed average cross section data for straight wires and circular wire arcs, and dipoles have been treated by Borison,[23] Palerno and Bauer,[24] Hessemer,[25] and Morrow.[26] This tumble average would be the "best estimate" or the expected value of the cross section of an object placed with arbitrary orientation in the radar beam or, from another viewpoint, the average cross section of a large number of the particular object, assuming sufficient separation that the elements may be considered decoupled. The mode approach discussed in Chapter III provides an efficient method for obtaining tumble average cross section data as well as other subsidiary information, such as the input impedance of an arbitrarily placed gap on the scattering element, and bistatic and monostatic cross sections.

An $e^{i\omega t}$ time convention is assumed throughout this work and is suppressed for convenience. Matrices and column vectors are denoted by [ ] and ( ), respectively.

CHAPTER II

BASIS TRANSFORMATION AND LEAST SQUARE TECHNIQUES WITH APPLICATION TO SCATTERING BY THIN WIRES

A. A Numerical Basis Transformation

In the following discussion a method of transforming the basis of a set of linear equations is described. The resulting transformation technique may be applied, in conjunction with existing methods, to the solution of scattering by thin wires. In succeeding discussions some uses and advantages of the technique are demonstrated by means of specific applications.

Assume that the set of linear equations,

$$[Z]\ (I) + (E) = (0) \tag{2}$$

has as a basis the set of orthonormal functions $i_1, i_2, \cdots, i_N$. We can, if we choose, refer Eq. (2) to a new basis $i'_1, i'_2, \cdots, i'_N$, by means of a linear transformation[27]

$$(I) = [T]\ (I'), \tag{3}$$

where [T] is the transformation matrix and (I') is a column vector representing the current I on the wire relative to the new basis functions, i.e.,

$$I = I'_1\, i'_1 + I'_2\, i'_2 + \cdots + I'_N\, i'_N, \tag{4}$$

where the I'_n, n=1,2,...,N, are the components of the vector (I'). Substituting Eq. (3) into Eq. (2),

(5) $$[Z]\ [T]\ (I') + (E) = (0).$$

Letting

(6) $$[Z'] = [Z]\ [T]\ ,$$

we write

(7) $$[Z']\ (I') + (E) = (0).$$

Equation (7) is equivalent to Eq. (2), referred to the new basis.

Consider, for example, the transformation from the basis of the piecewise uniform method to a basis of modal orthonormal functions, such as the cosine and sine functions. In this application we find that the matrix [T] of Eq. (3) is very simply defined. In fact, inspection of Eq. (3) reveals that each member of the new set of basis functions forms a column of the matrix [T]. (Note: Moving from top to bottom in a column of [T] in this case corresponds to moving segment-by-segment from one end of the wire to the other.) If, for example, the cosine functions $\cos(n\pi\ell)/L$, n=1,2,...,N, form the new basis, then the n^{th} column of [T] represents an n^{th} order cosine function distributed over the wire, i.e., the mn^{th} element of [T] is $\cos(n\pi\ell_m)/L$, where ℓ_m is the location of the m^{th} match point on the center-line of the wire. Equation (3) would be,

$$(8)\quad \begin{pmatrix} I_1 \\ I_2 \\ \cdot \\ \cdot \\ \cdot \\ I_N \end{pmatrix} = \begin{bmatrix} \cos\frac{\pi\ell_1}{L} & \cos\frac{2\pi\ell_1}{L} & \cdots & \cos\frac{N\pi\ell_1}{L} \\ \cos\frac{\pi\ell_2}{L} & \cos\frac{2\pi\ell_2}{L} & \cdots & \cos\frac{N\pi\ell_2}{L} \\ \cdot & \cdot & & \cdot \\ \cdot & \cdot & & \cdot \\ \cdot & \cdot & & \cdot \\ \cos\frac{\pi\ell_N}{L} & \cos\frac{2\pi\ell_N}{L} & \cdots & \cos\frac{N\pi\ell_N}{L} \end{bmatrix} \begin{pmatrix} I'_1 \\ I'_2 \\ \cdot \\ \cdot \\ \cdot \\ I'_N \end{pmatrix} .$$

The simple definition of the transformation matrix afforded by this example is a consequence of the fact that each component I_n of the current vector (I) in the piecewise uniform basis system equals the current at ℓ_n, ($-L/2 \leq \ell_n \leq L/2$), on the wire. This is true since only the n^{th} basis function is nonzero at ℓ_n. It is not true in general, however. For example, it is not true of the new current vector (I').

Having determined the desired basis and having thus specified the transformation matrix [T], the impedance matrix [Z] is transformed as in Eq. (6), and the new set of equations, Eq. (7), is obtained with reference to the new basis.

B. Least Square Solutions of Scattering by Thin Wires

Often one finds that the components I'_m of the current solution vector (I') of Eq. (7) are negligible for $m > M$ ($M<N$), i.e., the solution

$$(9) \qquad I = I'_1 i'_1 + I'_2 i'_2 + \cdots + I'_M i'_M + \cdots + I'_N i'_N$$

is quite well approximated by retaining only the first M terms (assuming proper ordering of the I'_m). In fact, it is not unusual to obtain sufficient accuracy with $M < N/10$. Recalling that the computer solution time for N linear equations is proportional to N^3, one of the advantages afforded by such a basis transformation is evident.

When this approximation can be made we need only to solve Eq. (7) for M of the N unknowns. The N x N impedance matrix [Z'] may be replaced by an N x M rectangular matrix $[Z'_a]$ formed by taking the first M columns of [Z'], and the column vector (I') is replaced by an M-dimensional column vector (I'_a) whose components are the first M components of (I'). The field vector (E) remains unchanged. The result is the overdetermined set of N equations in M unknowns,

$$(10) \qquad \begin{bmatrix} Z'_{a_{11}} & Z'_{a_{12}} & \cdots & Z'_{a_{1M}} \\ Z'_{a_{21}} & Z'_{a_{22}} & \cdots & Z'_{a_{2M}} \\ \cdot & \cdot & & \cdot \\ \cdot & \cdot & & \cdot \\ \cdot & \cdot & & \cdot \\ Z'_{a_{N1}} & Z'_{a_{N2}} & \cdots & Z'_{a_{NM}} \end{bmatrix} \begin{pmatrix} I'_{a_1} \\ I'_{a_2} \\ \cdot \\ \cdot \\ \cdot \\ I'_{a_M} \end{pmatrix} + \begin{pmatrix} E_1 \\ E_2 \\ \cdot \\ \cdot \\ \cdot \\ E_N \end{pmatrix} = \begin{pmatrix} 0 \\ 0 \\ \cdot \\ \cdot \\ \cdot \\ 0 \end{pmatrix},$$

for which several solutions exist, depending upon which subset of M equations is chosen. To avoid this non-uniqueness in an unambiguous fashion, we multiply (10) by the complex conjugate transpose of $[Z'_a]$ to get

$$(11)\quad \begin{bmatrix} Z'^{c}_{a_{11}} & Z'^{c}_{a_{21}} & \cdots & Z'^{c}_{a_{N1}} \\ Z'^{c}_{a_{12}} & Z'^{c}_{a_{22}} & \cdots & Z'^{c}_{a_{N2}} \\ \vdots & \vdots & & \vdots \\ Z'^{c}_{a_{1M}} & Z'^{c}_{a_{2M}} & \cdots & Z'^{c}_{a_{NM}} \end{bmatrix} \begin{bmatrix} Z'_{a_{11}} & Z'_{a_{12}} & \cdots & Z'_{a_{1M}} \\ Z'_{a_{21}} & Z'_{a_{22}} & \cdots & Z'_{a_{2M}} \\ \vdots & \vdots & & \vdots \\ Z'_{a_{N1}} & Z'_{a_{N2}} & \cdots & Z'_{a_{NM}} \end{bmatrix} \begin{pmatrix} I'_{a_1} \\ I'_{a_2} \\ \vdots \\ I'_{a_M} \end{pmatrix}$$

$$+ \begin{bmatrix} Z'^{c}_{a_{11}} & Z'^{c}_{a_{21}} & \cdots & Z'^{c}_{a_{N1}} \\ Z'^{c}_{a_{12}} & Z'^{c}_{a_{22}} & \cdots & Z'^{c}_{a_{N2}} \\ \vdots & \vdots & & \vdots \\ Z'^{c}_{a_{1M}} & Z'^{c}_{a_{2M}} & \cdots & Z'^{c}_{NM} \end{bmatrix} \begin{pmatrix} E_1 \\ E_2 \\ \vdots \\ E_N \end{pmatrix} = \begin{pmatrix} 0 \\ 0 \\ \vdots \\ 0 \end{pmatrix},$$

where the superscript c denotes the complex conjugate. The product $[Z'_a]^*$ $[Z'_a]$, where * denotes the matrix complex conjugate transpose, yields an M x M complex symmetric matrix. The solution[28-31] of Eq. (11) provides a least mean square "match" by M modes of the boundary conditions at N points on the wire.* Only M simultaneous equations need be solved, where M, the number of modes, may be less than 10, while the number of match points, N, may be greater than 100, for example. There can be substantial savings in computer time and storage requirements when this technique is used, as is demonstrated by examples given in later discussions (Sec. C-iii).

The above mentioned least square solution of problems associated with wires of closed configuration, such as circular and elliptical loops, causes no problems, but the application of least square methods to wires of open configuration, such as straight wires and open circular arcs, requires special consideration.

The field in the vicinity of the ends of wires of open configuration exhibits certain discontinuities depending on the geometry of the wire termination. In the case where flat ends are assumed, an edge-type singularity results. The approximations inherent in numerical calculations cause this singularity to introduce erroneous values for the scattered field on the wire in the vicinity of the ends. Any solution method which satisfies the boundary conditions on the wire in a least square sense must account for this approximation effect.

---

*See Appendix A.

A simple example will serve to clarify the effect which the field near the wire ends will have on a least square solution. Consider a straight wire scatterer with a plane wave incident from the broadside aspect. The incident electric field is assumed to have unit magnitude and zero phase on the wire axis. Ideally the induced current would produce the scattered field shown in Fig. 1-a, so that the total tangential field ($E^i + E^s$) on the wire is zero. Numerical solutions, however, provide only an approximation (Fig. 1-b) to that field. In deriving a least square solution it is seen that, roughly speaking, the scaling coefficient A in Fig. 1-b will be adjusted to produce a least mean squared error in the total field. The large error in the approximate fields near the wire ends forces A to be less than unity. The associated induced current is thus reduced in magnitude and is in error. If, however, in obtaining a least square solution, the match points within a certain distance, d (Fig. 1-b), from the wire ends are ignored (i.e., the equations corresponding to these points are deleted from the set of equations) a better solution results. This procedure may be viewed in the context of least square solutions as the inclusion of a weighting function in the integral to be minimized which is unity for all values of the differential (arc length, in this case) except for incremental regions near the limits of integration (wire ends), where it is zero.

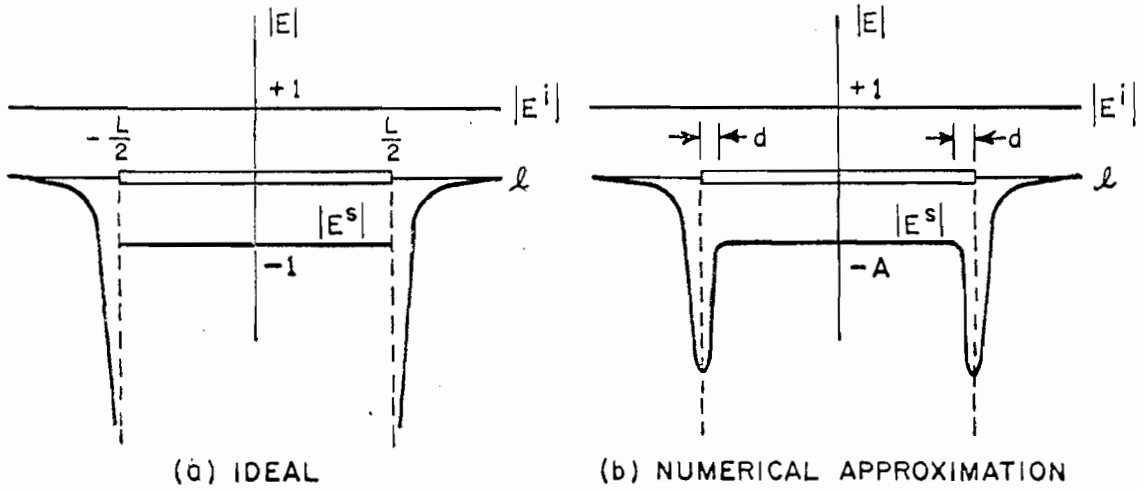

Fig. 1.--Incident and scattered fields on axis for a plane wave incident on a straight wire.

The need for these special considerations is not unusual. Other numerical solution methods[32-34] have shown a critical dependence on the choice of match points.

There is a need, then, for some measure of the error in the field matching achieved by a given solution both for the purpose of optimizing the solution conditions just discussed and to serve as an estimate of the accuracy of the final solution. A useful figure of merit[32,33,35] is

$$P = -\frac{1}{2}\,\mathrm{Re}\left\{\int_L J^c \cdot E^T \, d\ell\right\} \quad , \tag{12}$$

where J^c is the complex conjugate of the induced current density and E^T is the total electric field (i.e., the error field) on the wire. P is the average power radiated, in the absence of the scatterer, by

an equivalent source current J which generates an electric field intensity E^T. A negative value for P corresponds to the absorption of power while a positive value corresponds to radiation. Because the wire is a perfectly conducting scatterer it can neither absorb nor radiate power. In this case the condition P = 0 corresponds to satisfying the condition of conservation of power. It is desirable, then, to minimize the magnitude of P.

It must be pointed out, however, that to obtain $|P| = 0$ in a numerical solution such as that being discussed here does not necessarily imply that the solution is exact, for the figure of merit is itself computed by approximate methods. Equation (12) is, in this work, approximated by

$$(13) \qquad P \approx -\frac{1}{2} \mathrm{Re}\left\{ \sum_{n=1}^{N} I_n^c \cdot E_n^T \right\},$$

where I_n and E_n^T are the current and the total electric field intensity at the N match points.

In Table 1 are given figures of merit for a straight wire of length $L = 0.465\lambda$ with radius $a = 0.005\lambda$ as a function of the distance from the wire ends within which corresponding equations were ignored. The number of equations ignored at each end is also given for each case. A very significant improvement is often obtained by simply deleting the point nearest each end, though this is not the optimum in this case. The optimum distance depends on the wire radius and on the accuracy of the numerical impedance matrix. The impedance matrix $[Z_a']$ used to obtain these solutions was derived by a transformation from a piecewise

uniform basis [1-3] of dimension N = 100 to a cosine basis. Only the ten most significant cosine terms were retained, i.e., M = 10.

TABLE 1
FIGURES OF MERIT FOR LEAST SQUARE SOLUTIONS OF SCATTERING FROM A STRAIGHT WIRE OF LENGTH 0.465λ AND RADIUS 0.005λ

NUMBER OF EQUATIONS DELETED AT EACH END	DISTANCE FROM WIRE ENDS IN WIRE RADIUS	FIGURE OF MERIT
0	0.00	0.75×10^{-2}
1	0.93	0.33×10^{-5}
2	1.86	0.27×10^{-5}
3	2.79	0.37×10^{-6}
4	3.72	0.60×10^{-5}
5	4.65	0.11×10^{-4}

Two curves of least square solutions for the total tangential electric field for the same straight wire are given in Fig. 2. One (the upper, dashed line) was derived using all N equations. The other (the lower, solid line), which shows a significant improvement in field matching, was derived from the same N equations minus the six equations corresponding to the three points nearest each end. The figures of merit for these two cases are the first and fourth values given in Table 1. The values for the broadside echo area are, respectively, $0.712\lambda^2$ and $0.813\lambda^2$, the latter value corresponding to the minimum

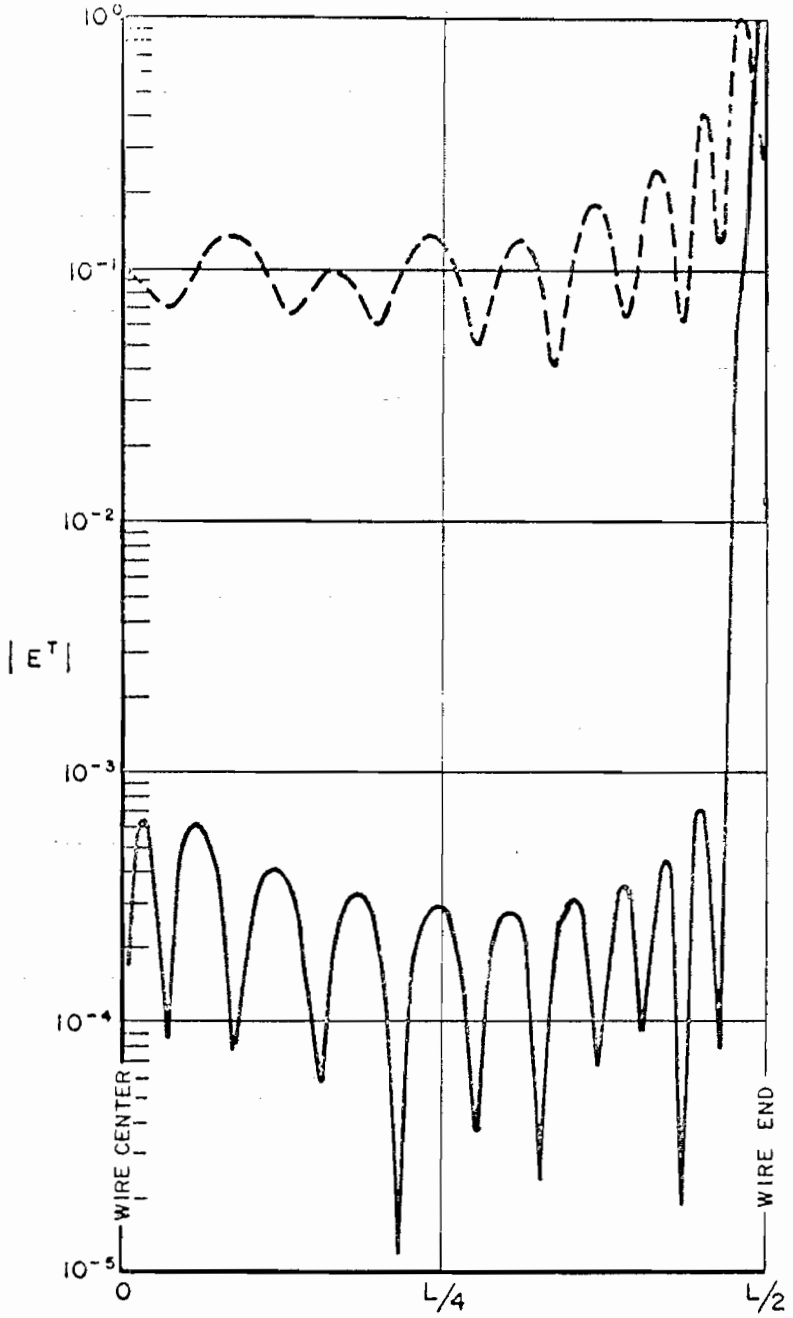

Fig. 2.--Least square solutions for the total tangential electric field on a straight wire of near resonant length.

figure of merit. (Reference 12 gives a value of approximately $0.82\lambda^2$ for the same wire by means of a linear equation method.)

C. Application to Scattering by Thin Wires

Application of the basis transformation and least square techniques just discussed follows the general procedure outlined below. In each case the wire is considered perfectly conducting and its radius is assumed to be much smaller than its length L and the wavelength λ. The assumption is made that the surface current density on the thin wire has only an axial component and is distributed uniformly around the circumference of the wire.

A segmental approximation to the wire is computed, giving the x, y, and z coordinates of the center of each linear wire segment along with orientation angles β, the angle of rotation from the positive x-axis, and α, the angle out of the xy plane (α is considered positive if the segment is tilted toward the negative z-axis). The matrix [T] of Eq. (3) is then derived with each column equal to one of the set of new basis functions. Having computed and stored [T], the transformation of Eq. (6) is performed. The piecewise uniform impedance matrix coefficients* are computed[1-3] one at a time while forming the new impedance matrix $[Z'_a]$ of Eq. (10) by means of running sums. The tangential component of the incident electric field (plane wave excitation is assumed) is then computed for each of the N match points, completing the

*See Appendix B.

formation of Eq. (10). Following pre-multiplication of the matrix equation by the complex conjugate transpose of $[Z_a']$, the resultant complex symmetric matrix equation (Eq. (11)) is solved.[31]

Substituting the solution (I_a') into Eq. (3), a piecewise uniform representation of the current is obtained from which the far field is computed. Solution for the cross section follows by application of the definition

$$\sigma = \lim_{r_o \to \infty} 4\pi r_o^2 \frac{|E^s|^2}{|E_o|^2} \quad , \tag{14}$$

where E^s is the scattered electric field intensity at a far distance r_o from the origin in the scatterer and E_o is the electric field intensity incident on the scatterer.

(i) Closed Loops

The backscattering cross section of circular loops (Fig. 3) was computed by transforming from the piecewise uniform basis to a basis of cosine functions, $\cos(2(m-1)\pi\ell)/L$, $m = 1,2,\cdots,M$, where L is the wire length (the loop circumference) and ℓ is measured along the wire center-line. The loop was approximated by N = 120 straight-wire segments and M = 5.

In Fig. 4 the broadside echo area is compared with measured values[36] and with values derived[36] by a variational method. A similar comparison is made in Fig. 5 of the ratio of the echo area at broadside aspect to that at edge aspect. In both cases the loop radius varies from 0.06λ to 0.40λ. Figure 6 gives the backscattering cross

section as a function of incidence angle for both theta- and phi-polarization for a 0.2λ radius loop. The wire radius for these examples is 0.005λ.

A suitable basis for elliptical loops is the set of cosine and sine functions, $\cos(2(m-1)\pi\ell)/L$ and $\sin(2m\pi\ell)/L$, $m = 1,2,\cdots,M$, where L is the circumference of the ellipse. Just as for the circular loops, N = 120 straight wire segments approximate the elliptical configuration. Six cosine functions and five sine functions were retained in the solutions. Backscattering cross sections are shown in Fig. 7 for both theta- and phi-polarizations at broadside- and edge-aspects as a function of the axial ratio of the ellipse. The wire radius is a = 0.00175λ.

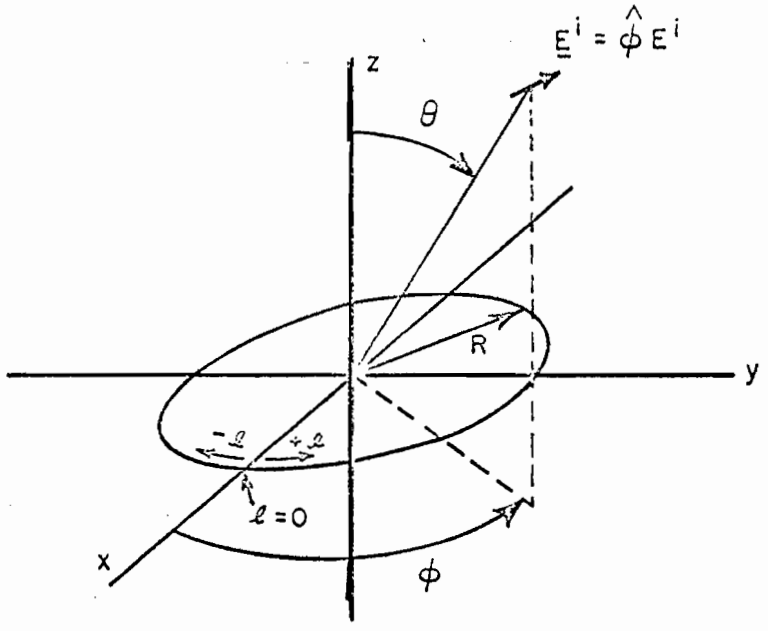

Fig. 3.--Geometry for the circular loop.

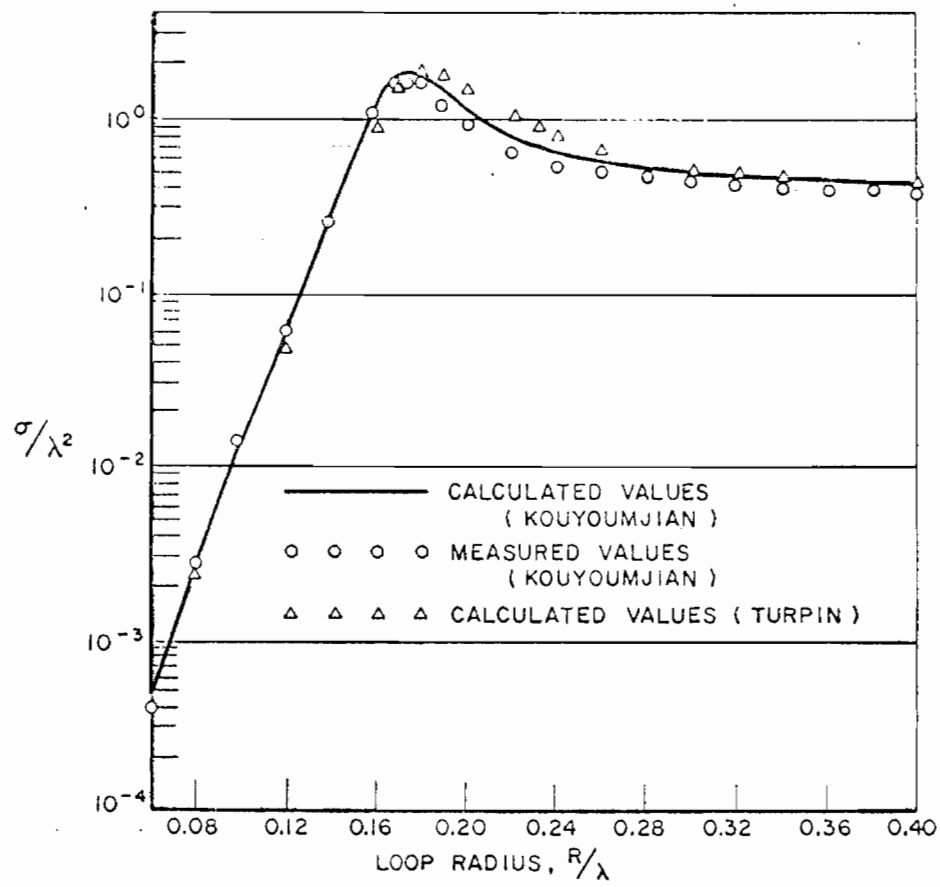

Fig. 4.--Echo area of circular loops at the broadside aspect.

(ii) Wires of Open Configuration

It has been shown[37] that the asymptotic form of the current distribution along any portion of a perfectly conducting wire, whether the wire is straight or curved, is

$$(15) \qquad I(\ell) = A \cos \frac{2\pi\ell}{\lambda} + B \sin \frac{2\pi\ell}{\lambda}$$

as the wire radius approaches zero. This sinusoidal approximation was

first discovered by Pocklington.[38] For wires of finite radius, however, the current distribution deviates from this sinusoidal behavior, especially near the wire ends. Knowing this, it might be expected that an accurate solution may be obtained for smaller M if some functions other than the sine and cosine functions are chosen as basis functions, in particular if the basis functions selected more closely approximate the true current distribution or perhaps better approximate the behavior of the current near the wire ends. A comparison is given in Fig. 8 of the broadside echo area of a wire of first resonant length as a function of M, the number of basis functions retained, for cosine functions* $\cos(n\pi\ell)/L$ and Chebyshev polynomials of the second kind.[39] The Chebyshev polynomials, which better approximate the current near the wire ends, are seen to give a slight improvement in this case.

The broadside echo area was computed for straight wires of lengths from 0.3λ to 0.6λ and of 0.005λ radius (Fig. 9), with N = 80 match points and M = 6 even Chebyshev polynomials as basis functions. Also shown are data derived[12] by a linear equation method based on the expansion of the current distribution in a series of 15 cosine modes. Figure 10 gives the backscattering cross section at the broadside aspect of straight wires with a length-to-diameter ratio L/2a = 100. Six even

---

*It was found that for least square solutions a complete, though truncated, set of basis functions is needed. In other words, when using the sine and cosine functions as basis functions, for example, it is necessary to retain all orders including the constant term and those which are non-zero at the wire ends. This differs from the usual practice of retaining only those functions which vanish at the wire ends, where the current must be zero.

Chebyshev modes were used with from N = 100 to 160 match points evenly spaced along the wires. Comparison is made with similar results[40] obtained by an independent method.

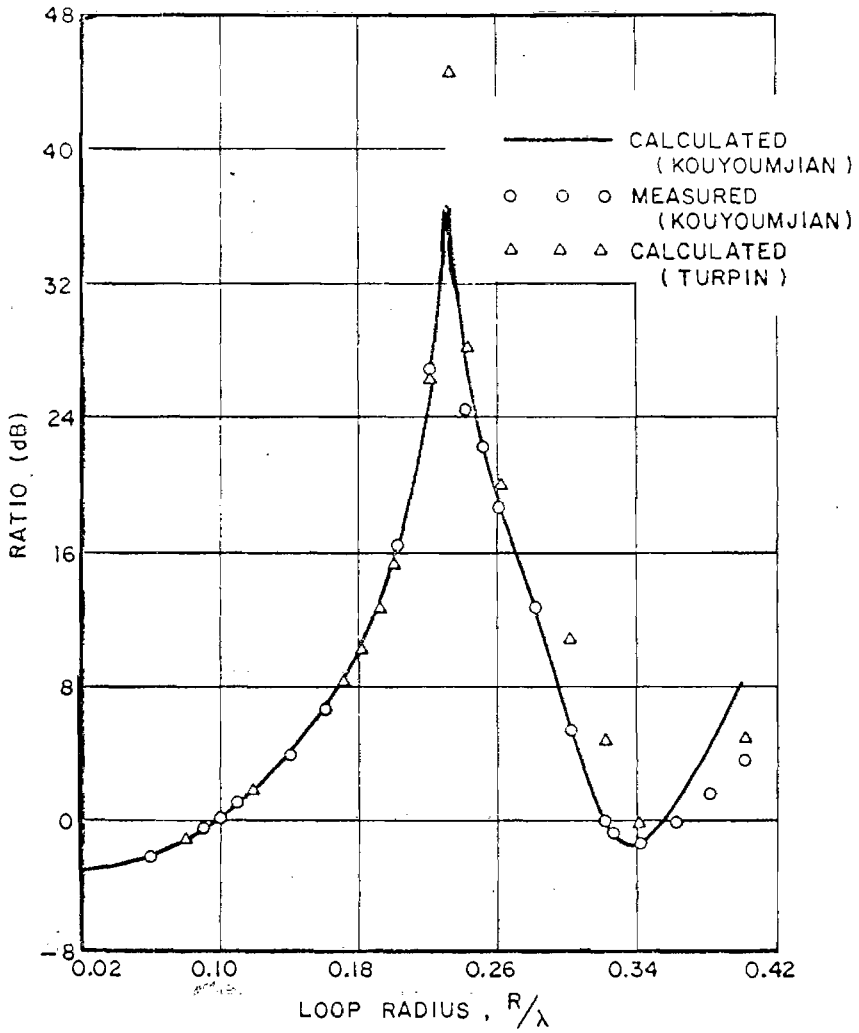

Fig. 5.--The ratio of the echo area at broadside aspect to the echo area at edge aspect for circular loops. (The ratio in dB = $\log_{10}$ (ratio).)

The broadside backscattering cross section of an open circular arc is shown in Fig. 11 as a function of arc radius. The wire length

and radius are 0.45λ and 0.00388λ, respectively, and the arc was approximated by N = 150 straight-wire segments. The currents were derived with M = 10 even Chebyshev polynomials as basis functions. Included in the figure are piecewise uniform results using N = 80 match points.[41,42]

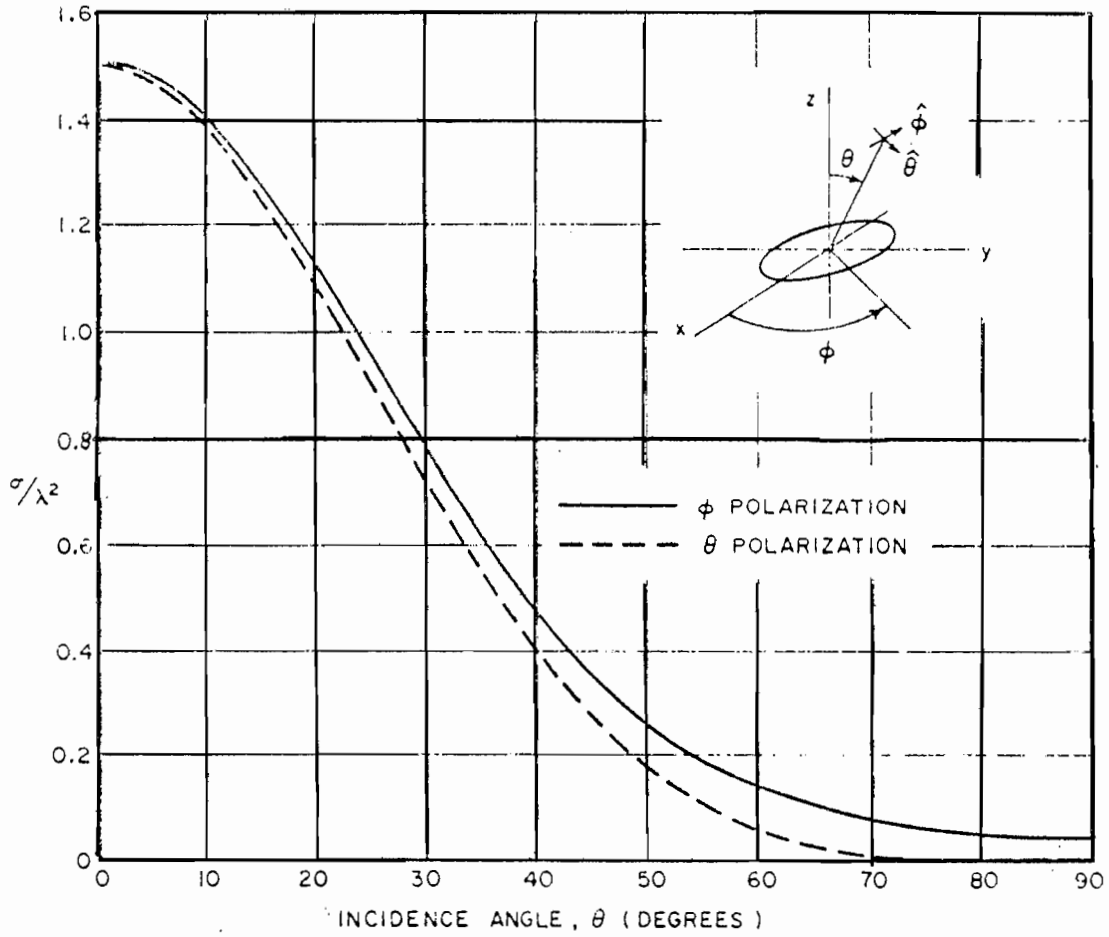

Fig. 6.--Backscattering cross section as a function of incidence angle θ for a circular loop of radius 0.2λ.

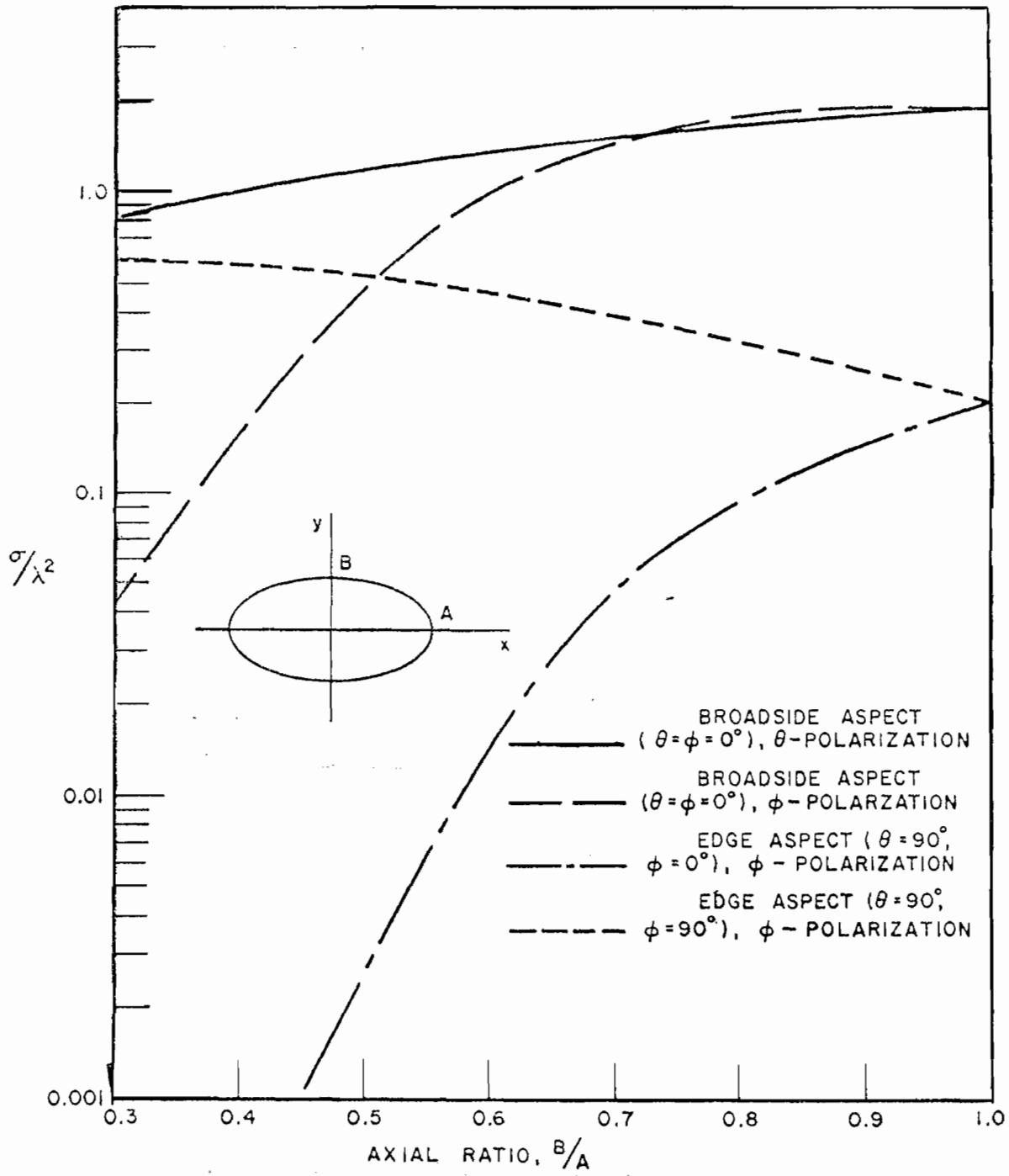

Fig. 7.--Broadside- and edge-aspect backscattering cross sections for an ellipse as a function of the axial ratio.

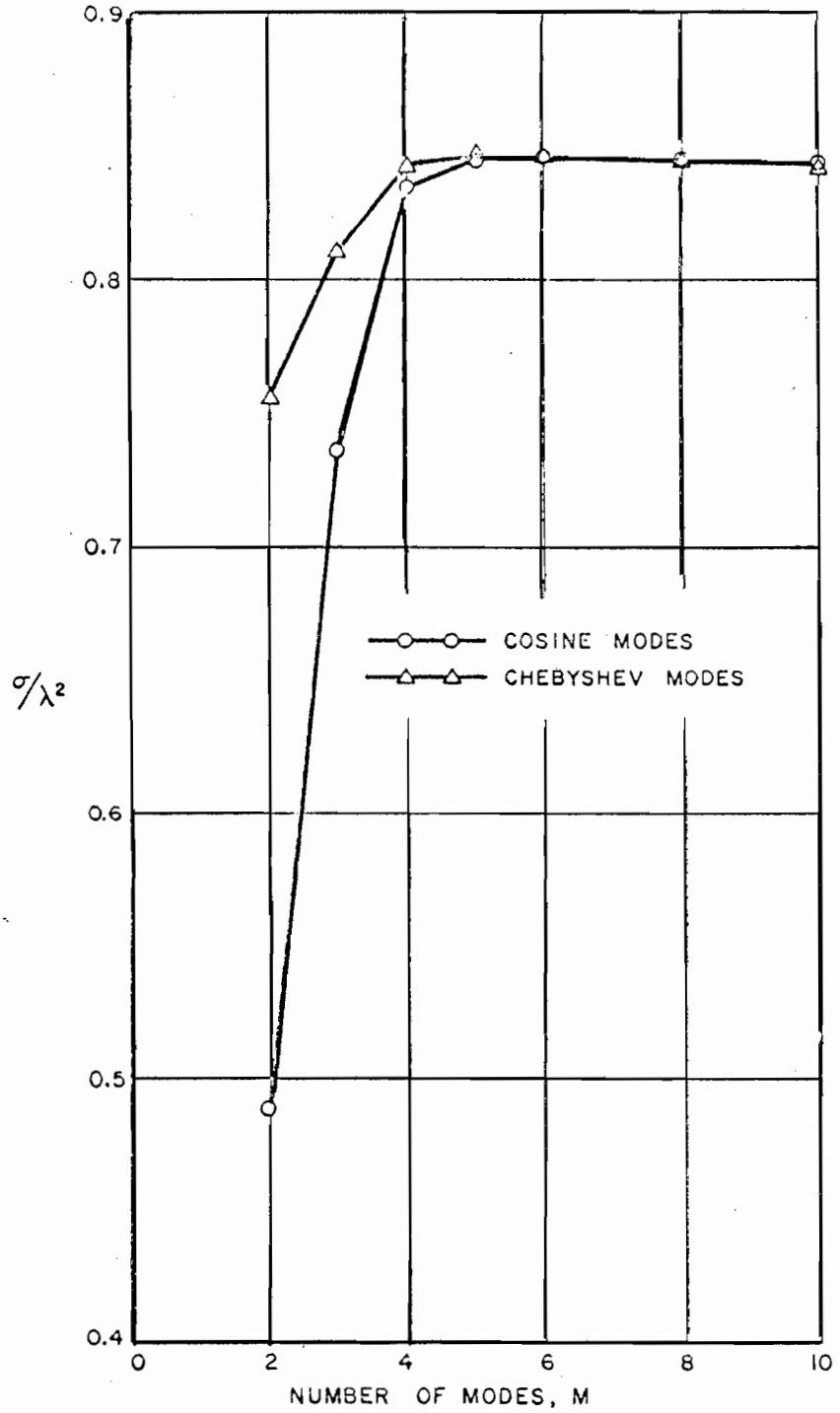

Fig. 8.--Broadside echo area for a straight wire of length 0.45λ and radius 0.005λ. A comparison of convergence as a function of M, the number of modes, using cosine functions and even Chebyshev polynomials of the second kind.

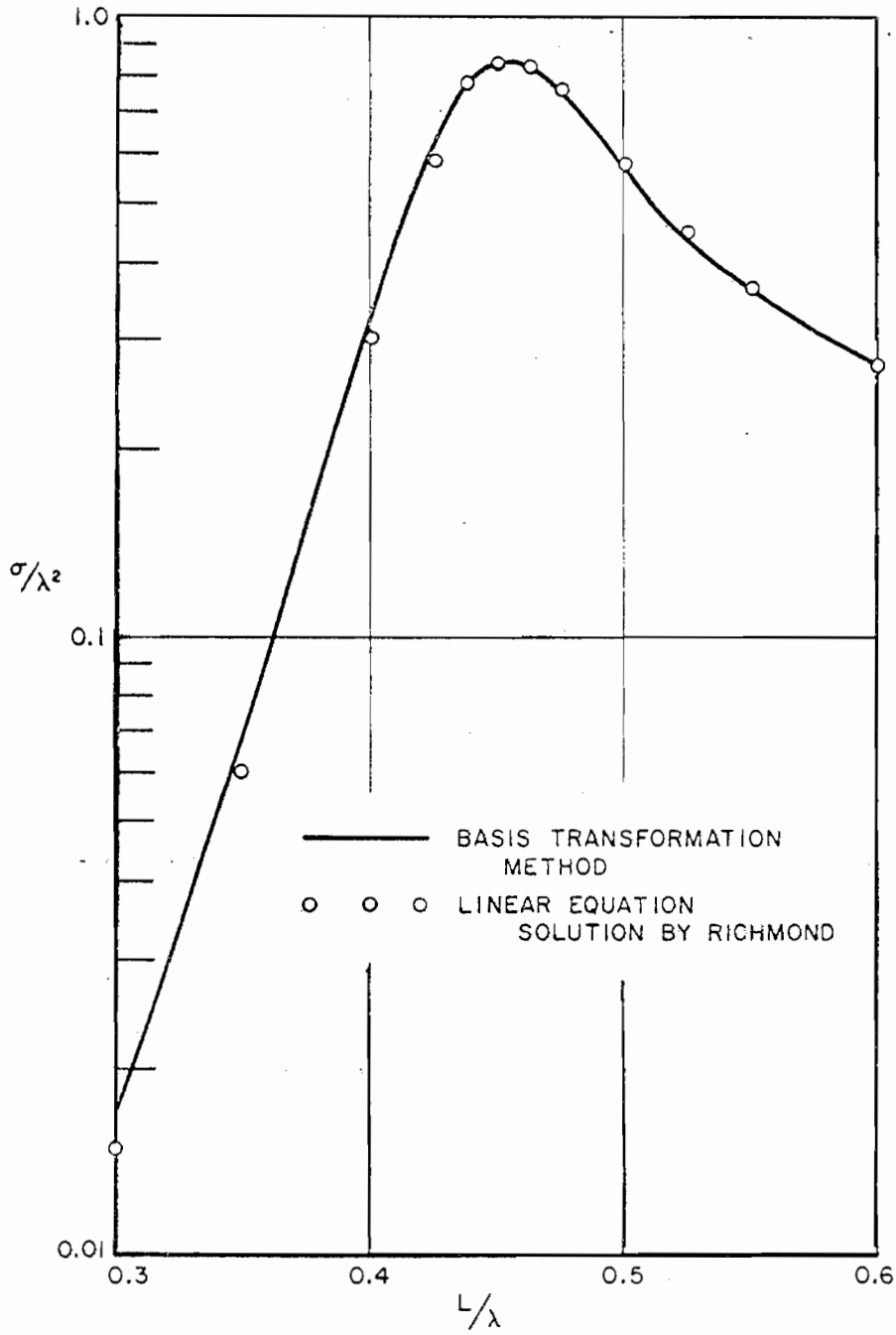

Fig. 9.--Broadside backscattering cross section for straight wires of near first resonant lengths and radius 0.005λ.

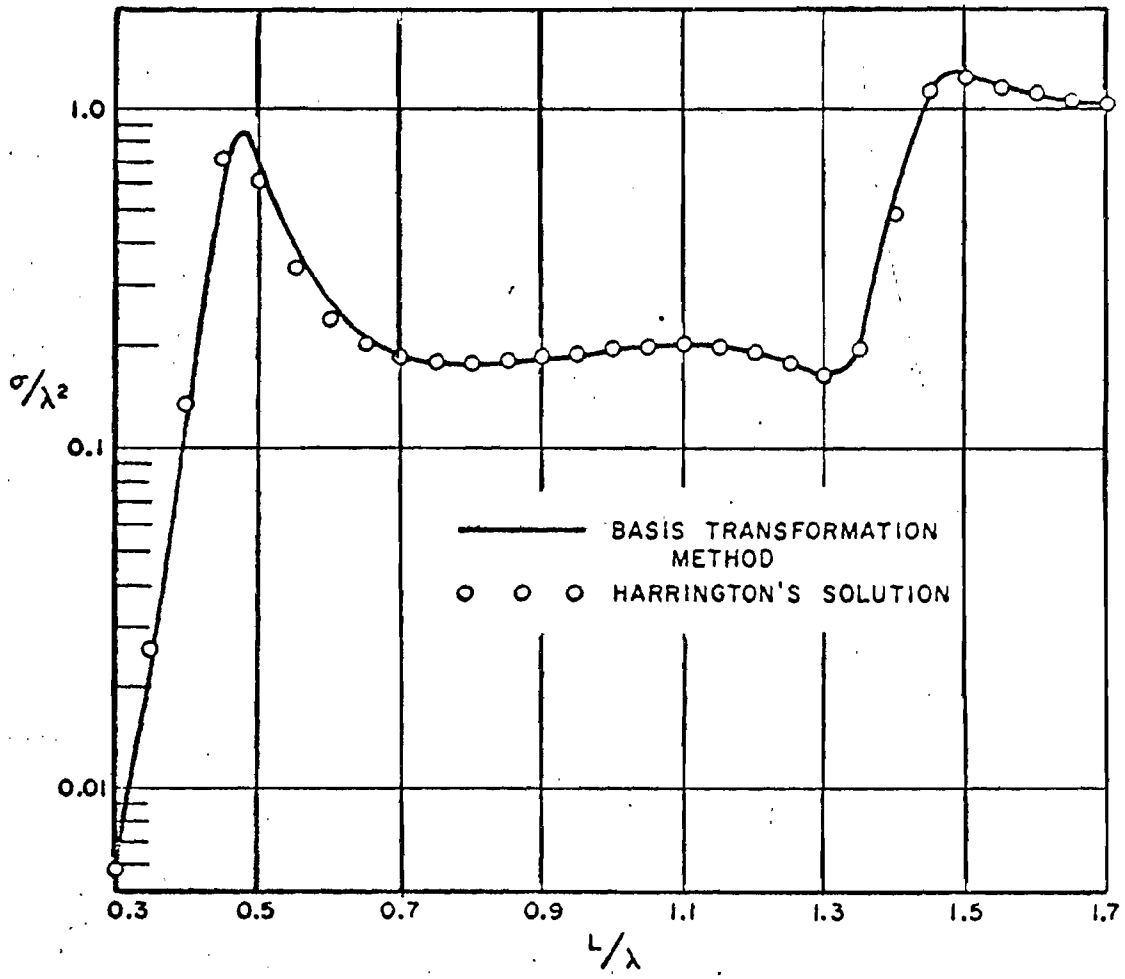

Fig. 10.--Broadside backscattering cross section of straight wires with length-to-diameter ratio, L/2a = 100.

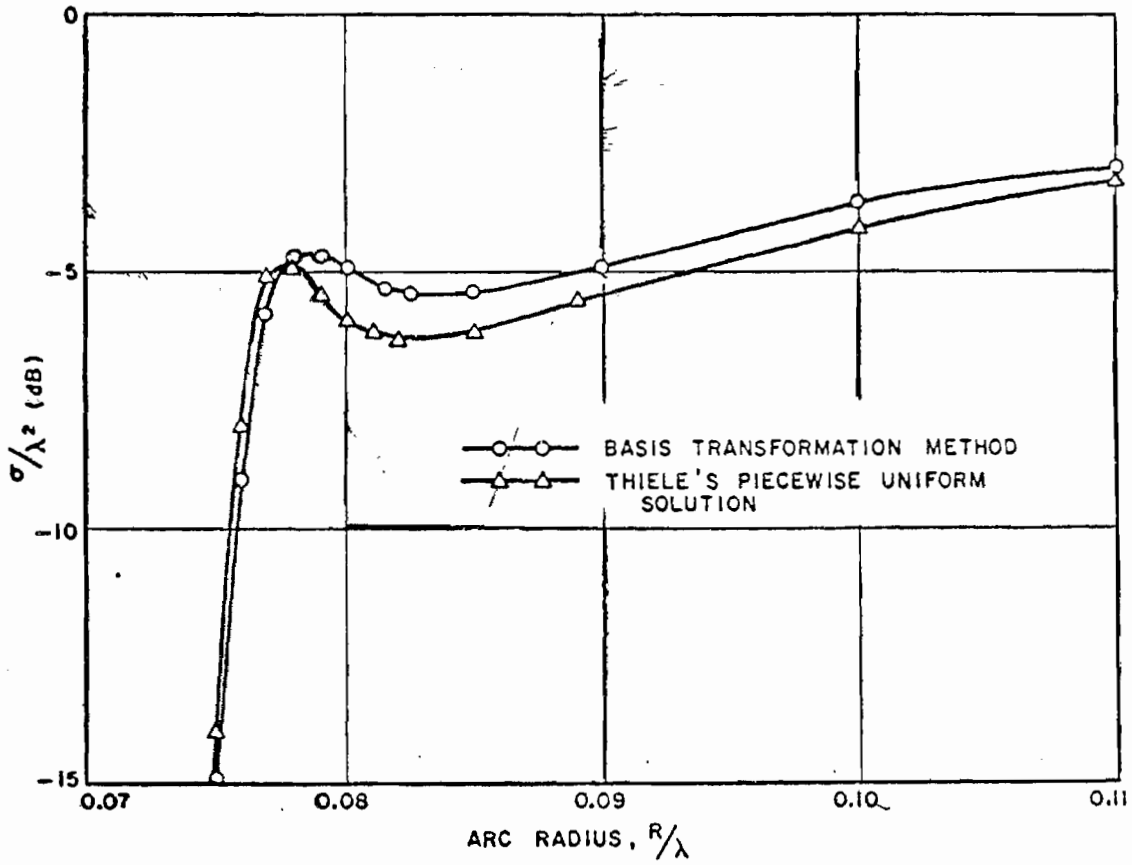

Fig. 11.--Broadside backscattering cross section of an open circular arc of fixed wire length (0.46λ) as a function of arc radius, with a wire of radius 0.00388λ.

(iii) Computer Time and Storage

A comparison was made between the computer time required to derive and solve a set of N linear equations for the unknown current using a piecewise uniform method and the time required if the same N equations were transformed to a new, continuous basis and reduced to a set of M equations from which a least square solution for the current was extracted. The wires for this comparison were two straight wires of lengths 0.45λ and 1.5λ with 0.005λ radii. The computer times and the

corresponding values for the backscattering cross sections (broadside aspect) are given in Table 2. A graphical time comparison is given in Fig. 12.

The piecewise uniform solution time is seen to have approximately a cubic dependence on N, being determined primarily by the time needed to invert an N-dimensional system of equations. By applying the basis transformation the time was reduced to a square law dependence on N, depending dominantly on the time required to compute the impedance matrix and to perform the transformation. The time consumed inverting the resultant M-dimensional system is almost negligible. Figure 13 shows the nearly linear dependence of computer time on M. Furthermore, the storage capacity of the computer (IBM 7094) limits the piecewise uniform program to $N \leq 100$, while application of a basis transformation allows an increase to $N \leq 500$ with $M \leq 20$.

TABLE 2

A COMPARISON OF COMPUTATION TIMES

NUMBER OF MATCH POINTS	PIECEWISE UNIFORM METHOD			PIECEWISE UNIFORM WITH BASIS TRANSFORMATION					
				M=6			M=10		
	T (SEC)	σ/λ^2		T (SEC)	σ/λ^2		T (SEC)	σ/λ^2	
N		L=0.45λ	L=1.5λ		L=0.45λ	L=1.5λ		L=0.45λ	L=1.5λ
20	0.65	0.7918	0.7323	0.97	0.7918	0.7323	1.58	0.7918	0.7323
40	3.33	0.7686	1.097	2.73	0.7801	1.097	4.45	0.7685	1.097
60	9.72	0.8391	1.080	5.32	0.8427	1.074	8.68	0.8377	1.080
80	21.50	0.8453	0.9354	8.78	0.8463	0.9911	14.35	0.8437	0.9639
100	40.35	0.8460	0.9202	12.12	0.8454	0.9652	21.45	0.8438	0.9430
120	—	—	—	18.35	—	1.027	30.05	—	1.016
150	—	—	—	27.88	—	1.115	45.46	—	1.124
200	—	—	—	47.76	—	1.136	78.24	—	1.145
250	—	—	—	73.17	—	1.124	119.88	—	1.139

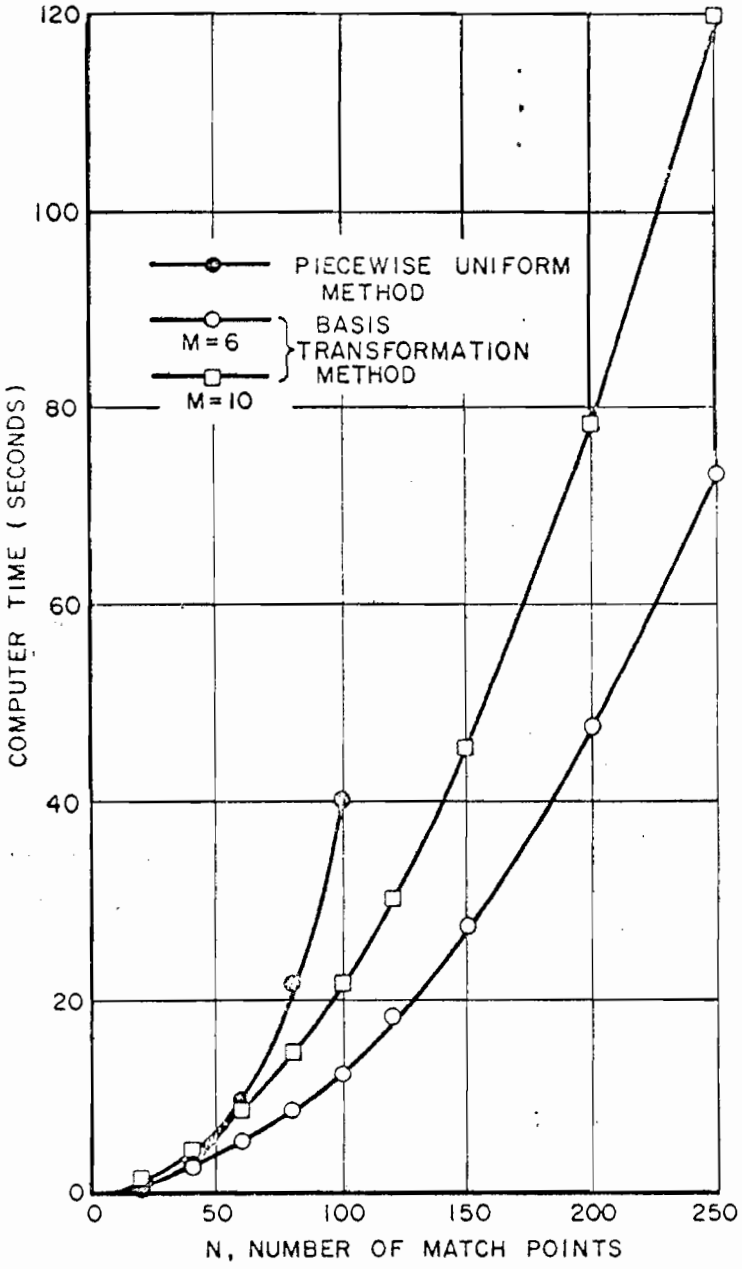

Fig. 12.--Computation times for a piecewise uniform method and for the basis transformation method.

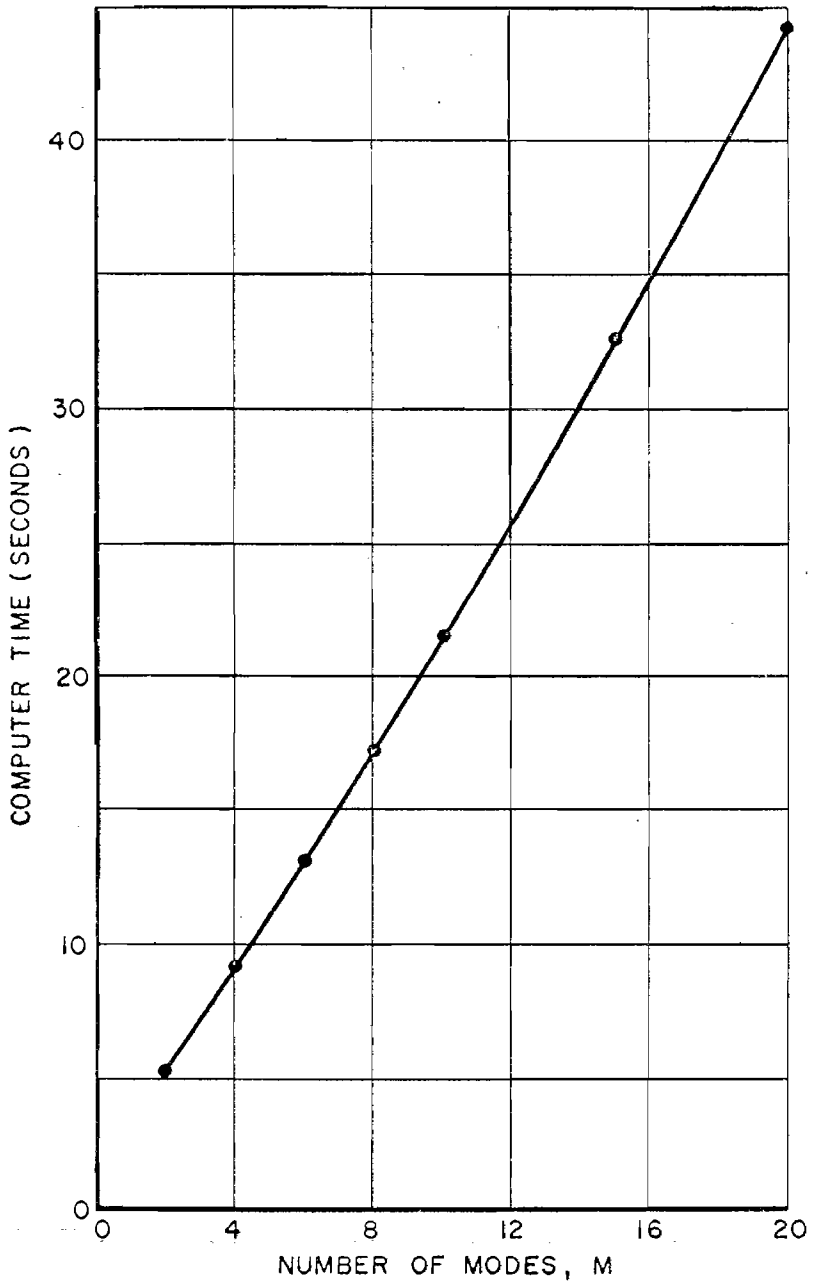

Fig. 13.--Computer time as a function of M, the number of modes, with N = 100.

CHAPTER III

THE DETERMINATION OF CHARACTERISTIC MODES AND THEIR USE IN THE SOLUTION OF SCATTERING BY THIN WIRES

Basis transformation and least square techniques have been discussed in the preceding chapter. Their use in conjunction with a piecewise uniform method has been demonstrated by application to the direct solution of scattering by thin wires. In the following discussion these same techniques are applied to the determination of characteristic modes of thin wires, which are in turn used to describe the scattering by these wires. The usefulness of this less direct approach to scattering problems will become evident later.

It has been shown[20,21] that every perfectly conducting obstacle has associated with it a particular set of surface currents and corresponding radiated fields which are characteristic of the obstacle shape and independent of any specific excitation. This set of so called "characteristic modes" forms a useful basis set in which to expand fields radiated or scattered at a great distance from the obstacle. Once these modes are known for a given obstacle, the scattering of plane waves incident from arbitrary source directions into arbitrary receiver directions may be evaluated concisely. In general, however, the determination of these characteristic modes is not a simple task.

Following a brief discussion of characteristic modes, a method for determining characteristic mode current distributions on wires of general shape is given. As examples of the method, the characteristic modes associated with a variety of perfectly conducting wires are derived and are then used to compute their backscattering properties.

A. Summary of Characteristic Mode Properties

The brief discussion of characteristic modes given in this section does not reflect the generality of the theory. For a more comprehensive treatment the reader is directed to References 20 and 21.

Consider a loss-free obstacle with a surface S. Assume a specified angular frequency ω. It has been shown[20] that a special set of characteristic vector fields, which are determined uniquely by the scatterer shape and composition and by the frequency, may be associated with this scatterer. Once they are found, these fields may be used in the solution of a variety of problems involving the obstacle; of particular interest here is their use in evaluating the field scattered in arbitrary directions for a plane wave incident on the obstacle from any direction.

If the obstacle is perfectly conducting there corresponds to this set of characteristic vector fields a set of characteristic current density distributions, $\underline{J}_m$, on S which satisfies the following conditions:

(i) Each member, $\underline{J}_m$, of the set is real on S.

(ii) Each $\underline{J}_m$, radiating in free space, generates an electric field intensity whose tangential component on S is equiphase and lags $\underline{J}_m$ by an angle α_m, where $\pi/2 \leq \alpha_m \leq 3\pi/2$. (The ordering of the $\underline{J}_m$ is chosen such that the magnitudes $|\cos \alpha_m|$ form a non-increasing sequence of numbers with increasing integers m.)

(iii) For each mode of finite order m, $\underline{J}_m$ is normalized so that it radiates unit power.

(iv) On the sphere $\sum$ at $r\to\infty$, $\underline{J}_m$ radiates the electric field

$$\underline{E}_m^{ext}(r,\theta,\phi) = -\frac{i\omega\mu}{4\pi}\frac{e^{-ikr}}{r}\underline{F}_m(\theta,\phi), \tag{16}$$

where $\underline{F}_m(\theta,\phi)$ is the m^{th} characteristic mode pattern function.

The normalization to unit radiated power ((iii) above) implies that

$$\langle \underline{F}_m, \underline{F}_m \rangle = \frac{1}{Z_o}\iint_\Sigma |F_m|^2 \sin\theta\, d\theta\, d\phi = (4\pi/kZ_o)^2, \tag{17}$$

where $\langle , \rangle$ denotes a scalar product. (RMS values are assumed here to agree with the notation of Reference 20.) Furthermore

$$\langle \underline{F}_m, \underline{F}_n \rangle = \frac{1}{Z_o}\iint_\Sigma \underline{F}_n \cdot \underline{F}_m^c \sin\theta\, d\theta\, d\phi = 0, \quad n\neq m, \tag{18}$$

where the superscript c denotes the complex conjugate. Equations (17) and (18) imply that the characteristic pattern functions, $\underline{F}_m(\theta,\phi)$, form an orthonormal set (with respect to radiated power) on the sphere Σ at infinity.

Knowledge of the $\underline{F}_m(\theta,\phi)$ and the associated characteristic values $a_m = |\cos \alpha_m| e^{i\alpha_m}$ permits a compact bilinear expansion for the far field scattered in any direction (r,θ^s,ϕ^s) due to a unit plane wave illuminating the obstacle from any direction (θ^i,ϕ^i). If both the source and the observer are at extreme distances from the scatterer,

$$(19) \qquad \underline{E}(r,\theta^s,\phi^s;\theta^i,\phi^i) = \frac{i\omega\mu}{4\pi} \frac{e^{-ikr}}{r} \sum_{m=1}^{M} a_m \underline{F}_m(\theta^s,\phi^s) \underline{F}_m(\theta^i,\phi^i) \cdot \hat{h}^i$$

$$= - \frac{i\omega\mu}{4\pi} \frac{e^{-ikr}}{r} \underline{\underline{F}}(\theta^s,\phi^s;\theta^i,\phi^i) \cdot \hat{h}^i$$

where $\hat{h}^i$ is the polarization state vector of the plane wave and

$$(20) \qquad \underline{\underline{F}}(\theta^s,\phi^s;\theta^i,\phi^i) = - \sum_{m=1}^{M} a_m \underline{F}_m(\theta^s,\phi^s) \underline{F}_m(\theta^i,\phi^i)$$

is the dyadic pattern function represented as a bilinear expansion in the characteristic pattern functions, $\underline{F}_m(\theta,\phi)$. The bilinear expansion has been truncated after M terms, all terms beyond these being negligible contributors to the scattered field. The bistatic cross section is then given by

$$(21) \qquad \sigma(\theta^s,\phi^s;\theta^i,\phi^i) = \frac{(\omega\mu)^2}{4\pi} |\underline{\underline{F}}(\theta^s,\phi^s;\theta^i,\phi^i) \cdot \hat{h}^i|^2.$$

Those characteristic modes for which the phase angle α_m is near π are the most effective contributors to radiated power. For this reason, if $\alpha_m = \pi$, the mode is said to be in scattering resonance. Modes for which $\alpha_m = \pi/2$ or $3\pi/2$ do not contribute at all to radiated power and are said to be in scattering null.

The determination of these characteristic fields and their characteristic values, α_m, is not a simple task. In the following section a computational technique is described and used to derive characteristic mode current distributions and the associated angles, α_m, for perfectly conducting thin wire scatterers of general configuration. Use is made of the defining conditions (i) and (ii), given in the above discussion, in developing the digital computer method.

B. A Technique for Determining Characteristic Modes of Wires

A modal impedance matrix, [Z], can be derived for a wire such that

$$[Z]\ (I) = (E), \tag{22}$$

where (E) is a vector representing the tangential component of the electric field intensity at N points on the wire due to a current I existing on the wire surface. (I) is a vector whose components are the coefficients of a Fourier expansion of the current I in terms of M orthonormal basis functions ($M \leq N$). The ij^{th} element of the impedance matrix, then, gives the tangential electric field at the i^{th} point on the wire due to the j^{th} basis function of current distributed over the wire length. Thus, [Z] is an N x M matrix and (I) and (E) are column vectors of dimensions M and N, respectively.

In a common application of Eq. (22) to scattering problems, the M dimensional current vector (I) is sought which generates a scattered

field equal to the negative of the incident field (i.e., $(E) = -(E^i)$) at M points along the wire, thereby approximating the exact boundary condition of zero total tangential electric field everywhere along the wire in a "point-matching" sense. A less common application[16], (Chapter II) of Eq. (22) is the approximation of the exact boundary condition in a "least mean square" sense. In this method, an M dimensional current vector (I) is sought which generates a scattered field that differs from the negative of the incident field such that the norm, $|(E) + (E^i)|^2$, of the difference vector, when averaged over N > M points on the wire, is a minimum. Application of Eq. (22) to the determination of characteristic modes will make rather novel use of the least mean square criterion by minimizing the phase variation along the wire rather than the field differences. This is accomplished by imposing, as constraints on Eq. (22), conditions (i) and (ii) of the preceding section, which specify that the m^{th} characteristic current I_m, represented by the vector (I_m) in the chosen basis system, be real and that the associated characteristic field E_m, represented by the vector (E_m) in the chosen basis system, be equiphase over the wire surface and lag I_m in phase by an angle α_m. The problem is to determine the phase angles α_m and the associated characteristic current distributions I_m for the significant modes. The characteristic pattern functions $\underline{F}_m(\theta,\phi)$ derived from the I_m, together with the characteristic values a_m derived from the α_m, then provide a concise evaluation of the scattered electric field according to Eq. (19).

To this end, Eq. (22) is rewritten as

$$[Z]\ (I) = (E')e^{-i\alpha}\ , \tag{23}$$

where a constant phase term, α, is removed from the field vector and is shown explicitly. This phase factor is then transferred to the left side of Eq. (23) and finally is absorbed into the impedance matrix, i.e.,

$$e^{i\alpha}\ [Z]\ (I) = [Z'(\alpha)]\ (I) = (E'), \tag{24}$$

where $[Z'(\alpha)] = e^{i\alpha}[Z]$.

If α and (I) of Eqs. (23) and (24) were the phase and corresponding real current vector associated with a characteristic mode, i.e., if $\alpha = \alpha_m$ and $(I) = (I_m)$, (E') would be a real vector. At this point in the problem, however, both α_m and (I_m) are unknown. Thus it is expected that, initially, (E') has some residual phase factor which is a function of the distance ℓ along the wire center-line. To reflect this fact, Eq. (24) is rewritten as

$$[Z'(\alpha)]\ (I) = (\mathrm{RE}\{E'\}) + i(\mathrm{Im}\{E'\}). \tag{25}$$

Letting $(\delta) = (\mathrm{Im}\{E'\})$, and assuming that (I) is a real vector,

$$[\mathrm{Im}\{Z'(\alpha)\}]\ (I) = (\delta), \tag{26}$$

where $[\mathrm{Im}\{Z'(\alpha)\}]$ is a real matrix. The real vector (δ) is thereby related to the deviation of the phase of (E') from an equiphase

condition. Ideally, (δ) would equal the null vector when $(I) = (I_m)$. We shall approximate this null vector with one which is minimum in a least mean square sense, i.e., one whose norm,

$$\varepsilon = (\delta)^T (\delta), \tag{27}$$

is minimized. (The superscript T denotes the transpose operation.)

Following the suggestion of Eq. (27), Eq. (26) is multiplied by its transpose, with the result,

$$(I)^T [\mathrm{Im}\{Z'(\alpha)\}]^T [\mathrm{Im}\{Z'(\alpha)\}] (I) = (\delta)^T(\delta) = \varepsilon(\alpha), \tag{28}$$

where the mean squared error, $\varepsilon(\alpha)$, is recognized explicitly as a function of α. Let

$$[B(\alpha)] = [\mathrm{Im}\{Z'(\alpha)\}]^T [\mathrm{Im}\{Z'(\alpha)\}] \quad , \tag{29}$$

where $[B(\alpha)]$ is a real symmetric matrix of dimensions M x M. Assume for convenience that the normalization $(I)^T(I) = 1$ applies. Then Eq. (28) becomes

$$[B(\alpha)] (I) = \varepsilon(\alpha) (I) \tag{30}$$

or

$$[B(\alpha) - \varepsilon(\alpha)I] (I) = (0), \tag{31}$$

where [I] is the identity matrix and (0) is the null vector. The equation

(32) $\det [B(\alpha) - \varepsilon(\alpha)I] = 0$

is recognized as the characteristic equation of the matrix $[B(\alpha)]$. The M roots $\varepsilon(\alpha) = \varepsilon_m(\alpha)$, m=1,2,···,M, of this equation are the eigenvalues of $[B(\alpha)]$ and the associated M vectors $(I) = (I_m(\alpha))$ are its eigenvectors. Because $[B(\alpha)]$ is real and symmetric the $\varepsilon_m(\alpha)$ must be real;[43]furthermore, because of the mean square condition enforced by Eq. (13) they must be non-negative. To assist in the following discussion, the eigenvalues $\varepsilon_m(\alpha)$ have been plotted in Fig. 14 as a function of the phase angle α for a specific example to be developed later.

Equation (32) determines the functional dependence of the eigenvalues ε_m on α. At this point it may be well to remember that $\varepsilon_m(\alpha)$ is a measure of the deviation of the phase of (E) from an equiphase condition. The smaller the $\varepsilon_m(\alpha)$ the closer this ideal condition is approached. In this light it is clear that we are interested in those values of α which cause relative minima in $\varepsilon_{min}(\alpha)$, where $\varepsilon_{min}(\alpha)$ denotes the smallest of the M eigenvalues $\varepsilon_m(\alpha)$ for a specified α. These relative minima, denoted by $\varepsilon_{min}(\alpha_m)$, will occur for $\alpha = \alpha_m$, m=1,2,···,M, corresponding to each of the eigenvectors $(I_{min}(\alpha_m))$ of Eq. (31). The angle α_m is the phase of the m^{th} equiphase surface field (E_m) and the associated eigenvector $(I_{min}(\alpha_m))$, hereafter denoted simply by (I_m), describes the m^{th} characteristic current distribution. For each pair, α_m and (I_m), the equiphase constraint on the tangential electric field is satisfied in a least mean square sense at the N selected points along the wire. The m^{th} characteristic

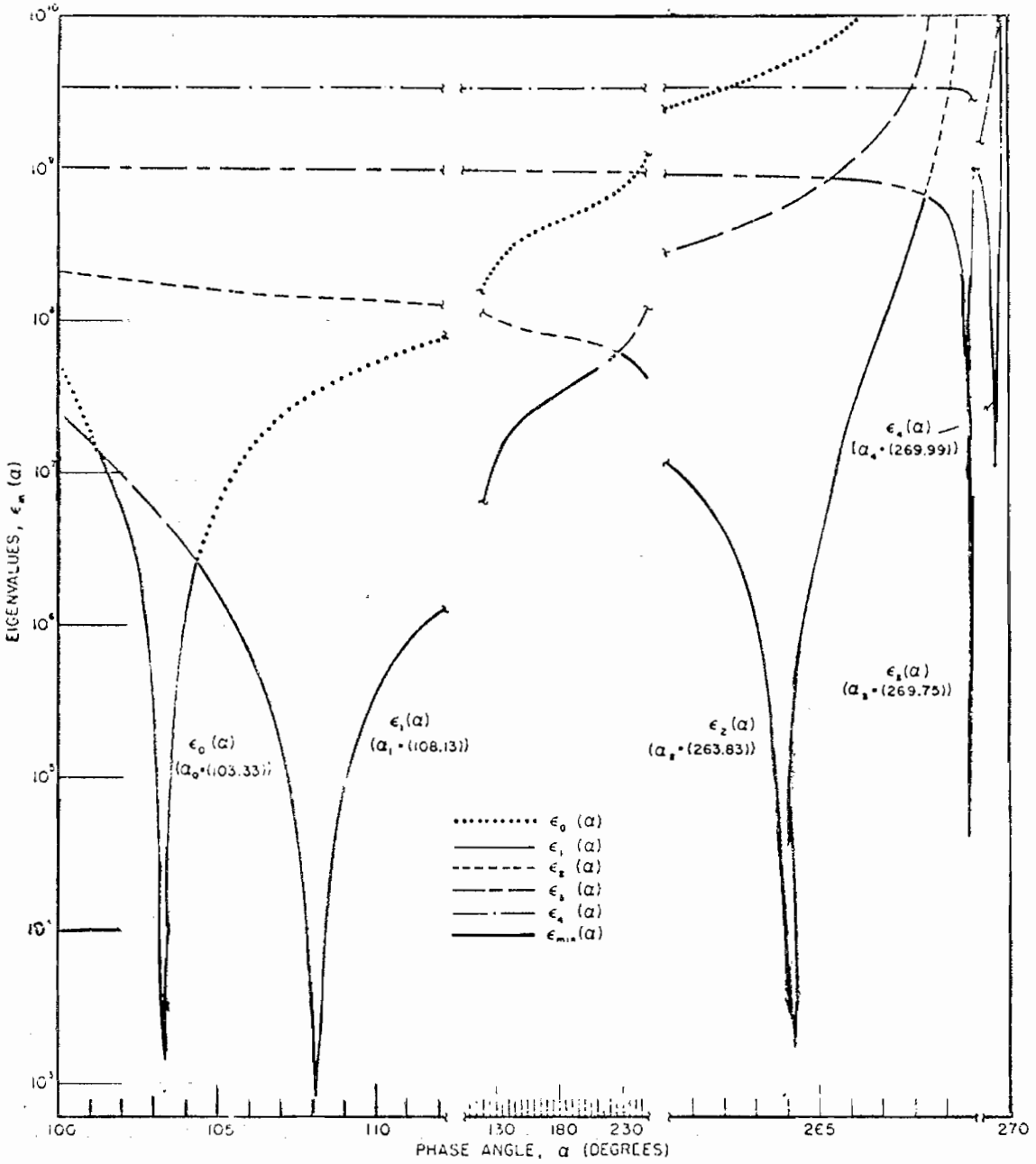

Fig. 14.--Eigenvalues $\epsilon_m(\alpha)$ for a circular loop of radius 0.25λ with a wire radius of 0.0025λ.

mode current distribution may now be expressed explicitly as a Fourier expansion in terms of the aforementioned set of orthonormal basis functions (e.g., cosine and sine functions), the coefficients of which are the components of the real vector (I_m).

In applying this procedure it is convenient to break up the matrix $[B(\alpha)]$ of Eq. (29), separating out those parts which are independent of α. Recalling that $[Z'(\alpha)] = e^{i\alpha}[Z]$, where $[Z]$ is a complex matrix, let

$$(33) \qquad [A] = [\mathrm{Im}\{Z'(\alpha)\}] = [\mathrm{Im}\{e^{i\alpha}[Z]\}]$$
$$= [\mathrm{Im}\{Z\} + \tan\alpha\ \mathrm{Re}\{Z\}]\cos\alpha.$$

Then, according to Eq. (29),

$$(34) \qquad [B(\alpha)] = [A]^T [A]$$
$$= [\mathrm{Im}\{Z\}^T\ \mathrm{Im}\{Z\} + \tan\alpha(\mathrm{Re}\{Z\}^T\ \mathrm{Im}\{Z\}$$
$$+ \mathrm{Im}\{Z\}^T\ \mathrm{Re}\{Z\}) + \tan^2\alpha\ \mathrm{Re}\{Z\}^T\ \mathrm{Re}\{Z\}] \cdot \cos^2\alpha$$

Letting

$$(35) \qquad [P] = [\mathrm{Im}\{Z\}^T\ \mathrm{Im}\{Z\}] \quad ,$$

$$(36) \qquad [Q] = [\mathrm{Re}\{Z\}^T\ \mathrm{Im}\{Z\} + \mathrm{Im}\{Z\}^T\ \mathrm{Re}\{Z\}] \quad ,$$

and

$$(37) \qquad [R] = [\mathrm{Re}\{Z\}^T\ \mathrm{Re}\{Z\}] \quad ,$$

Eq. (34) may be written as

$$(38) \qquad \frac{1}{\cos^2\alpha}\ [B(\alpha)] = [P] + \tan\alpha[Q] + \tan^2\alpha[R] \quad .$$

It is efficient to derive the matrices [P], [Q], and [R] from which the matrix [B (α)] can be formed for each α as α is varied in seeking relative minima of $\varepsilon_{min}(\alpha)$. The term $1/\cos^2\alpha$ is ignored from this point on since it has no effect on the location of these minima.

When both even and odd basis functions are used for the current expansion and these functions are ordered so that the first M_e components of the current vector (I) correspond to the even and the last M_o components correspond to the odd basis functions (where $M = M_e+M_o$ is the total number of basis functions), the matrix [B(α)] has a block diagonal form, i.e.,

$$[B(\alpha)] = \begin{bmatrix} [B_e(\alpha)] & 0 \\ 0 & [B_o(\alpha)] \end{bmatrix} , \tag{39}$$

where the matrices $[B_e(\alpha)]$ and $[B_o(\alpha)]$ are associated with the even and the odd basis functions, respectively. The even and odd characteristic mode current distributions can then be derived separately from the respective even and odd characteristic equations

$$\det [B_e(\alpha) - \varepsilon_e(\alpha)I] = 0 \tag{40}$$

and

$$\det[B_o(\alpha) - \varepsilon_o(\alpha)I] = 0. \tag{41}$$

Solution of the two above equations of dimensions M_e and M_o, respectively, consumes less computer time than the solution of one characteristic equation of dimension $M = M_e + M_o$. As an added

benefit, the separation into even and odd problems aids the location of minima in $\varepsilon_{min}(\alpha)$ when an even and an odd characteristic mode both have equal or very nearly equal phase angles.

An example of the behavior of the eigenvalues, $\varepsilon_m(\alpha)$, as functions of α has been given in Fig. 14. The scatterer in this example is a circular loop of radius 0.25λ, with a wire radius of 0.0025λ. The loop is approximated by 120 straight-wire segments and five cosine functions form the basis of the Fourier expansion of the current distributions. Due to the rotational symmetry of the loop and the resulting second order degeneracy of the modes, the eigenvalues associated with the sine functions are the same as those associated with the cosine functions. The characteristic phase angles,* α_m, m=0,1,2,3,4, corresponding to the relative minima $\varepsilon_{min}(\alpha_m)$, are given in Table 3 where they are compared with those angles calculated[20] analytically by independent methods.

The circular loop is a very special example in that the characteristic mode current distributions and the basis functions used for their expansion are one and the same, i.e., cosine and sine functions. For this reason each eigenvalue $\varepsilon_m(\alpha)$ of $[B(\alpha)]$ assumes a minimum $\varepsilon_{min}(\alpha_m)$ for its respective angle α_m as seen in Fig. 14. For more general scatterers the eigenvalue behavior is not this simple but

---

*Because the characteristic currents turn out to be the familiar cos $m\phi$ functions in this example, we have chosen to order the modes on m in the conventional manner, beginning with m = 0. In more general problems one would order the modes so as to make $|\cos \alpha_m|$ a non-increasing sequence with increasing m.

no extra complications arise. In any case, the smallest eigenvalue, $\varepsilon_{min}(\alpha)$, is the only eigenvalue of interest and regardless of which $\varepsilon_m(\alpha)$ happens to be the smallest eigenvalue for the choice of α under study, it is the relative minima of this $\varepsilon_{min}(\alpha)$ which are sought. To emphasize this point $\varepsilon_{min}(\alpha)$ is shown for the preceding example as a heavy line in Fig. 14.

TABLE 3
PHASE ANGLES α_m FOR A CIRCULAR LOOP OF RADIUS 0.25λ WITH WIRE RADIUS 0.0025λ

MODE m	α_m (DEGREES)	
	ANALYTICAL METHOD	NUMERICAL METHOD
0	103.4	103.33
1	107.5	108.13
2	263.1	263.83
3	269.7	269.75
4	~270.0	269.99

C. Scattering Solutions Using Characteristic Modes

(i) Backscattering Cross Section

Assuming a unit plane wave incident field, the scattered electric field intensity for an object is given by Eq. (19). The equation is repeated here for convenience.

$$(42) \qquad \underline{E}^s = -\frac{i\omega\mu}{4\pi}\,\frac{e^{-ikr}}{r}\;\underline{\underline{F}}(\theta^s,\phi^s;\theta^i,\phi^i)\cdot\hat{h}^i$$

The matrix equivalent of $\underline{\underline{F}}$ is

$$(43) \quad [F]=-\begin{bmatrix} \sum_{m=1}^{M} a_m F_{m_\theta}(\theta^i,\phi^i)F_{m_\theta}(\theta^s,\phi^s) & \sum_{m=1}^{M} a_m F_{m_\theta}(\theta^i,\phi^i)F_{m_\phi}(\theta^s,\phi^s) \\ \sum_{m=1}^{M} a_m F_{m_\phi}(\theta^i,\phi^i)F_{m_\theta}(\theta^s,\phi^s) & \sum_{m=1}^{M} a_m F_{m_\phi}(\theta^i,\phi^i)F_{m_\phi}(\theta^s,\phi^s) \end{bmatrix}$$

$$= \begin{bmatrix} F_{\theta\theta} & F_{\theta\phi} \\ F_{\phi\theta} & F_{\phi\phi} \end{bmatrix}$$

where F_{m_θ} and F_{m_ϕ} are the θ- and ϕ-components of the vector $\underline{F}_m$. The quantities $F_{\theta\theta}$, $F_{\theta\phi}$, $F_{\phi\theta}$ and $F_{\phi\phi}$ are functions (complex in general) of the incidence direction (θ^i,ϕ^i) and the scattering direction (θ^s,ϕ^s) although the dependence is not explicitly shown for simplicity in later discussions.

Both bistatic and monostatic scattering solutions may be derived from these expressions. Only the backscattering (monostatic) case, for which $\theta^i = \theta^s = \theta$, $\phi^i = \phi^s = \phi$ and $F_{\theta\phi} = F_{\phi\theta}$, is considered here. The matrix representation of Eq. (42) is

$$(44) \qquad (E^s) = -\frac{i\omega\mu}{4\pi}\,\frac{e^{-ikr}}{r}\,[F]\,(h^t),$$

where (h^t) is the transmitting antenna vector height[44] expressed in the θ-ϕ basis system.

The radar cross section is proportional[44] to $|V|^2$, with

$$V(\theta,\phi) = (h^r)^T\ (E^s), \tag{45}$$

where (h^r) is the vector height of the receiving antenna and the superscript T denotes the vector transpose. Substituting Eq. (44) into Eq. (45),

$$V(\theta,\phi) = -\frac{i\omega\mu}{4\pi}\ \frac{e^{-ikr}}{r}\quad (h^r)^T\ [F]\ (h^t) \tag{46}$$

The backscattering cross section is then

$$\sigma_{bs}(\theta,\phi) = \lim_{r\to\infty} 4\pi r^2 |V(\theta,\phi)|^2 = \frac{(\omega\mu)^2}{4\pi}\quad |(h^r)^T\ [F]\ (h^t)|^2. \tag{47}$$

It may be helpful at this point to note the similarity between the matrix [F] and the familiar scattering or polarization matrix[44] which will be denoted by [S]. In fact, [S] = [F], so that

$$s_{11} = -\sum_{m=1}^{M} a_m F_{m_\theta}(\theta^i,\phi^i)\ F_{m_\theta}(\theta^s,\phi^s), \text{ etc.} \tag{48}$$

Thus, the matrix [F] is simply an explicit expression of the polarization matrix in terms of the characteristic mode pattern functions $\underline{F}_m(\theta,\phi)$.

Equation (47) compactly expresses the plane wave backscattering cross section of an obstacle in terms of its characteristic pattern functions and the transmitter and receiver vector antenna heights. Since it will be useful later on to have explicit expressions for

certain vector antenna height combinations, we now devote some effort to their derivation. Of general interest are the transmitter-receiver polarization combinations of (1) vertical-to-vertical, (2) horizontal-to-horizontal, (3) vertical-to-horizontal (equal to horizontal-to-vertical in the monostatic case), (4) right circular-to-right circular, (5) left circular-to-left circular, and (6) right circular-to-left circular (equal to left circular-to-right circular in the monostatic case).

Letting the theta- and phi-components of the transmitter and receiver vector antenna heights be expressed explicitly, i.e.,

$$(h^t) = \begin{pmatrix} h_\theta^t \\ h_\phi^t \end{pmatrix} \quad \text{and} \quad (h^r) = \begin{pmatrix} h_\theta^r \\ h_\phi^r \end{pmatrix} ,$$

and substituting into Eq. (47),

$$\begin{aligned} (49) \qquad \sigma_{bs} = \frac{(\omega\mu)^2}{4\pi} \Big[& |F_{\theta\theta}|^2 |h_\theta^t|^2 |h_\theta^r|^2 + |F_{\phi\phi}|^2 |h_\phi^t|^2 |h_\phi^r|^2 \\ & + |F_{\theta\phi}|^2 (|h_\phi^t|^2 |h_\theta^r|^2 + |h_\theta^t|^2 |h_\phi^r|^2 \\ & \quad + h_\phi^{t^c} h_\theta^t h_\theta^{r^c} h_\phi^r + h_\theta^{t^c} h_\phi^t h_\phi^{r^c} h_\theta^r) \\ & + 2\,\mathrm{Re}\{F_{\theta\theta}^c F_{\theta\phi} (h_\theta^{t^c} h_\phi^t |h_\theta^r|^2 + |h_\theta^t|^2 h_\theta^{r^c} h_\phi^r) \\ & \quad + F_{\theta\theta}^c F_{\phi\phi} h_\theta^{t^c} h_\phi^t h_\theta^{r^c} h_\phi^r \\ & \quad + F_{\theta\phi}^c F_{\phi\phi} (|h_\theta^t|^2 h_\theta^{r^c} h_\phi^r + h_\theta^{t^c} h_\phi^t |h_\phi^r|^2)\} \Big] . \end{aligned}$$

The backscattering cross section for specific transmitter and receiver polarizations are obtained from Eq. (49) by assigning the

proper values to the vector antenna height components. Expressions for the polarizations mentioned earlier are given here:

(1) vertical-to-vertical $(h_\theta^t = h_\theta^r = 1,\ h_\phi^t = h_\phi^r = 0)$,

$$\sigma_{VV} = \frac{(\omega\mu)^2}{4\pi} |F_{\theta\theta}|^2 \tag{50}$$

(2) horizontal-to-horizontal $(h_\theta^t = h_\theta^r = 0,\ h_\phi^t = h_\phi^r = 1)$,

$$\sigma_{HH} = \frac{(\omega\mu)^2}{4\pi} |F_{\phi\phi}|^2 \tag{51}$$

(3) vertical-to-horizontal $(h_\theta^t = h_\phi^r = 1,\ h_\phi^t = h_\theta^r = 0)$,

$$\sigma_{VH} = \frac{(\omega\mu)^2}{4\pi} |F_{\theta\phi}|^2 \tag{52}$$

(4) right circular-to-right circular $(h_\theta^t = h_\theta^r = \frac{1}{\sqrt{2}},\ h_\phi^t = h_\phi^r = -\frac{j}{\sqrt{2}})$,

$$\sigma_{RR} = \frac{(\omega\mu)^2}{4\pi} \left[\frac{1}{4} \left(|F_{\theta\theta}|^2 + |F_{\phi\phi}|^2 \right) + |F_{\theta\phi}|^2 \right. \tag{53}$$

$$\left. - \frac{1}{2} \operatorname{Re} \{F_{\theta\theta} F_{\phi\phi}^c\} + \operatorname{Im} \{(F_{\theta\theta} - F_{\phi\phi}) F_{\theta\phi}^c\} \right] ,$$

(5) left circular-to-left circular $(h_\theta^t = h_\theta^r = \frac{1}{\sqrt{2}},\ h_\phi^t = h_\phi^r = \frac{j}{\sqrt{2}})$,

$$\sigma_{LL} = \frac{(\omega\mu)^2}{4\pi} \left[\frac{1}{4} \left(|F_{\theta\theta}|^2 + |F_{\phi\phi}|^2 \right) + |F_{\theta\phi}|^2 \right. \tag{54}$$

$$\left. - \frac{1}{2} \operatorname{Re} \{F_{\theta\theta} F_{\phi\phi}^c\} - \operatorname{Im}\{(F_{\theta\theta} - F_{\phi\phi}) F_{\theta\phi}^c\} \right] ,$$

and (6) right circular-to-left circular $(h_\theta^t = h_\theta^r = \frac{1}{\sqrt{2}},\ h_\phi^t = -h_\phi^r = -\frac{j}{\sqrt{2}})$,

$$\sigma_{RL} = \frac{(\omega\mu)^2}{4\pi} \left[\frac{1}{4} \left(|F_{\theta\theta}|^2 + |F_{\phi\phi}|^2 \right) + \frac{1}{2} \operatorname{Re} \{F_{\theta\theta} F_{\phi\phi}^c\} \right] . \tag{55}$$

The θ- and ϕ-dependence of the elements of the matrix [F] and of the cross section σ is assumed and is suppressed for ease in notation. The θ and ϕ subscripts signify the particular elements of the matrix [F] (see Eq. (43)).

(ii) Tumble Average Backscattering Cross Section

Having determined a suitable number of characteristic values and characteristic pattern functions for a given obstacle, it is a simple matter to apply the bilinear expansion of Eq. (42) and obtain plane wave scattering data, bistatic or monostatic, in an economical fashion. The ensuing compact expression (Eq. (47)) for backscattering cross section is particularly useful when one must consider an obstacle which is tumbling in space, and the quantity of interest is not backscattering cross section for some fixed orientation, but backscattering cross section averaged over all tumble aspects of the obstacle. Thus, if we denote the backscattering cross section with transmitter and receiver located in a direction (θ,ϕ) by $\sigma_{bs}(\theta,\phi)$, and if we assume a spherical probability density function for aspect likelihood, then the tumble average cross section can be defined by

$$(56) \qquad \langle\sigma_{bs}\rangle = \frac{1}{\pi}\int_0^{\pi}\frac{1}{4\pi}\int_0^{2\pi}\int_0^{\pi}\sigma_{bs}(\theta,\phi)\sin\theta\, d\theta\, d\phi\, d\alpha\ .$$

The angle α is a measure of the rotation of the obstacle about the line-of-sight. Since $\sigma_{bs}(\theta,\phi)$ is expressible so concisely in terms of characteristic pattern functions via Eq. (21) or Eq. (47), the calculation of $\langle\sigma_{bs}\rangle$ is greatly expedited.

In the following discussion the average over α will be performed analytically for arbitrary transmitter and receiver polarizations. The average over θ and ϕ, however, must be done numerically in general.

In the far field, the most general polarization, elliptical polarization, may be represented[45-47] by a combination of right circular and left circular polarization vectors, i.e.,

$$(57) \qquad (h_e) = (h_L) + (h_R)e^{j2\alpha}$$

where the subscripts L and R denote left and right circular polarization, respectively. The angle α (not to be confused with the characteristic phase angles α_m) is the angle of rotation, measured in a C.C.W. direction (looking in the direction of propagation), of the major axis of the polarization ellipse from the vertical axis. From the general expression of Eq. (57) can be derived left circular ($(h_R) = 0$), right circular ($(h_L) = 0$), vertical ($(h_L) = (h_R)$, $\alpha = 0$), and horizontal ($(h_L) = (h_R)$, $\alpha = \pi/2$) polarization vectors.

The norm of (h_e) will be set equal to unity, i.e.,

$$(58) \qquad |\underline{h}_e| = \sqrt{|\underline{h}_L|^2 + |\underline{h}_R|^2} = 1.$$

The axial ratio, r, of the ellipse is

$$(59) \qquad r = \frac{|\underline{h}_R| + |\underline{h}_L|}{|\underline{h}_R| - |\underline{h}_L|}$$

It is desired to obtain an expression for the average backscattering cross section for general transmitter and receiver polarization states. To this end assume a transmitter polarization

(60) $$(h^t) = (h_L^t) + (h_R^t)\, e^{j2\alpha_t}$$

and a receiver polarization

(61) $$(h^r) = (h_L^r) + (h_R^r) e^{j2\alpha_r}.$$

Substituting Eqs. (60) and (61) into Eq. (46) (suppressing the constant terms for convenience),

(62) $$V(\theta,\phi) \propto (h_L^r + h_R^r\, e^{j2\alpha_r})^T\, [F]\, (h_L^t + h_R^t\, e^{j2\alpha_t}).$$

Then

(63) $$\begin{aligned} |V(\theta,\phi)|^2 &\propto |(h_L^r + h_R^r\, e^{j2\alpha_r})^T\, [F]\, (h_L^t + h_R^t\, e^{j2\alpha_t})|^2 \\ &\propto |(h_L^r)^T\, [F]\, (h_L^t)|^2 + |(h_R^r)^T\, [F]\, (h_L^t)|^2 \\ &+ |(h_L^r)^T\, [F]\, (h_R^t)|^2 + |(h_R^r)^T\, [F]\, (h_R^t)|^2 \\ &+ 2\, \mathrm{Re}\Big\{[(h_R^r)^T\, [F]\, (h_L^t)]\, [(h_L^r)^T\, [F]\, (h_R^t)]^c\, e^{-j2(\alpha_t-\alpha_r)} \\ &+ [(h_L^r)^T\, [F]\, (h_L^t)][(h_R^r)^T\, [F]\, (h_L^t)]^c\, e^{-j2\alpha_r} \\ &+ [(h_L^r)^T\, [F]\, (h_L^t)][(h_L^r)^T\, [F]\, (h_R^t)]^c\, e^{-j2\alpha_t} \\ &+ [(h_L^r)^T\, [F]\, (h_L^t)][(h_R^r)^T\, [F]\, (h_R^t)]^c\, e^{-j2(\alpha_t+\alpha_r)} \\ &+ [(h_R^r)^T\, [F]\, (h_L^t)][(h_R^r)^T\, [F]\, (h_R^t)]^c\, e^{-j2\alpha_t} \\ &+ [(h_L^r)^T\, [F](h_R^t)][(h_R^r)^T\, [F]\, (h_R^t)]^c\, e^{-j2\alpha_r}\Big\}, \end{aligned}$$

where c denotes the complex conjugate. Let $\alpha_r = \alpha_t + \delta$. The last five terms of Eq. (63), then, contain terms $e^{-j2\alpha_t}$ and $e^{-j4\alpha_t}$. Integrating over α_t corresponds to an averaging of the backscattering cross section as the object rotates on an axis parallel to the direction of propagation. Since

$$\frac{1}{\pi}\int_0^{\pi} e^{-j2\alpha}\, d\alpha = \frac{1}{\pi}\int_0^{\pi} e^{-j4\alpha}\, d\alpha = 0,$$

these five terms will not contribute to the average.

The first five terms of Eq. (63) are seen to be independent of α_t. The fifth term is dependent on δ, the angle of separation between the transmitter and the receiver major axes of polarization.

Denoting the average over α_t by $\hat{}$, Eq. (63) reduces to

$$\begin{aligned}(64)\qquad \hat{\sigma}_{bs}(\theta,\phi) \propto\ & |(h_L^r)^T\ [F]\ (h_L^t)|^2 + |(h_R^r)^T\ [F]\ (h_L^t)|^2 \\ & + |(h_L^r)^T\ [F]\ (h_R^t)|^2 + |(h_R^r)^T\ [F]\ (h_R^t)|^2 \\ & + 2\ \mathrm{Re}\left\{ [(h_R^r)^T\ [F]\ (h_L^t)]\ [(h_L^r)^T\ [F]\ (h_R^t)]^c\ e^{j2\delta} \right\}.\end{aligned}$$

The vector antenna heights expressed in the θ-ϕ basis system are now specified as noted by their subscripts, i.e.,

(65)

a) $$(h_L^r) = L_r \begin{pmatrix} \frac{1}{\sqrt{2}} \\ \frac{j}{\sqrt{2}} \end{pmatrix}, \quad \text{left circular receive;}$$

b) $$(h_R^r) = R_r \begin{pmatrix} \frac{1}{\sqrt{2}} \\ \frac{-j}{\sqrt{2}} \end{pmatrix}, \quad \text{right circular receive;}$$

(65) (cont.) c) $(h_L^t) = L_t \begin{pmatrix} \frac{1}{\sqrt{2}} \\ \frac{j}{\sqrt{2}} \end{pmatrix}$, left circular transmit; and

d) $(h_R^t) = R_t \begin{pmatrix} \frac{1}{\sqrt{2}} \\ \frac{-j}{\sqrt{2}} \end{pmatrix}$, right circular transmit;

where R and L represent the right circular and left circular magnitudes, respectively. Substituting into Eq. (64), normalizing according to Eq. (58), averaging over θ and ϕ to obtain the average over all tumble angles (denoted by $< >$), and expressing the proportionality constant explicitly, we get

$$(66) \quad \langle\sigma_{bs}\rangle = \frac{(\omega\mu)^2}{4\pi} \frac{1}{4(R_r^2 + L_r^2)(R_t^2 + L_t^2)} \Big\{ [(R_r R_t)^2 + (L_r L_t)^2]$$

$$\cdot [\langle|F_{\theta\theta}|^2\rangle + \langle|F_{\phi\phi}|^2\rangle + 4\langle|F_{\theta\phi}|^2\rangle - 2\langle \mathrm{Re}\{F_{\theta\theta} F_{\phi\phi}^2\}\rangle]$$

$$+ 4[(R_r R_t)^2 - (L_r L_t)^2] \langle \mathrm{Im}\{(F_{\theta\theta} - F_{\phi\phi}) F^c\}\rangle$$

$$+ [(R_r L_t)^2 + (L_r R_t)^2 + 2(R_r L_t)(L_r R_t)\cos 2\delta]$$

$$\cdot [\langle|F_{\theta\theta}|^2\rangle + \langle|F_{\phi\phi}|^2\rangle + 2\langle \mathrm{Re}\{F_{\theta\theta} F_{\phi\phi}^c\}\rangle] \Big\} \quad .$$

From Eq. (66) we obtain tumble average expressions for the following specific transmitter-receiver polarizations:

(i) right circular-to-right circular ($R_r = R_t = 1$, $L_r = L_t = 0$)

$$(67) \quad \langle\sigma_{RR}\rangle = \frac{(\omega\mu)^2}{4\pi} \frac{1}{4} \Big(\langle|F_{\theta\theta}|^2\rangle + \langle|F_{\phi\phi}|^2\rangle + 4\langle|F_{\theta\phi}|^2\rangle$$

$$-2\langle \mathrm{Re}\{F_{\theta\theta} F_{\phi\phi}^c\}\rangle + 4\langle \mathrm{Im}\{(F_{\theta\theta} - F_{\phi\phi}) F_{\theta\phi}^c\}\rangle \Big)$$

(ii) left circular-to-left circular ($R_r=R_t=0$, $L_r=L_t=1$)

$$(68)\qquad \langle\sigma_{LL}\rangle = \frac{(\omega\mu)^2}{4\pi}\ \frac{1}{4}\Big(\langle|F_{\theta\theta}|^2\rangle + \langle|F_{\phi\phi}|^2\rangle + 4\langle|F_{\theta\phi}|^2\rangle$$

$$-2\langle\mathrm{Re}\{F_{\theta\theta}\ F^c_{\phi\phi}\}\rangle - 4\langle\mathrm{Im}\{(F_{\theta\theta} - F_{\phi\phi})F^c_{\theta\phi}\}\rangle\Big),$$

(iii) right circular-to-left circular ($R_r=L_t=0$, $R_t=L_r=1$)

$$(69)\qquad \langle\sigma_{RL}\rangle = \frac{(\omega\mu)^2}{4\pi}\ \frac{1}{4}\ \Big(\langle|F_{\theta\theta}|^2\rangle + \langle|F_{\phi\phi}|^2\rangle + 2\langle\mathrm{Re}\{F_{\theta\theta}\ F^c_{\phi\phi}\}\rangle\Big),$$

(iv) left circular-to-right circular ($R_r=L_t=1$, $R_t=L_r=0$)

$$(70)\qquad \langle\sigma_{LR}\rangle = \frac{(\omega\mu)^2}{4\pi}\ \frac{1}{4}\Big(\langle|F_{\theta\theta}|^2\rangle + \langle|F_{\phi\phi}|^2\rangle + 2\langle\mathrm{Re}\{F_{\theta\theta}\ F^c_{\theta\phi}\}\rangle\Big),$$

(v) linear-to-linear ($R_r=L_r=R_t=L_t=1$, $\delta = 0$)

$$(71)\qquad \langle\sigma_{\parallel}\rangle = \frac{(\omega\mu)^2}{4\pi}\Big(\frac{3}{8}\ (\langle|F_{\theta\theta}|^2\rangle + \langle|F_{\phi\phi}|^2\rangle) + \frac{1}{2}\ \langle|F_{\theta\phi}|^2\rangle$$

and

$$+\frac{1}{4}\ \langle\mathrm{Re}\{F_{\theta\theta}\ F^c_{\phi\phi}\}\rangle\Big),$$

(vi) linear-to-cross linear ($R_r=L_r=R_t=L_t=1$, $\delta = \pi/2$)

$$(72)\qquad \langle\sigma_{\perp}\rangle = \frac{(\omega\mu)^2}{4\pi}\ \Big(\frac{1}{8}\ \ (\langle|F_{\theta\theta}|^2\rangle + \langle|F_{\phi\phi}|^2\rangle) + \frac{1}{2}\ \langle|F_{\theta\phi}|^2\rangle$$

$$-\frac{1}{4}\ \langle\mathrm{Re}\{F_{\theta\theta}\ F^c_{\phi\phi}\}\rangle\Big)\qquad .$$

Having expressions (67) through (72), Eq. (66) can be written as

$$(73)\qquad \langle\sigma_{bs}\rangle = \frac{1}{(R_r^2 + L_r^2)(R_t^2 + L_t^2)} \Big((R_rR_t)^2 \langle\sigma_{RR}\rangle + (L_rL_t)^2 \langle\sigma_{LL}\rangle$$

$$+ [(R_rL_t)^2 + (L_rR_t)^2 + 2(R_rL_t)(L_rR_t)\cos 2\delta] \langle\sigma_{RL}\rangle\Big)$$

or as

$$(74)\qquad \langle\sigma_{bs}\rangle = \frac{1}{(R_r^2 + L_r^2)(R_t^2 + L_t^2)} \Big([(R_rR_t)^2 - (L_rL_t)^2] \langle\sigma_{RR}\rangle$$

$$+ [4(L_rL_t)^2 - (R_rL_t)^2 - (L_rR_t)^2 - 2(R_rL_t)(L_rR_t)\cos 2\delta] \langle\sigma_{\perp}\rangle$$

$$+ [(R_rL_t)^2 + (L_rR_t)^2 + 2(R_rL_t)(L_rR_t)\cos 2\delta] \langle\sigma_{\parallel}\rangle\Big),$$

where Eq. (73) is in terms of circular polarization averages and Eq. (74) is in terms of circular and linear polarization averages.

(iii) Input Admittance

The design of loaded scatterers requires a knowledge of the driving point impedance (or admittance) of the element when it is excited as an antenna. The scatterer is usually resonated by placing a passive load at the set of terminals such that the reactive component is cancelled. The characteristic mode theory offers a new approach toward determining the desired antenna impedance for wire-type scatterers.

An expression for the input admittance can be derived[48] in terms of the characteristic currents and the characteristic values of a given wire. The current evaluated at point ℓ on the wire due to a unit plane wave incident from a direction (θ^i,ϕ^i) is[20,48]

$$(75) \qquad I(\ell) = \sum_{m=1}^{M} A_m \, I_m(\ell),$$

where $I_m(\ell)$ is real and represents the m^{th} normalized characteristic current distribution evaluated at ℓ, and A_m, the weight[20] of the m^{th} term in the expansion, is complex and is given by the reaction[49-51] of the m^{th} radiated field, $\underline{E}_m^{ext}(r,\theta,\phi)$, with the source current, i.e.,

$$(76) \qquad A_m = \iiint_V \underline{E}_m^{ext}(r,\theta,\phi) \cdot \underline{J}(r,\theta,\phi) \, dV,$$

where the integration is over the volume of the source. If the source is an electric dipole located at (r^i,θ^i,ϕ^i) which causes an essentially plane wave in the vicinity of the wire, Eq. (76) becomes

$$(77) \qquad A_m = a_m \underline{F}_m(\theta^i,\phi^i) \cdot \hat{h}^i,$$

where $\hat{h}^i$ is the polarization state vector of the plane wave, a_m is the characteristic value associated with the m^{th} mode, and $\underline{F}_m(\theta^i,\phi^i)$ is the m^{th} characteristic mode pattern function evaluated at (θ^i,ϕ^i). Substituting Eq. (77) into Eq. (75),

$$(78) \qquad I(\ell) = \sum_{m=1}^{M} a_m \, \underline{F}_m(\theta^i,\phi^i) \cdot \hat{h}^i \, I_m(\ell).$$

From reciprocity,

$$(79) \qquad I(\ell) = -\hat{h}^i \cdot \underline{F}^r(\theta^i,\phi^i),$$

Where $\underline{F}^r(\theta^i,\phi^i)$ is the radiation pattern in the (θ^i,ϕ^i) direction due to unit voltage, V = 1, across the gap at point ℓ along the wire. Then

$$(80) \qquad \underline{E}^r(\theta^i,\phi^i) = -\sum_{m=1}^{M} a_m \underline{E}_m(\theta^i,\phi^i)\, I_m(\ell) \ .$$

Recalling the orthonormality of the characteristic pattern functions, the complex power radiated is seen to be[20, 48]

$$(81) \qquad P = \sum_{m=1}^{M} |a_m|^2\, I_m(\ell)^2\, (1 - i\lambda_m),$$

where $a_m = -1/(1+i\lambda_m)$ and λ_m is the ratio of net reactive to net radiated power. The admittance is, then,

$$(82) \qquad Y(\ell) = \frac{P}{|V|^2} = -\sum_{m=1}^{M} a_m\, I_m(\ell)^2.$$

D. Examples of Characteristic Modes and Scattering Solutions

In this section the technique described in Section B above is used to determine characteristic mode current distributions and characteristic values of circular and elliptical loops, straight wires, circular arcs, and helices. The modes are used to compute backscattering and tumble average cross sections and input admittance data as outlined in Section C. Where possible, the results are compared with solutions derived by independent methods.

In each case, in deriving the impedance matrix [Z] of Eq. (22), the wire is considered perfectly conducting and its radius is assumed to be much smaller than its length L and the wavelength λ. The assumption is made that the surface current density on the thin wire has only an axial component and is distributed uniformly around the circumference of the wire.

The modal impedance matrix ([Z] of Eq. (22)) for each wire configuration is computed by means of the numerical basis transformation method used in conjunction with a piecewise uniform method.[1-3] The P, Q, and R matrices (Eqs. (35), (36), and (37)) are formed from [Z] and from them the matrix $[B(\alpha)]$ is derived explicitly in terms of α. The characteristic equation (Eq. (32)) is then solved for the smallest eigenvalue $\varepsilon_{min}(\alpha)$. By stepping through a range of α's, we can locate the relative minima of $\varepsilon_{min}(\alpha) = \varepsilon_{min}(\alpha_m)$, thereby specifying the phase angles α_m and allowing the determination of the corresponding eigenvectors (I_m) of Eq. (31). The components of these eigenvectors are the Fourier expansion coefficients of the characteristic mode current distributions in terms of the chosen set of basis functions.

More than one characteristic mode generally is needed to describe a scatterer. Often, however, one mode is sufficient, as is the case, for example, with short wires, i.e., wires of first resonant length or less. This single mode character holds true for quite general wire configurations. For short wires which are effective scatterers, the dominant mode has associated with it a phase angle α_m within about $\pm\pi/4$ of the $\alpha = \pi$ resonant angle; other modes characteristic of such a scatterer are found to have phase angles very near $\pi/2$ or $3\pi/2$, implying that their contributions to scattering are relatively small and usually negligible. As wires increase in length more modes are required to describe their scattering properties accurately. The number of modes needed is also dependent, though to a lesser degree, on the wire geometry.

Certain wire geometries support multiply degenerate modes. As mentioned previously, the circular loop is doubly degenerate since each phase angle α_m (i.e., each characteristic value, a_m) has associated with it two mode current distributions, one of the form $\cos m\phi$, the other of the form $\sin m\phi$. This fact is due, of course, to the rotational symmetry of the loop.

(i) Circular Loops

Characteristic modes were determined for circular loops with a loop radius-to-wire radius ratio R/a = 100. The first four phase angles α_m are shown in Fig. 15 for a range of frequencies. The curves

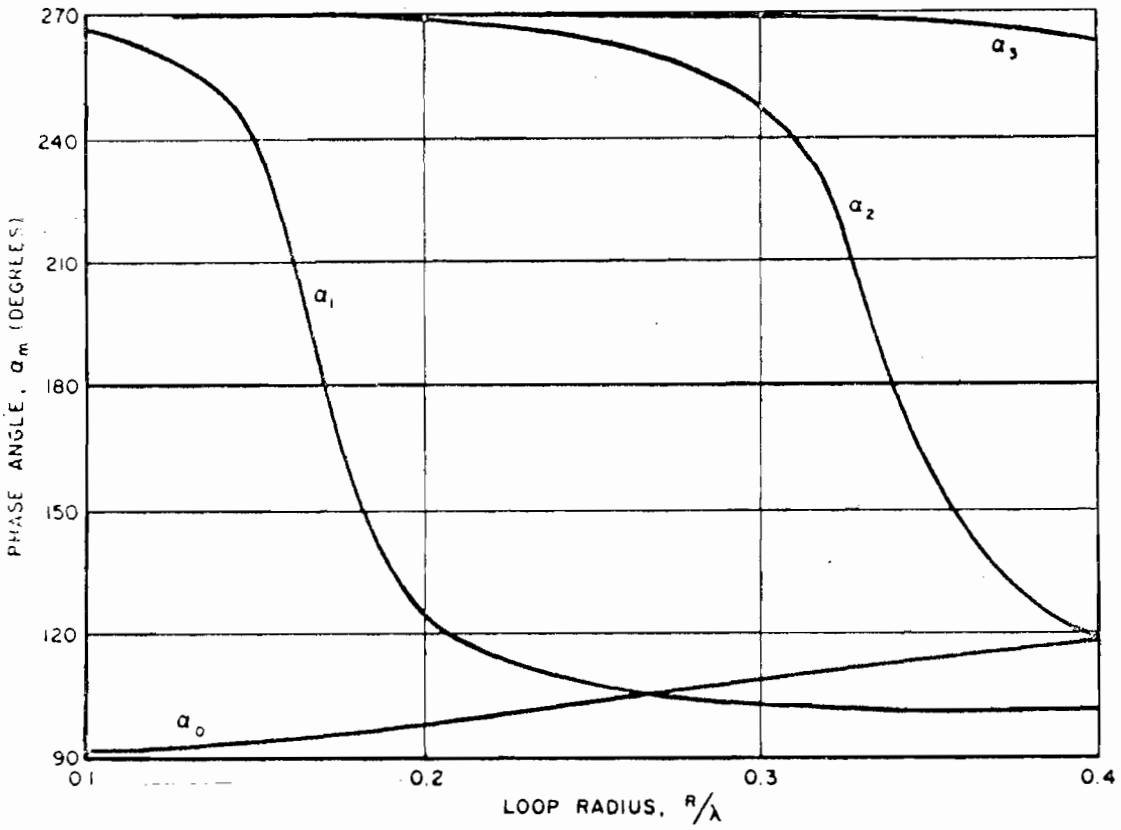

Fig. 15.--Phase angles α_m, m = 0,1,2,3, for circular loops as a function of loop radius.

compare favorably with independently derived results presented in Reference 20. The backscattering cross section data derived using these modes are shown in Figs. 16 and 17. The edge aspect results are compared with solutions obtained by Harrington.[52] The ratio of broadside-to-edge aspect cross section given in Fig. 17 is compared with similar data,[36] both measured and analytical, for loops with a wire radius $a = 0.005\lambda$.

The real and imaginary parts of the input admittance of circular loops with a loop radius-to-wire radius ratio $R/a = 100$ are plotted in Fig. 18 and are compared with Harrington's solutions.[52] The admittance, especially its imaginary part, is more difficult to compute accurately than the far zone scattering parameters. This example is given, together with part (iii) of Section C, above, to show the manner in which the admittance can be obtained from the characteristic modes. More demanding application to admittance calculations would require more accurate solutions for the characteristic modes, which would in turn require more sophisticated (than piecewise uniform) methods for computing the impedance matrix [Z] of Eq. (22).

(ii) Elliptical Loops

Having noted in the preceding discussion that the characteristic modes of a circular loop are doubly degenerate, it is of interest to observe the effect which distortions of the circular geometry have on the modes. For example, one may study the modes of a planar elliptical loop whose axial ratio diverges from unity. Figure 19 shows

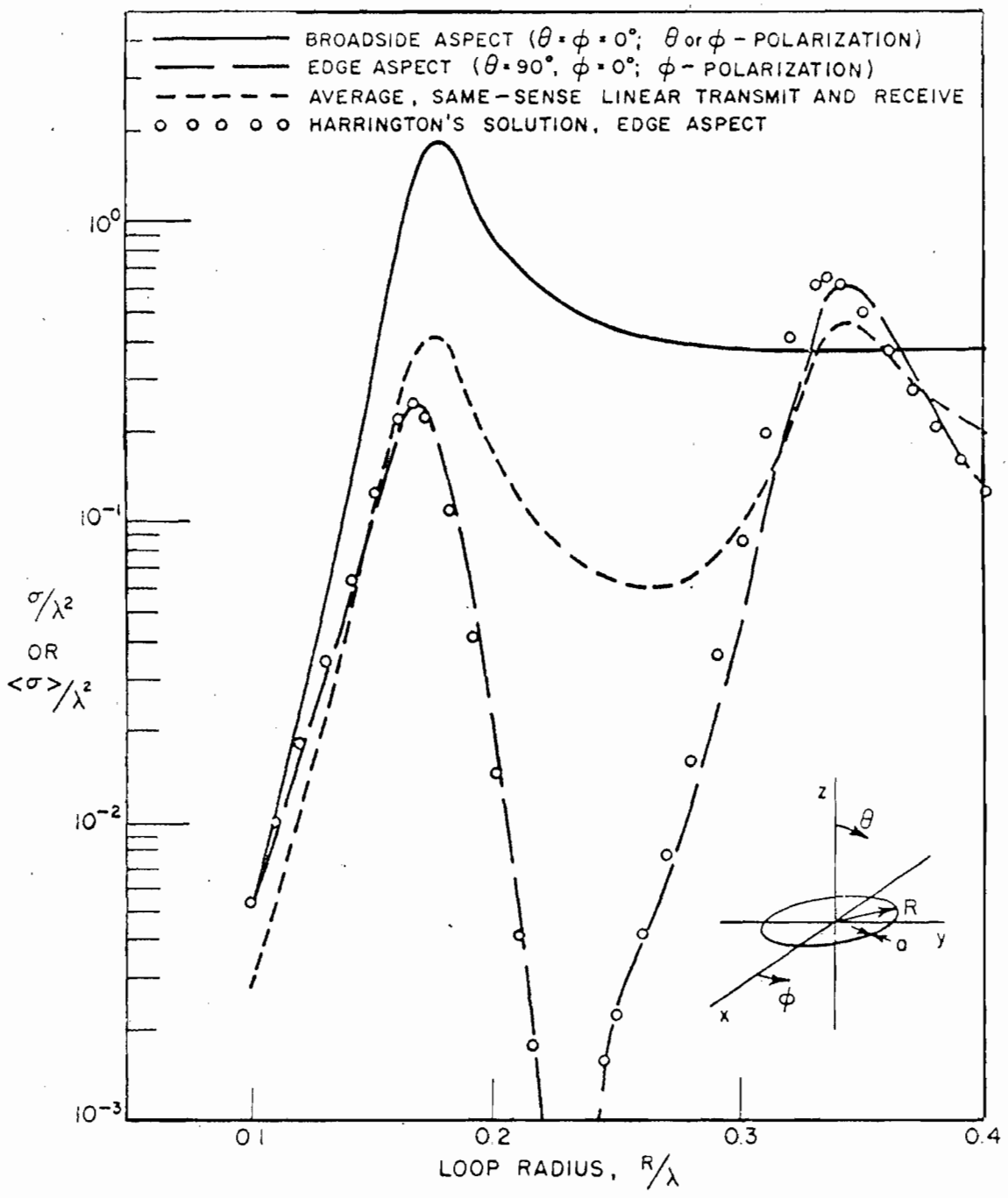

Fig. 16.--Backscattering and tumble average cross sections for circular loops with a loop radius-to-wire radius ratio R/a = 100.

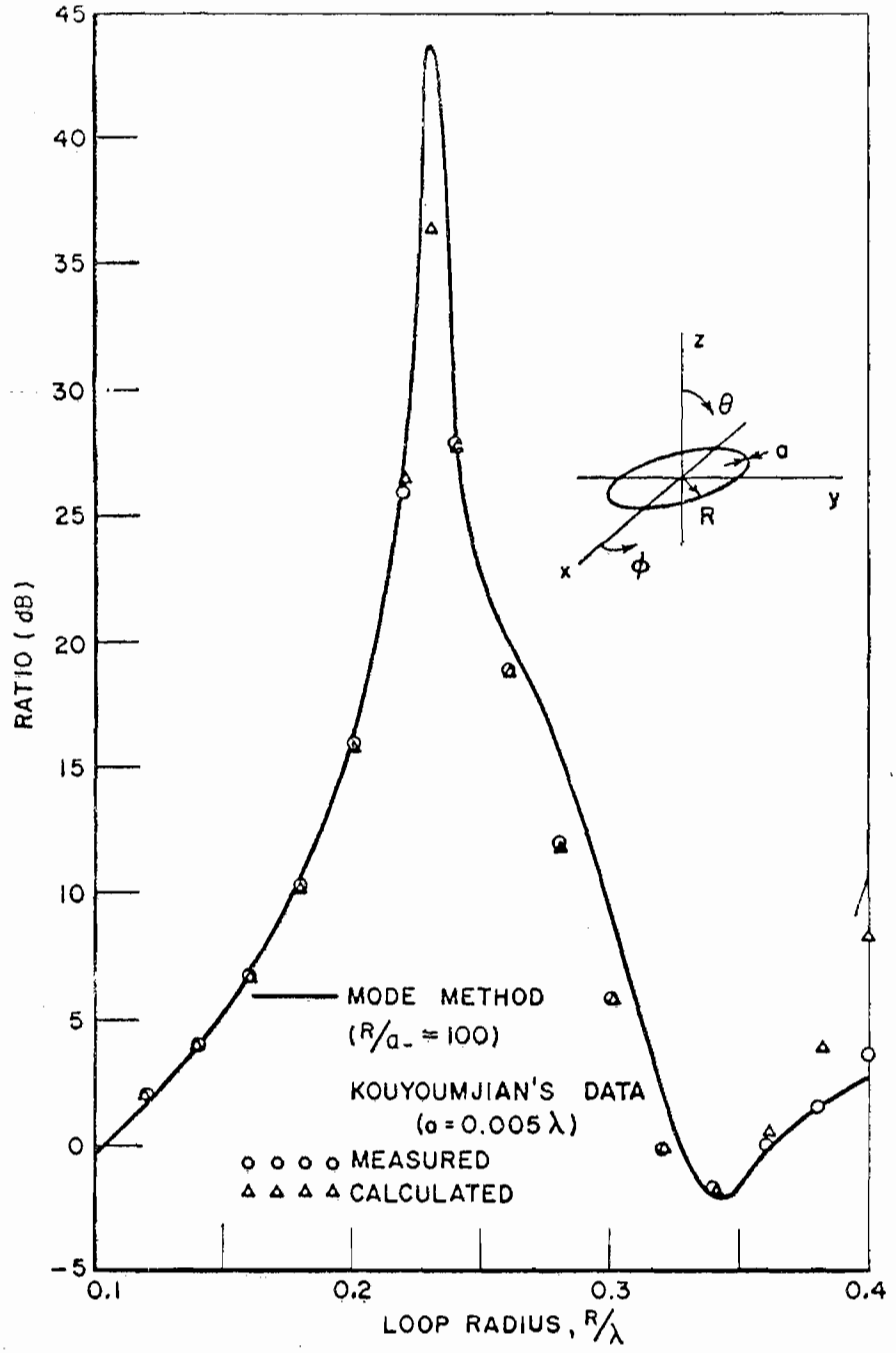

Fig. 17.--Ratio of the backscattering cross section at broadside aspect to that at edge aspect for circular loops with R/a = 100. (Ratio = 10 $\log_{10} \sigma_{bs}/\sigma_{edge}$.)

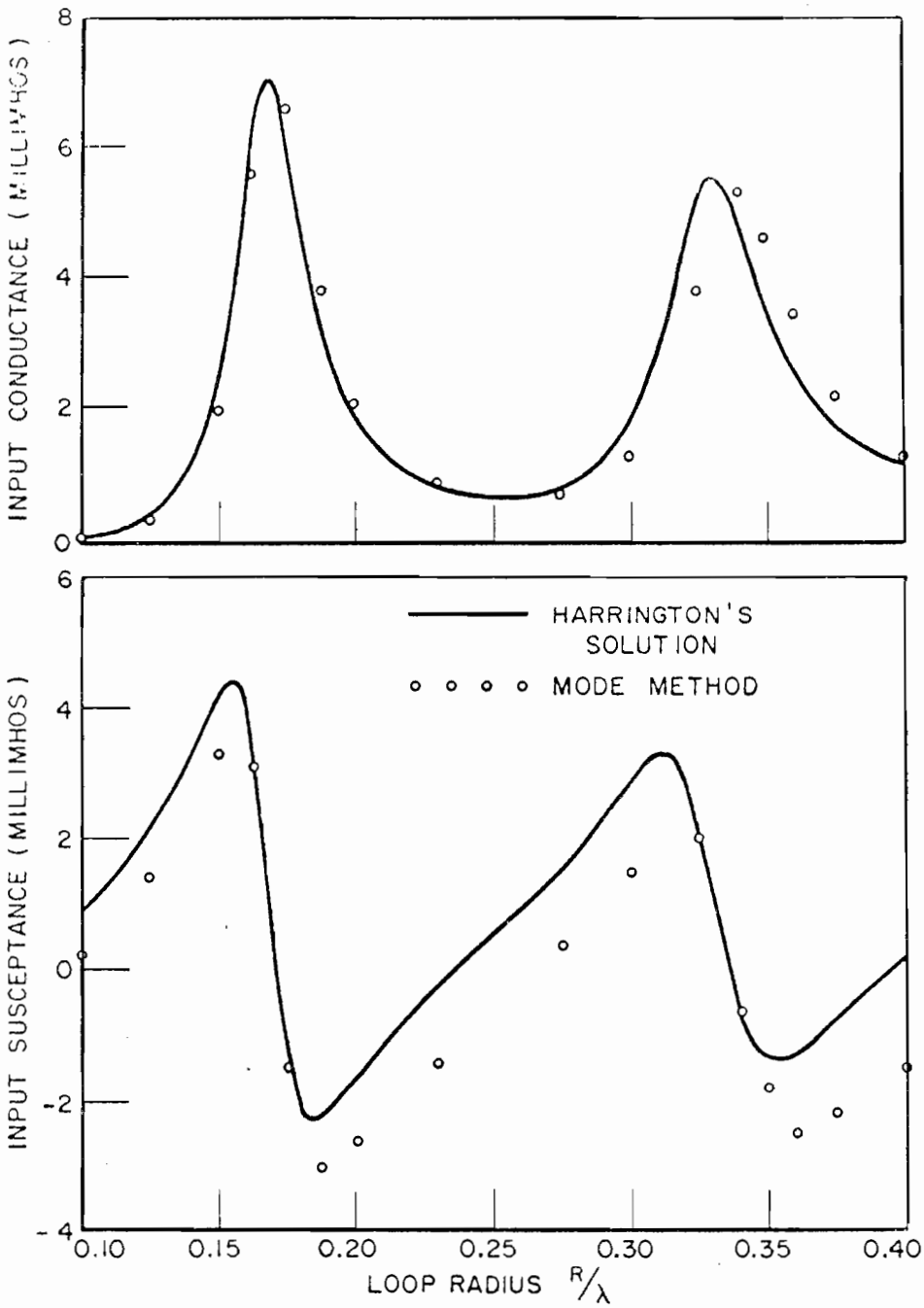

Fig. 18.--Input admittance for circular loops with loop radius-to-wire radius ratio R/a = 100.

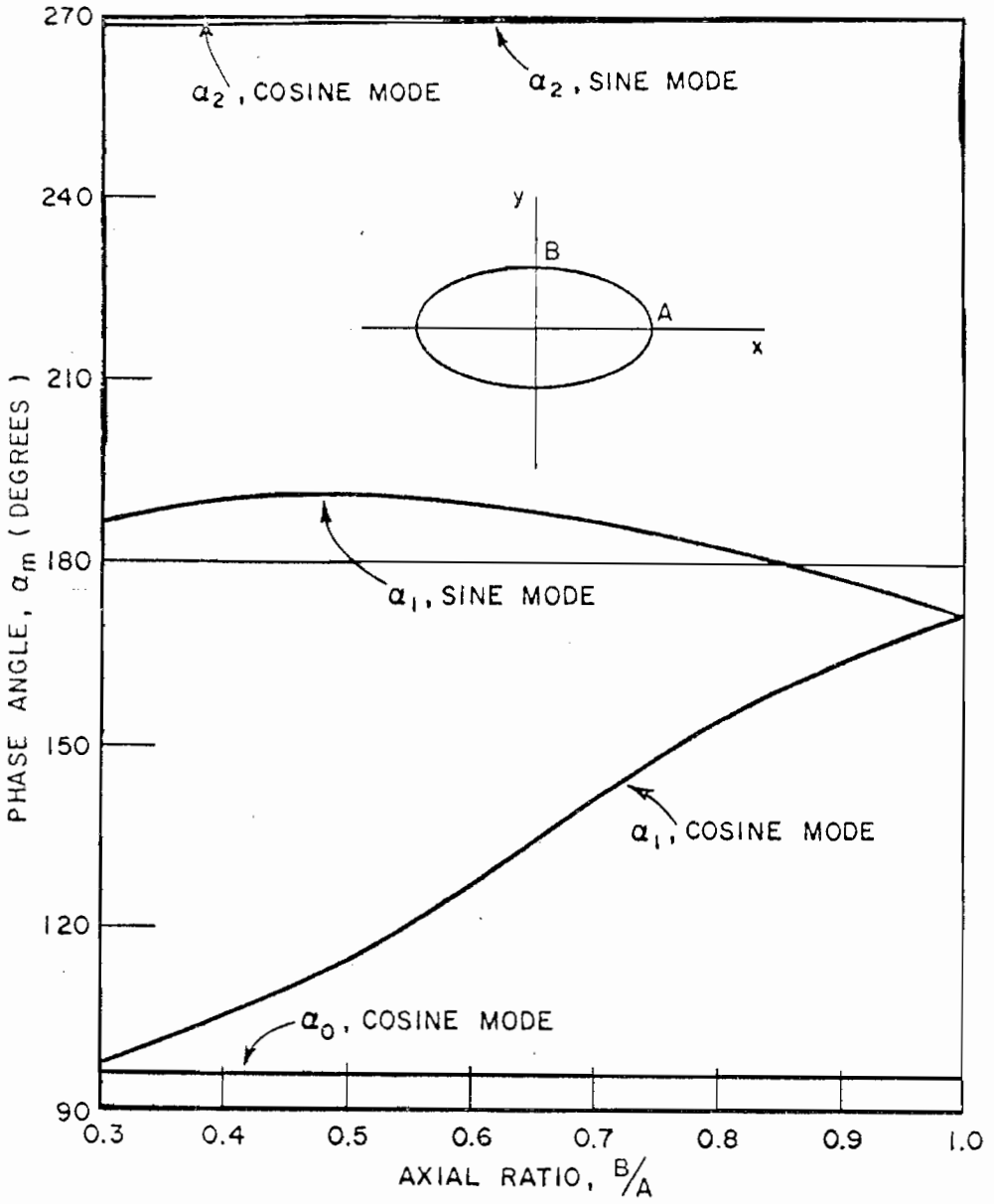

Fig. 19.--Phase angles α_m, m=0,1,2, for elliptical loops with circumference C = 1.1λ and wire radius a = 0.00175λ.

several phase angles associated with the modes of an ellipse as a function of the axial ratio. The circumference is held constant at 1.1λ. The wire radius is a = 0.00175λ and the circumference-to-wire radius ratio is 200π, i.e., the wire is of the same dimensions as

that used in the preceding circular loop example for a loop radius $R = 0.175\lambda$. For an axial ratio of unity the angles α_m are, of course, those shown in Fig. 15 for the corresponding circular loop. As the axial ratio is varied from unity the rotational symmetry of the loop is lost and the modes are no longer doubly degenerate. The backscattering cross section data for these examples are shown in Fig. 20.

In the loop examples just given 120 match points were used in solving for the modes, with six cosine and five sine terms in the Fourier expansions of the characteristic currents. The loops are in the xy-plane and the origin $\ell = 0$ is on the positive x-axis.

(iii) Straight Wires

The characteristic phase angles for straight wires with a length-to-diameter ratio L/2a = 100 are shown in Fig. 21 as a function of frequency. The characteristic current distributions $\underline{I}_m$ for a wire of length $L = 1.5\lambda$ are shown in Fig. 22, where each current has been normalized to radiate unit power. Figures 23 and 24 give backscattering and tumble average cross section data obtained using the characteristic modes associated with the phase angles of Fig. 21. The broadside data given in Fig. 23 are compared with results obtained by Harrington and Mautz.[40] The backscattering cross section as a function of incidence angle θ is shown in Fig. 24 for a wire length $L = 1.5\lambda$.

Similar phase angle and scattering data are shown in Figs. 25 and 26 for straight wires of radius $a = 0.005\lambda$. The results in Fig. 26 for the broadside backscattering cross section of wires of lengths near the first resonance are compared with those obtained by Richmond.[12]

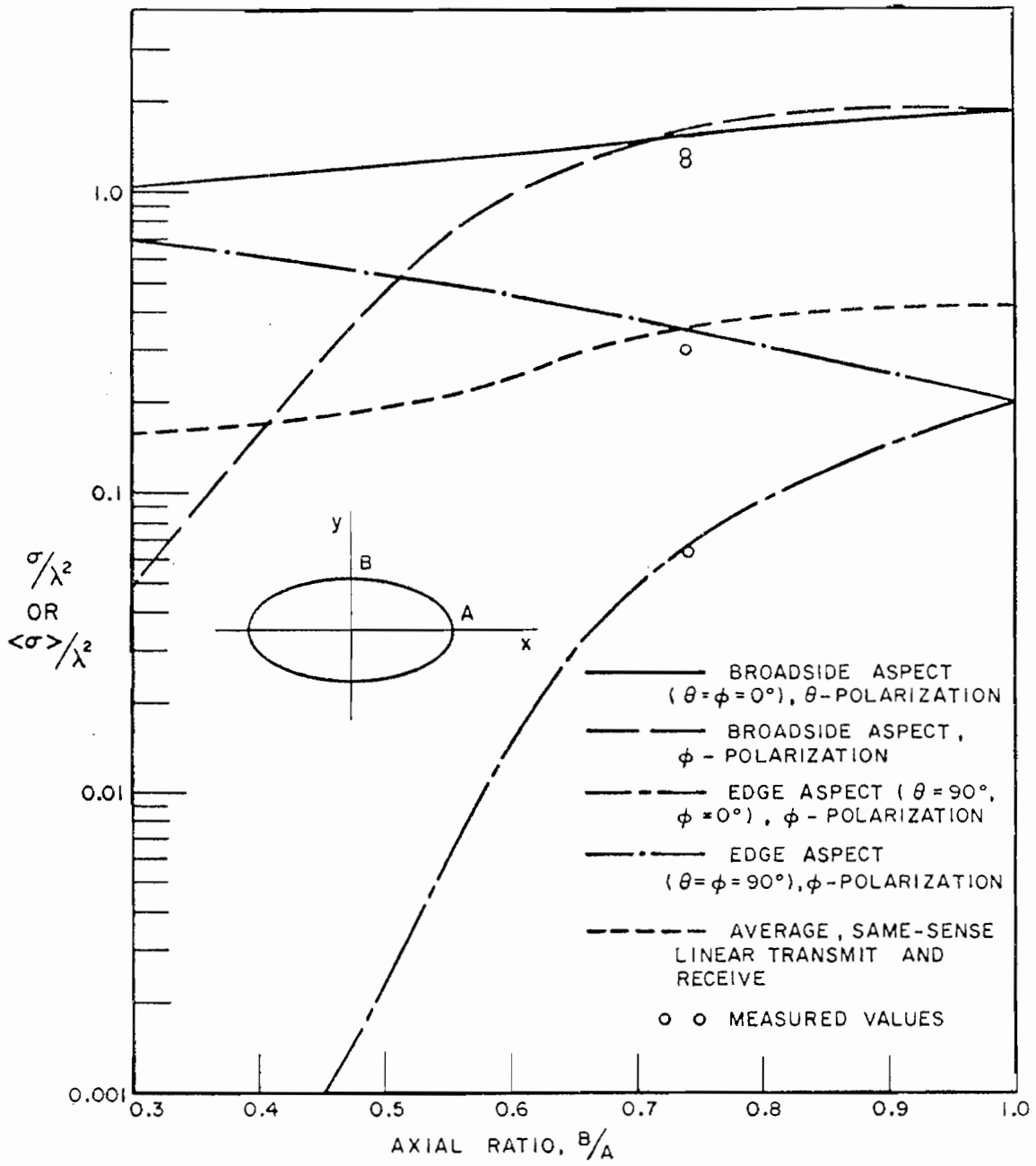

Fig. 20.--Backscattering and tumble average cross sections for elliptical loops with circumference C = 1.1λ and wire radius a = 0.00175λ.

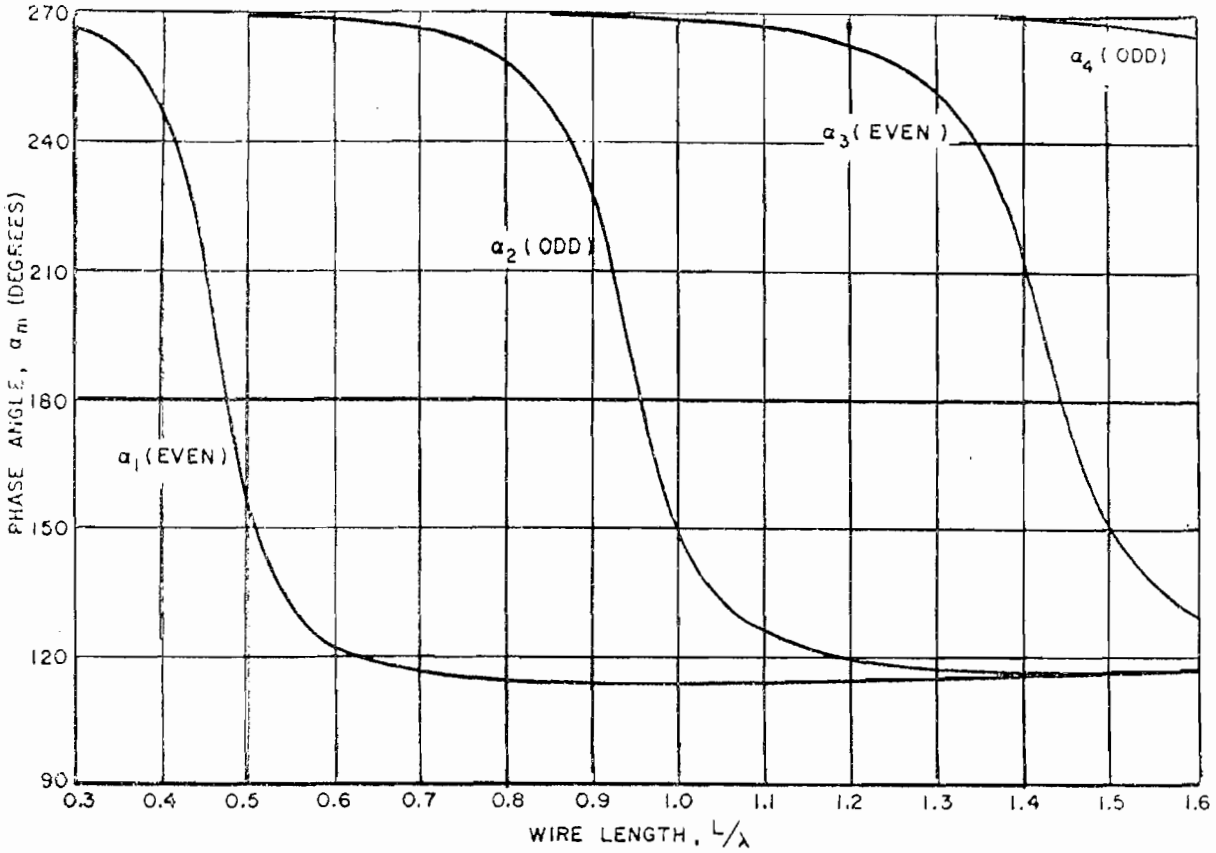

Fig. 21.--Phase angles α_m, m=1,2,3,4, for straight wires with a length-to-diameter ratio L/2a = 100.

A comparison of the phase angle curves with the scattering behavior as a function of wire length for the straight wire examples just given demonstrates the dependence of the scattering or radiating efficiency of a mode upon its characteristic value or phase. In each case considered (where one mode is the dominant contributor) a peak in the average cross section corresponds to a wire length for which the phase associated with the dominant mode is equal to or approximately equal to π.

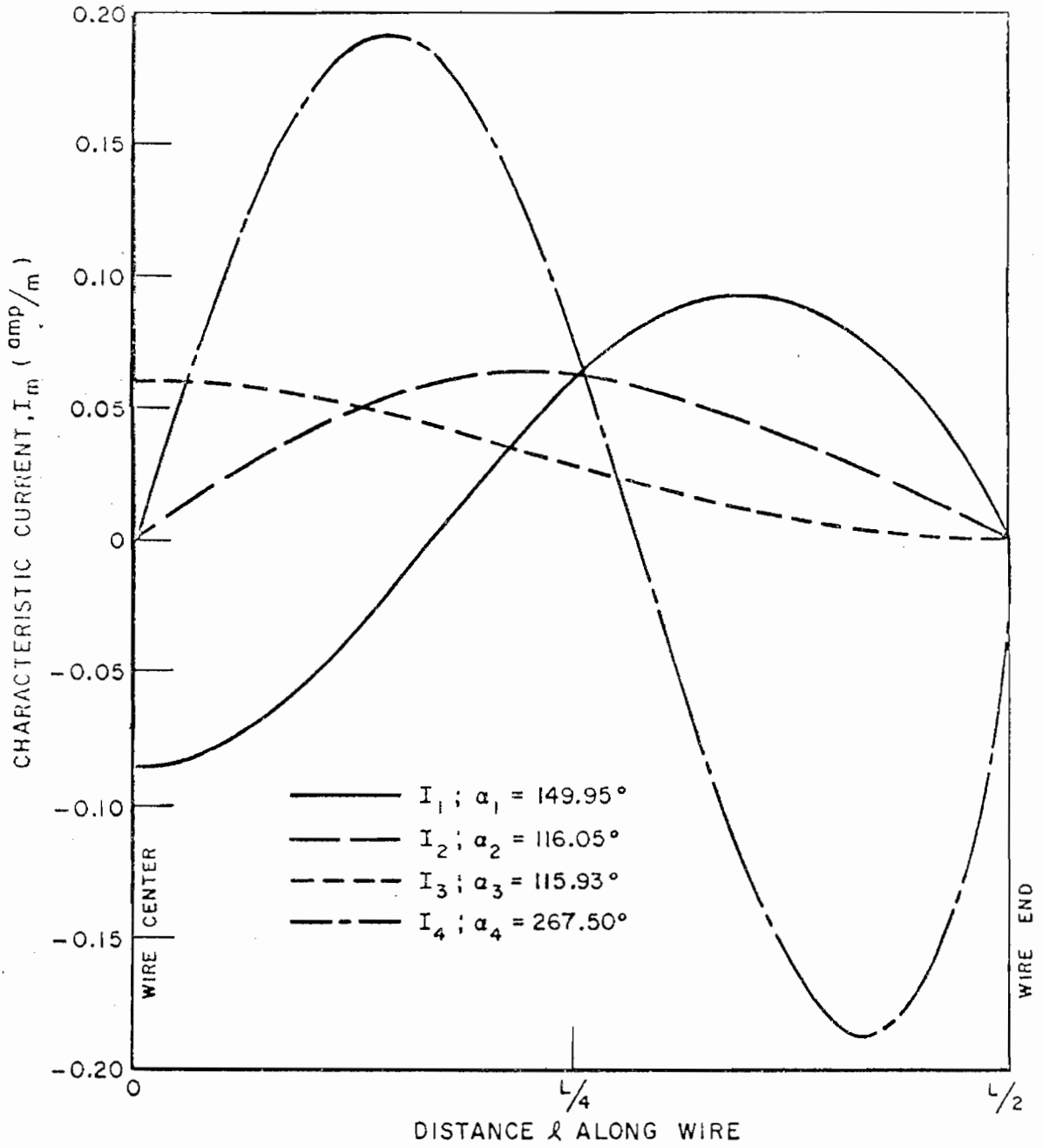

Fig. 22.--Normalized characteristic current distributions I_m, m=1,2,3,4, for a straight wire of length L = 1.5λ with L/2a = 100.

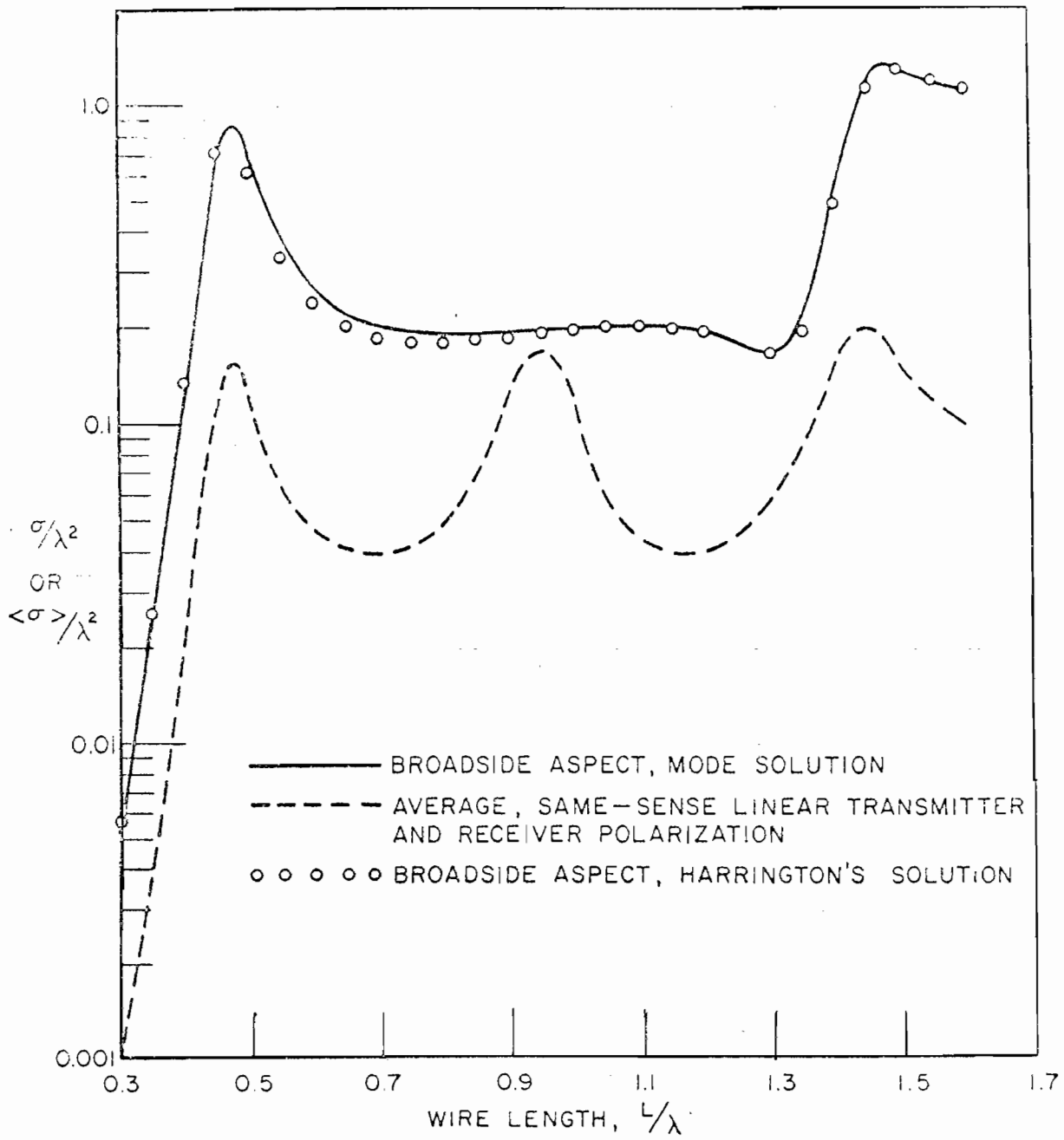

Fig. 23.--Broadside and tumble average backscattering cross sections of straight wires with L/2a = 100.

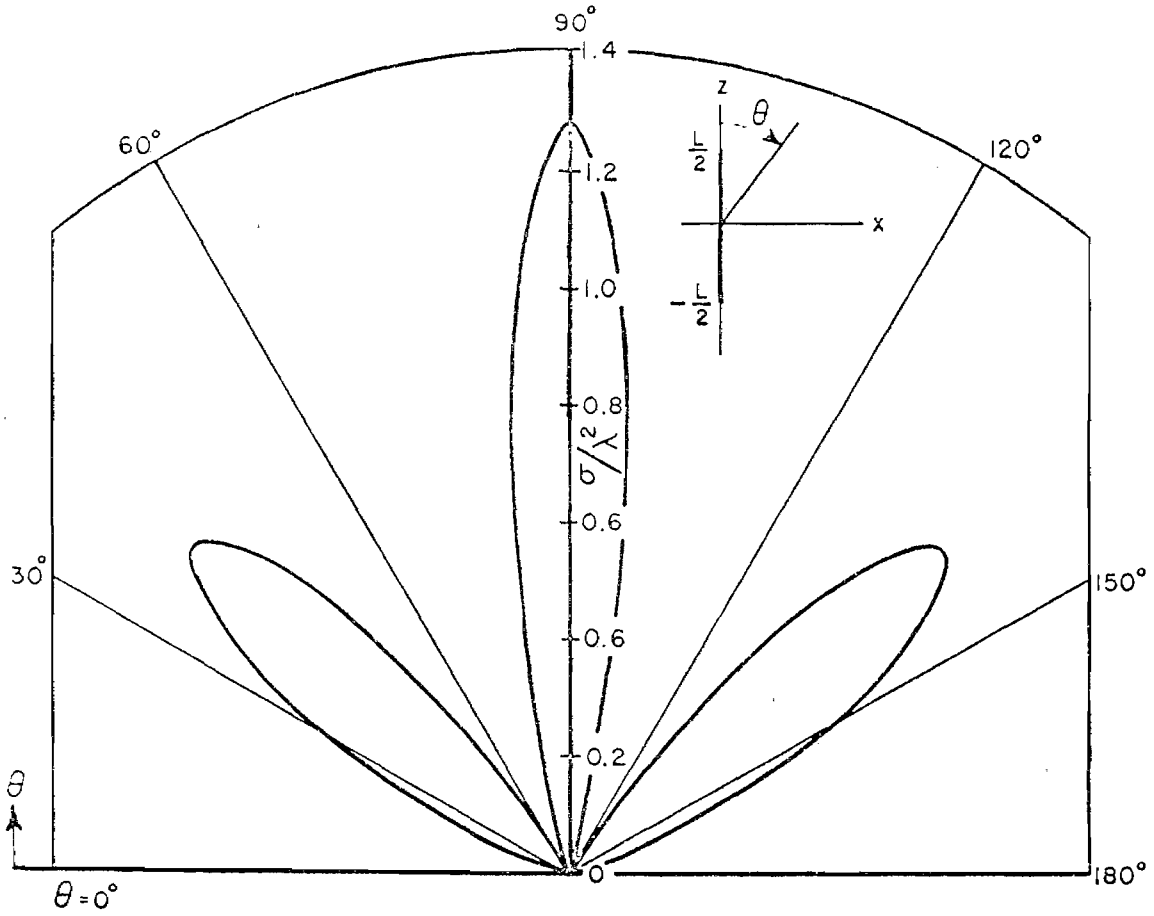

Fig. 24.--Backscattering cross section as a function of incidence angle θ for a straight wire of length L = 1.5λ with L/2a = 100.

In determining the characteristic modes for the straight wires considered above, up to 160 match points were used with six even and five odd Chebyshev polynomials of the second kind in the Fourier expansions of the characteristic currents.

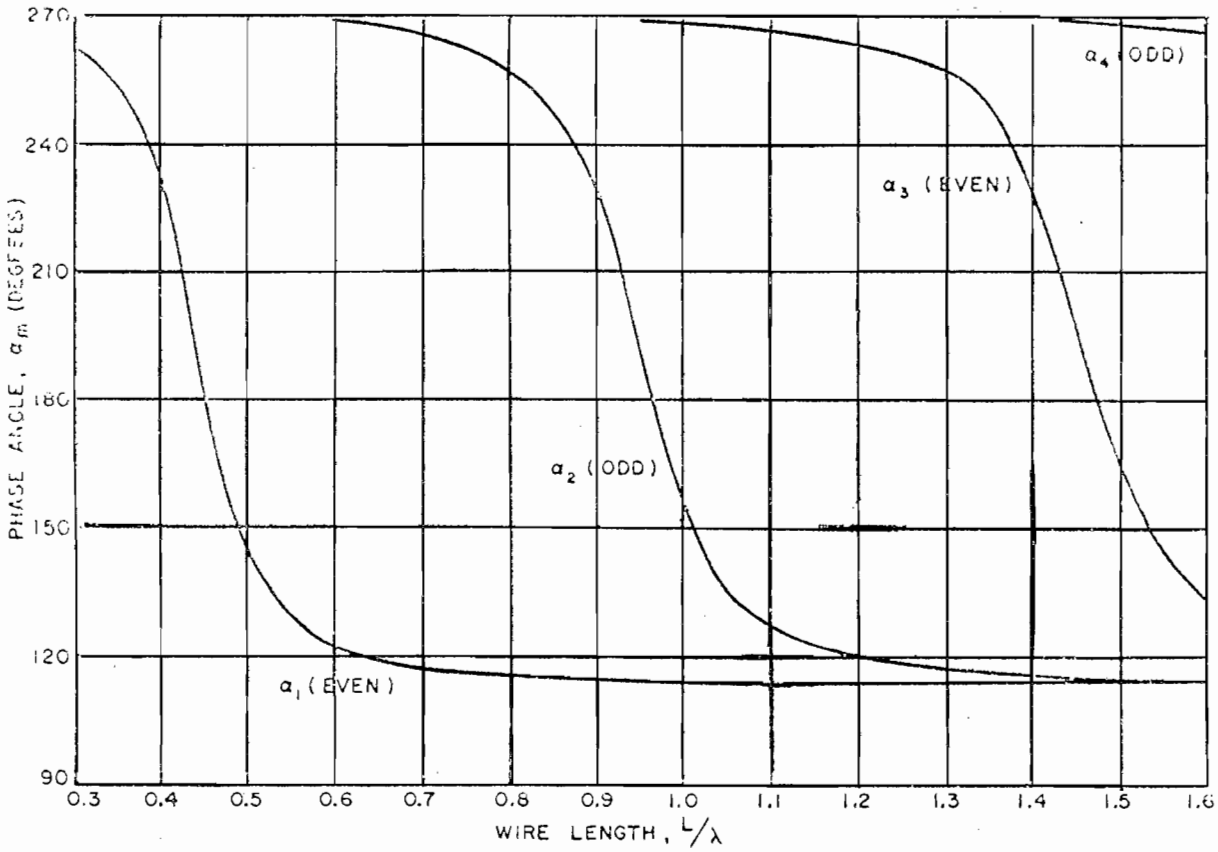

Fig. 25.--Phase angles α_m, m = 1,2,3,4, for straight wires of constant radius a = 0.005λ.

(iv) Circular Arcs

The examples given so far have been scatterers for which more than one mode were needed to describe the scattering properties accurately. In particular instances, e.g., the case of straight wires with $L \leq 0.6\lambda$, only one mode was needed to obtain reasonably accurate plane wave scattering data. In this section we show that such short

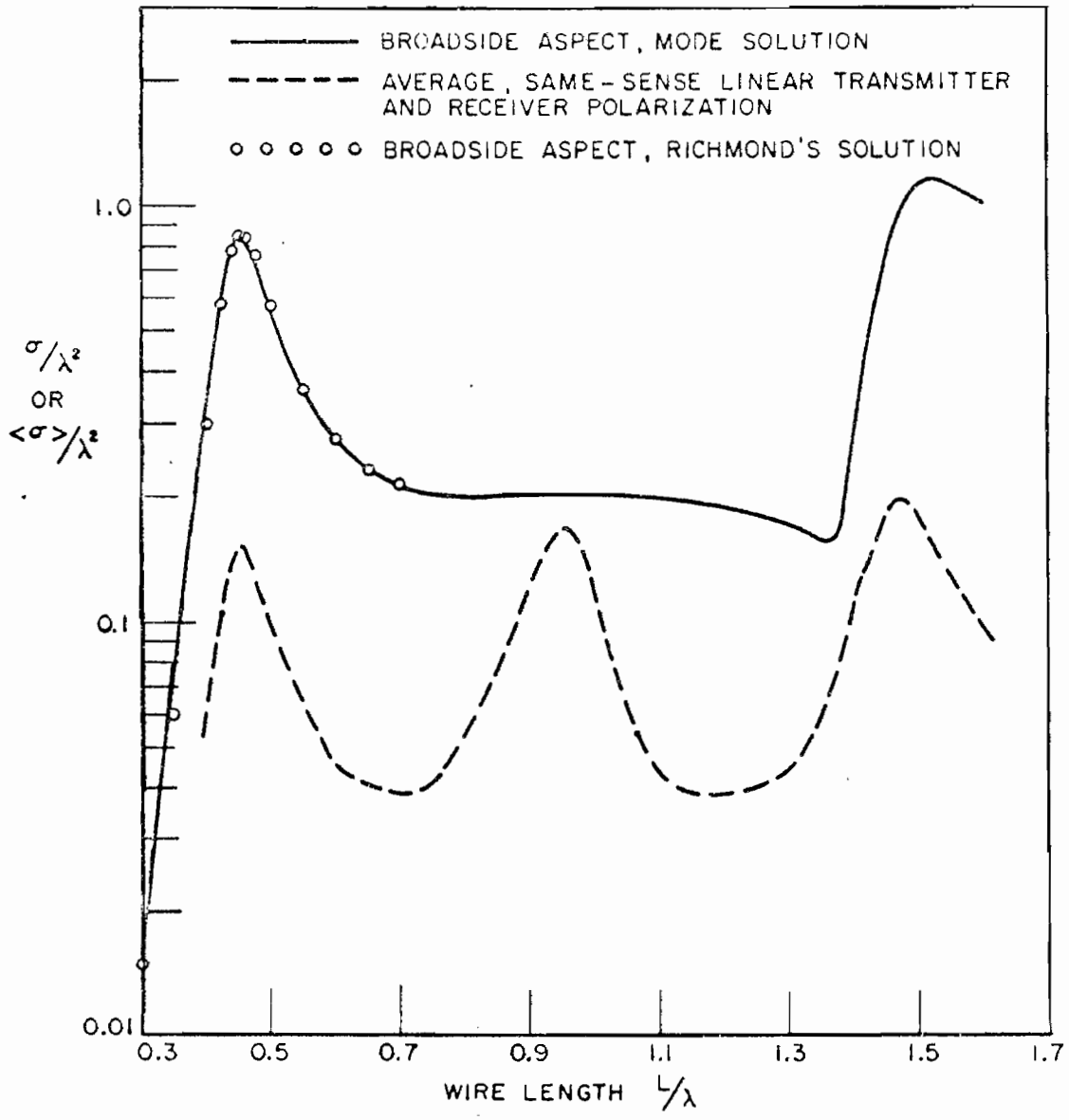

Fig. 26.--Broadside and tumble average backscattering cross sections of straight wires with a = 0.005λ.

wires, even when formed into circular arcs, retain this "single-mode" nature.

The phase angle associated with the dominant characteristic mode for a lossless open circular arc of wire of length L = 0.475λ and radius a = 0.0008467λ is shown in Fig. 27 as a function of the arc radius, R. Using only this dominant mode, the backscattering data of Fig. 28 were derived. The broadside- and edge-aspect cross section results are compared with solutions obtained[53] by a piecewise uniform, point-matching method for tungsten wires.

It is interesting to note the dependence of the dominant mode current distribution on the arc radius. The distribution appears to be nearly independent of the arc radius to a radius of approximately 0.085λ. This can be seen by noting the nearly constant values obtained for the Fourier coefficients of the series approximations to be current. Figure 29 shows the first five coefficients as a function of arc radius. Each coefficient has been normalized to its value for a radius R = 0.15λ for convenience in plotting. This suggests that the mode current distribution for a short wire of a given length may be, to a degree, independent of the wire configuration. The characteristic value, or phase angle, associated with the current, however, may show considerable variation and can give evidence of significant variations in scattering cross section. For example, Fig. 28 shows a variation of more than 3 dB in backscattering cross sections for circular arcs ranging in arc radii from 0.085λ to 0.15λ, in spite of

the constancy of current distribution implied by Fig. 29. Only a substantial change in phase angle can be the explanation, and Fig. 27 bears this out.

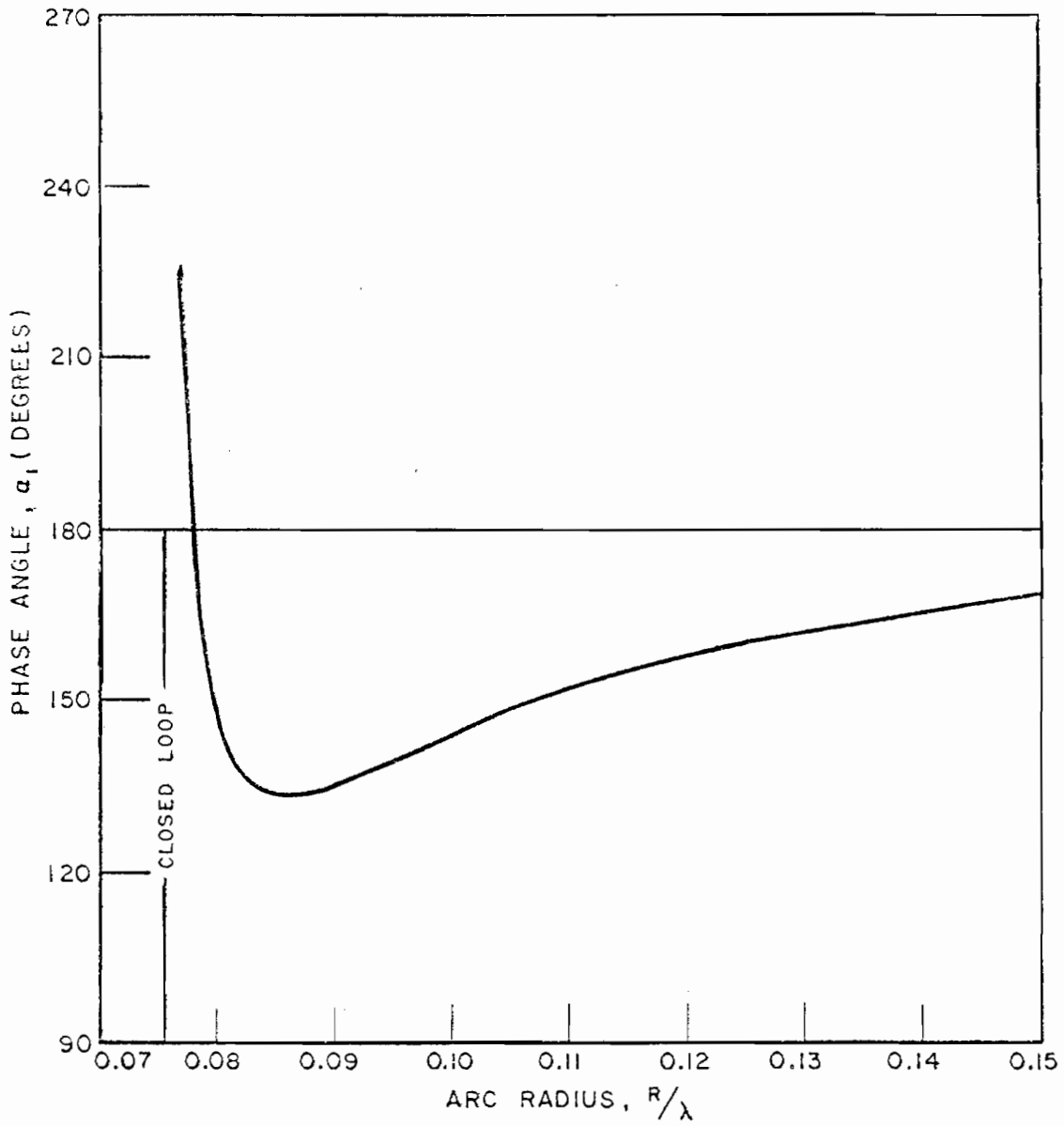

Fig. 27.--Phase angle α_1 as a function of arc radius for the dominant mode of a circular wire arc with wire length L = 0.475λ and wire radius a = 0.0008467λ.

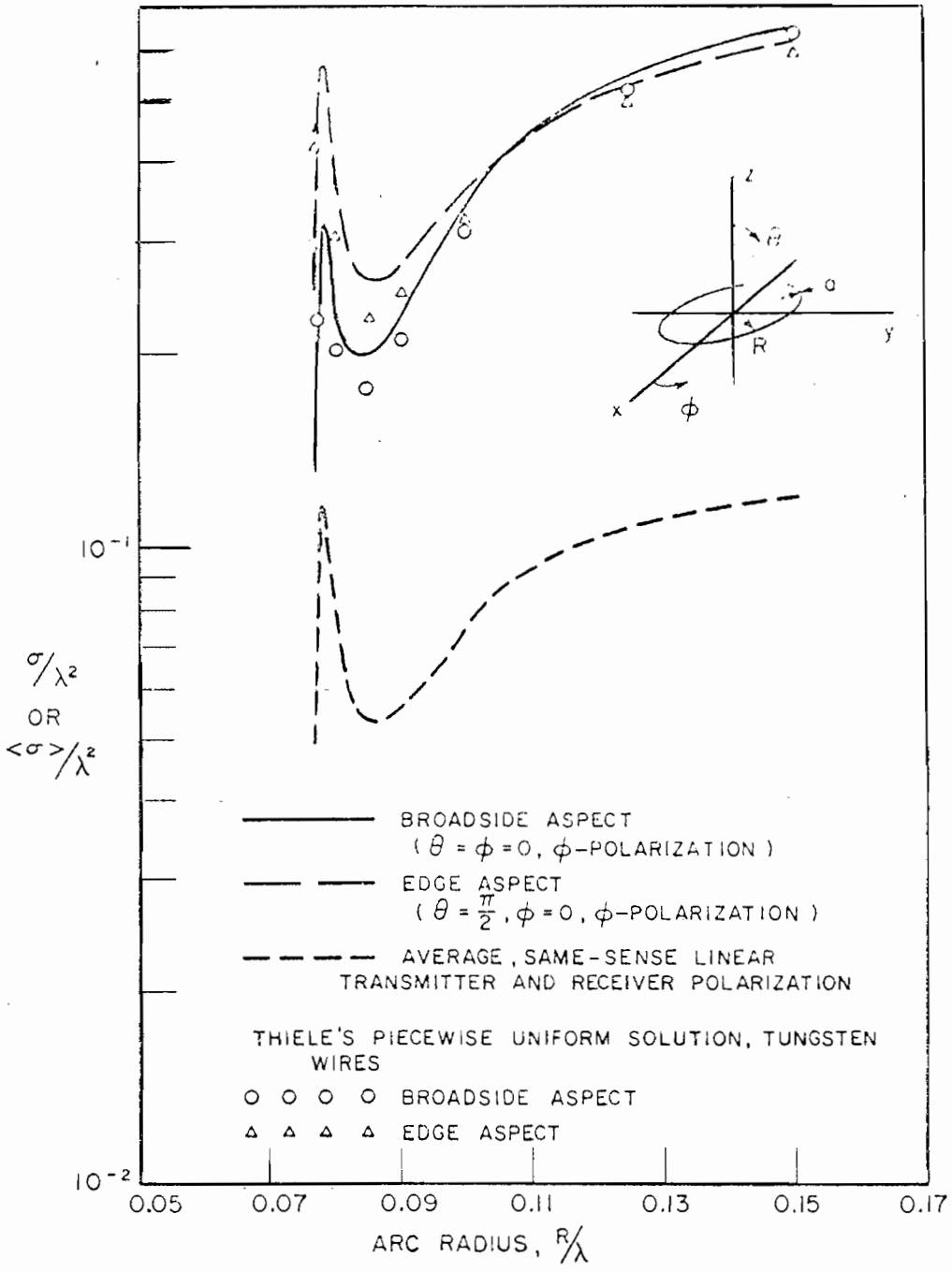

Fig. 28.--Backscattering and tumble average cross section data for a circular arc with L = 0.475λ and a = 0.0008467λ.

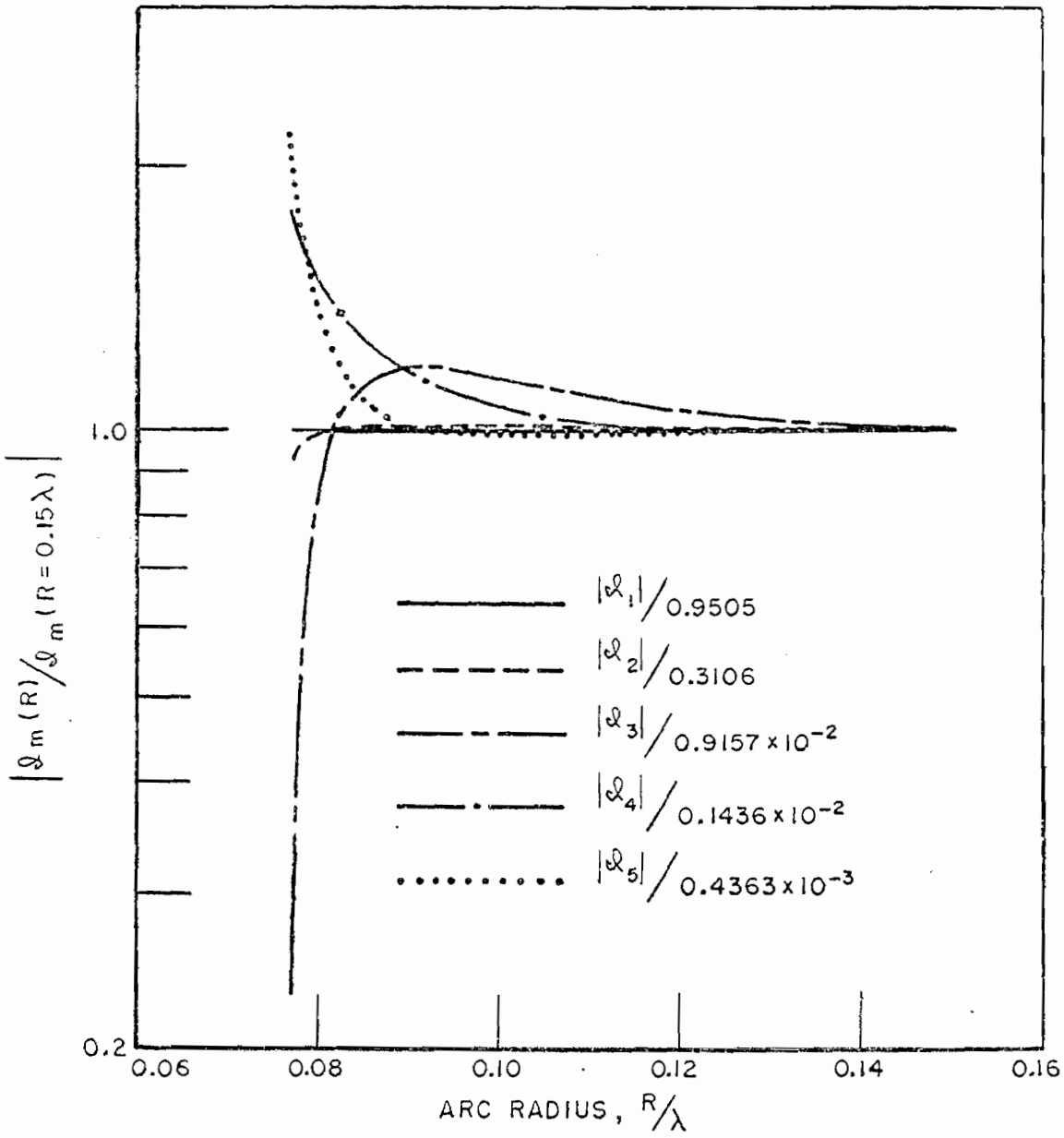

Fig. 29.--Characteristic mode current coefficients for the dominant mode of a circular arc with wire length $L = 0.475\lambda$ and wire radius $a = 0.0008467\lambda$. (Each coefficient is normalized to its value for a radius $R = 0.15\lambda$.)

(v) Helices

Helices were formed with a wire of length L = 0.475λ and radius a = 0.0008467λ. The helix pitch, p, the distance between turns, is equal to thirty times the wire radius. Just as for the circular arcs formed by wires of the same dimensions, a single mode describes the scattering with sufficient accuracy.

The phase angle associated with the dominant mode as a function of the helix radius, R, is shown in Fig. 30. Backscattering and tumble average cross section data for linear polarization are given in Fig. 31 and that for circular polarization in Fig. 32. The broadside aspect results in Fig. 31 are compared with Thiele's[54] piecewise uniform, point-matching solutions for tungsten wires.

A helix formed of a wire whose length, L, is slightly greater than the straight-wire resonant length, viz., L = 0.6λ, is considered next. In this case it is necessary to include the contributions of up to three modes, all of which are relatively small. The phase angles are given in Fig. 33 for the first two even modes and the first odd mode. With these modes the linear and circular polarization backscattering and tumble average cross section curves of Figs. 34 and 35 were calculated.

Finally, a one-turn helix with a wire length-to-diameter ratio L/2a = 100 and a pitch p = 10a is investigated as a function of frequency. The phase angles corresponding to the first four characteristic modes are shown in Fig. 36. Figures 37 and 38 give the backscattering cross sections at various fixed aspects, as well as the

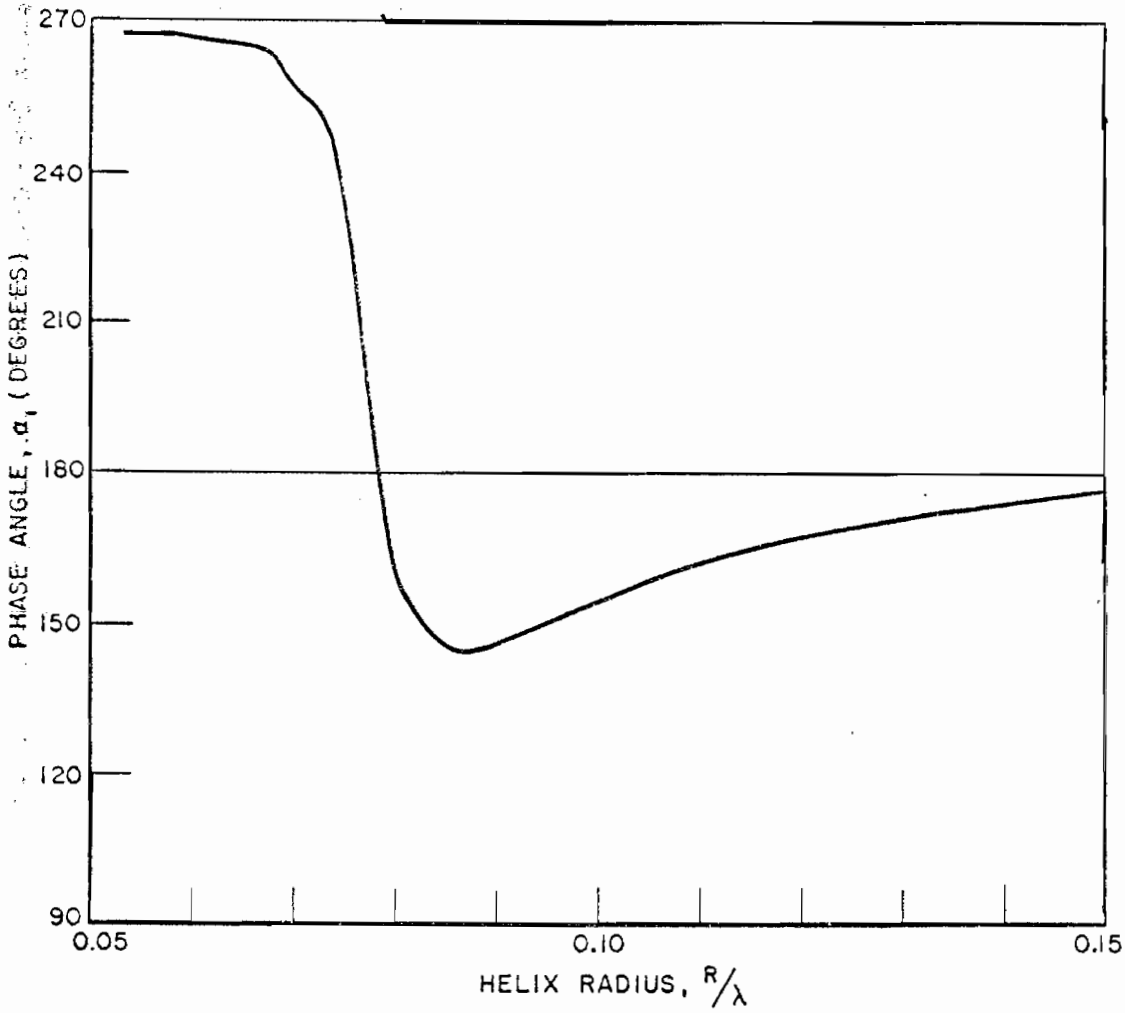

Fig. 30.--Phase angle α_1 for a helix with wire length L = 0.475λ, wire radius a = 0.0008467λ, and pitch p = 30a.

tumble average backscattering cross sections, for linear and circular polarizations, respectively. It is interesting to compare these results with those (Figs. 21 and 23) obtained for a straight wire of the same dimensions. A comparison is made in Fig. 39 of the tumble average cross sections of these configurations for linear-to-linear transmitter-receiver polarizations. Of particular interest, for

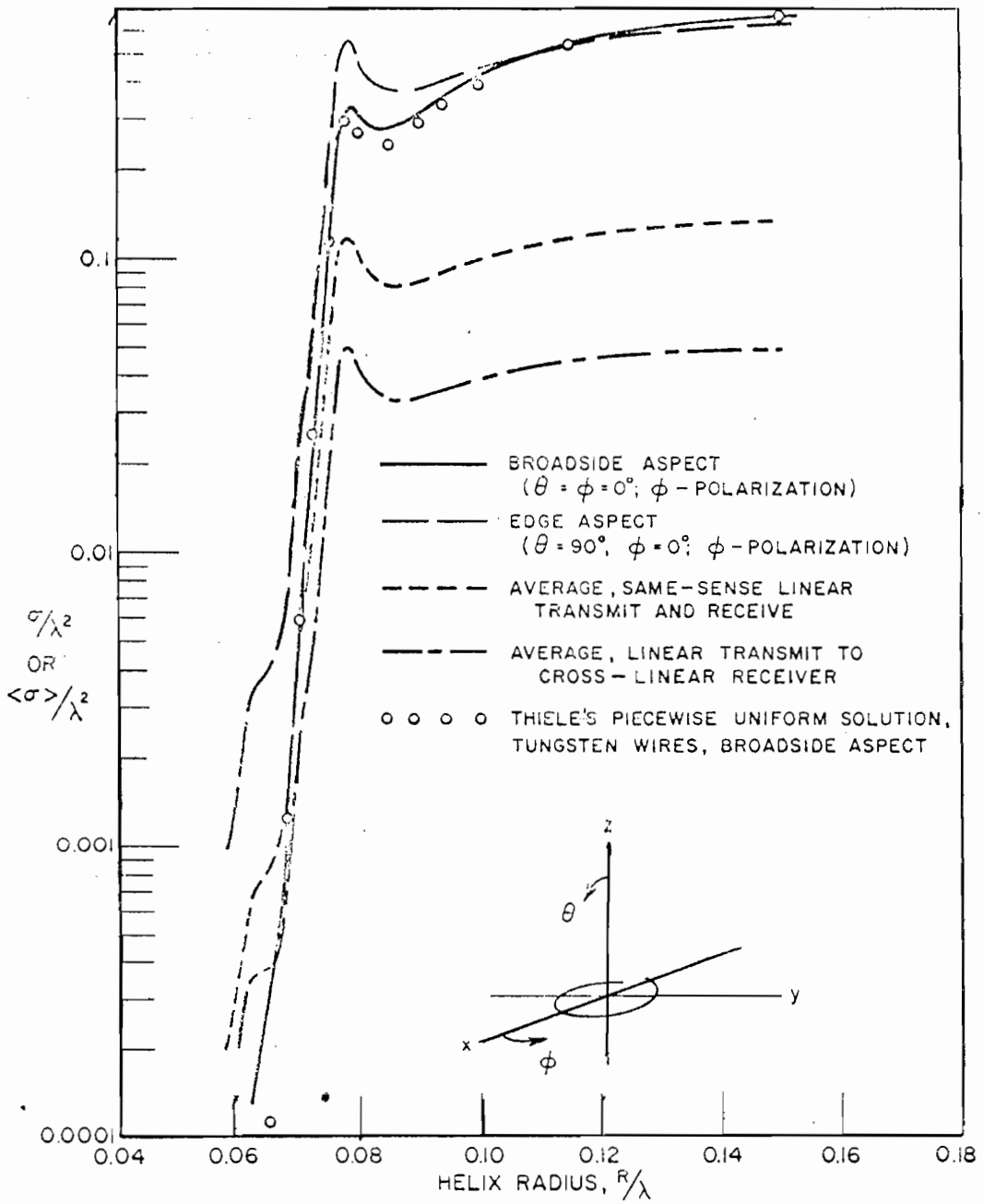

Fig. 31.--Backscattering and tumble average cross sections of a helix with L = 0.475λ, a = 0.0008467λ, and p = 30a for linear polarization.

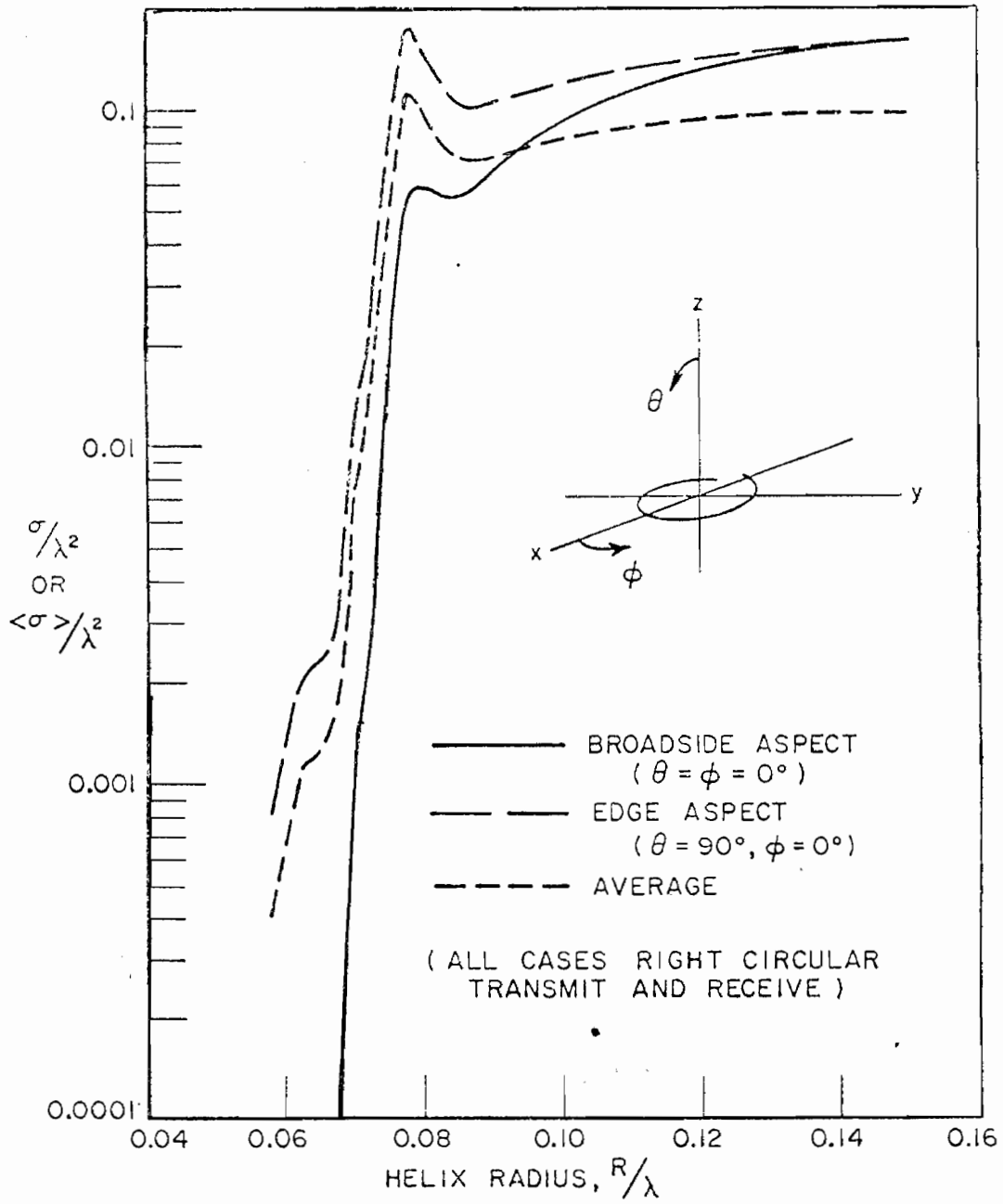

Fig. 32.--Backscattering and tumble average cross sections of a helix with L = 0.475λ, a = 0.0008467λ, and p = 30a for circular polarization.

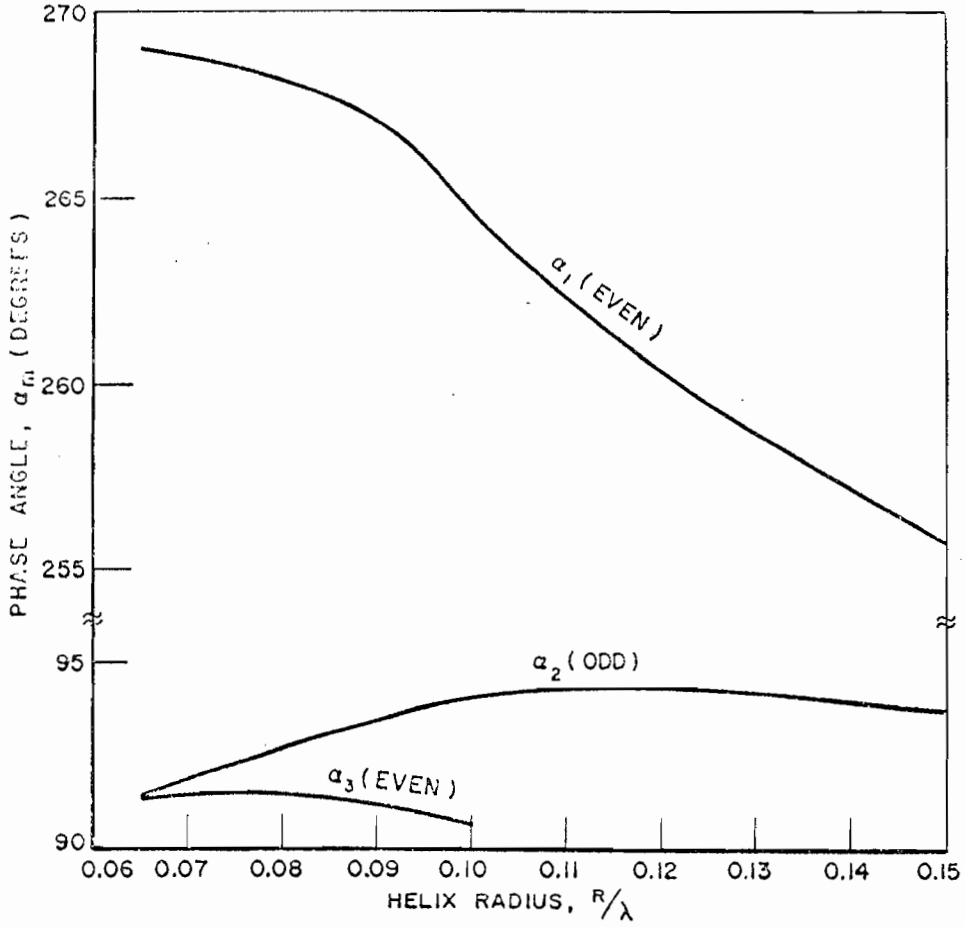

Fig. 33.--Phase angles α_m, m=1,2,3, for a helix with L = 0.6λ, a = 0.0008467λ, and p = 30a.

example, is the relation of the bandwidth of the first resonance to the slope of the corresponding phase angle curve for α_1 in the vicinity of 180°. The slope of the α_1-curve for the helix (Fig. 36) is noticeably greater than that for the straight wire (Fig. 21). The reduced bandwidth of the first resonance for the helix is evident in Fig. 39.

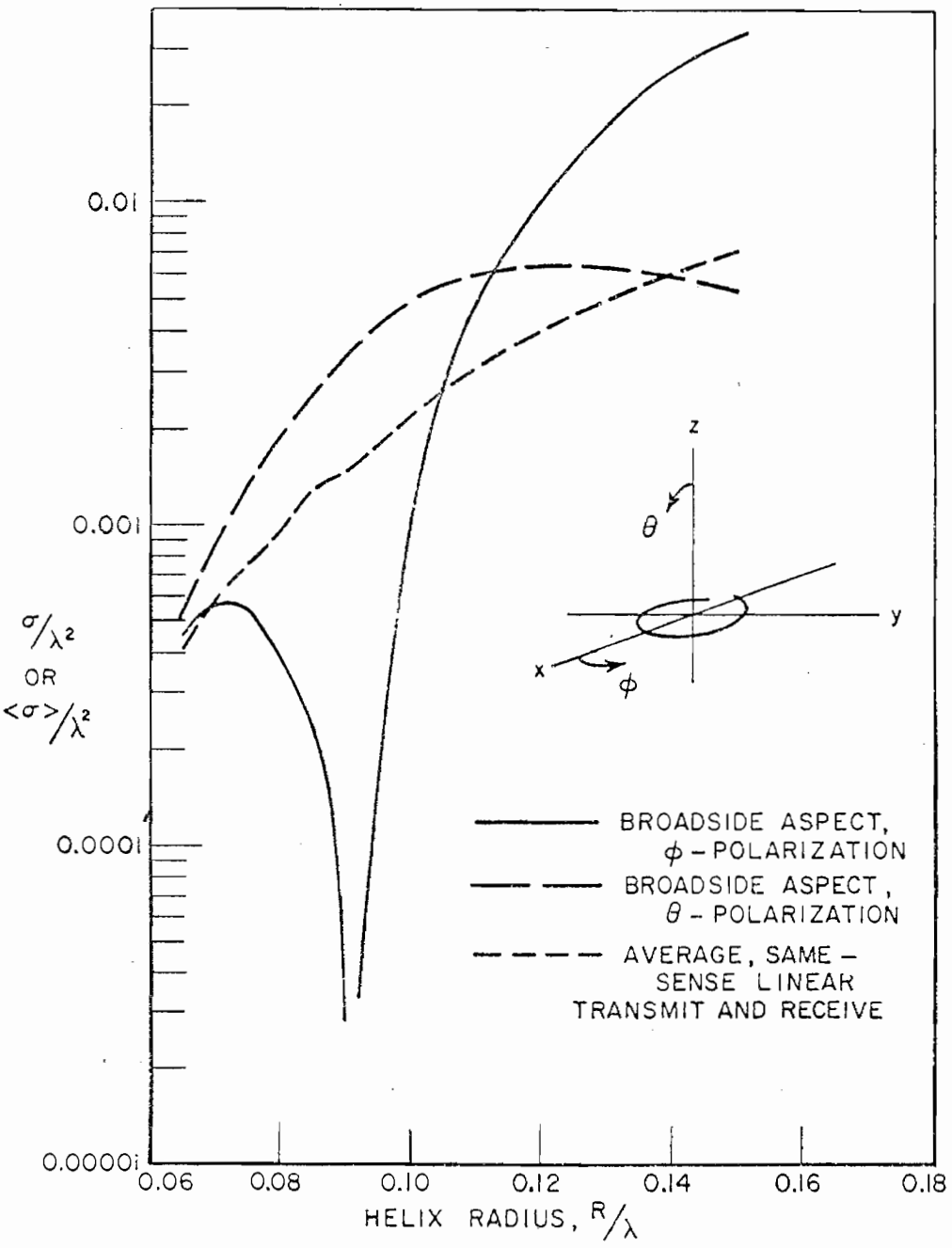

Fig. 34.--Backscattering and tumble average cross sections of a helix with L = 0.6λ, a = 0.0008467λ, and p = 30a for linear polarization.

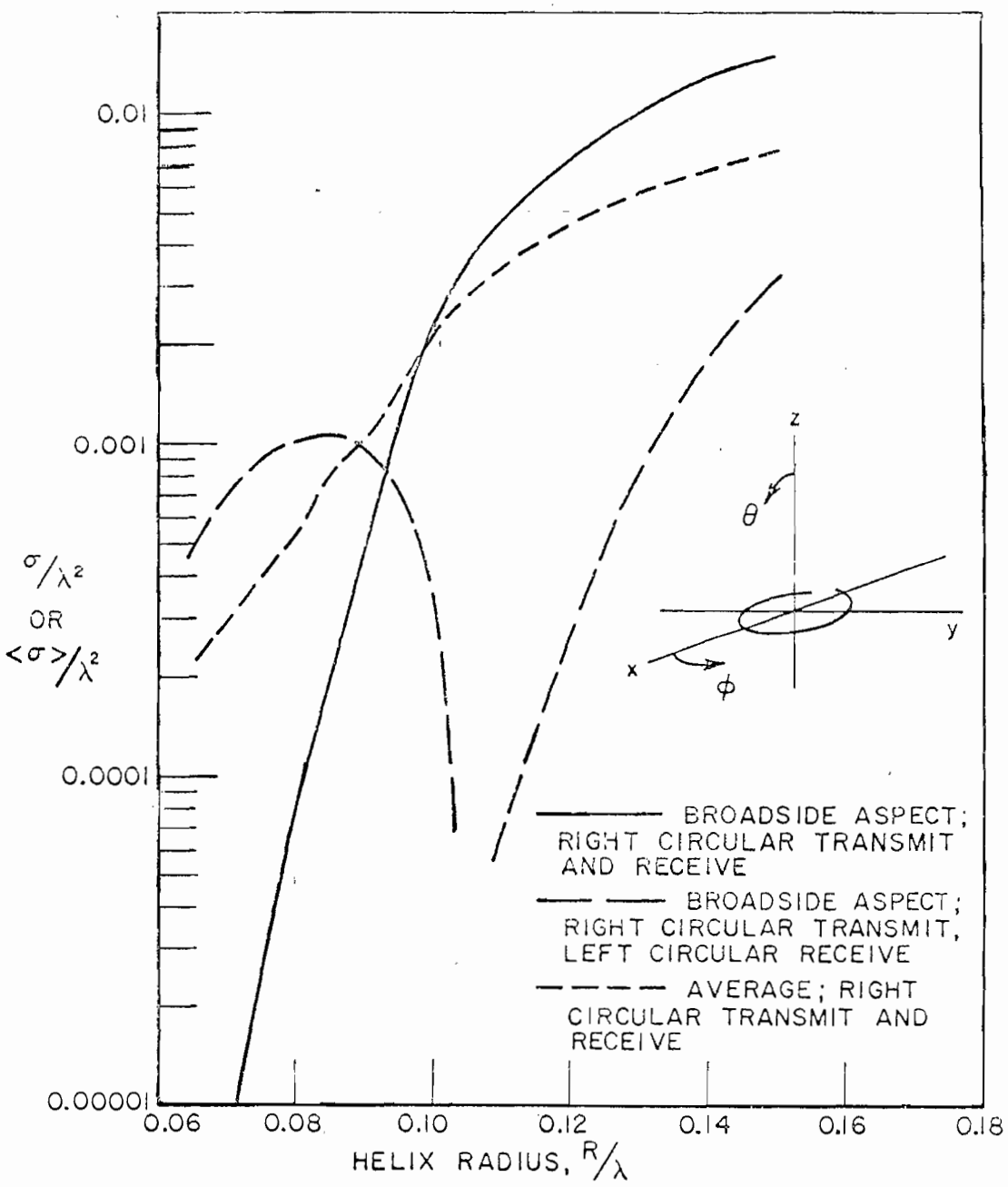

Fig. 35.--Backscattering and tumble average cross sections of a helix with $L = 0.6\lambda$, $a = 0.0008467\lambda$, and $p = 30a$ for circular polarization.

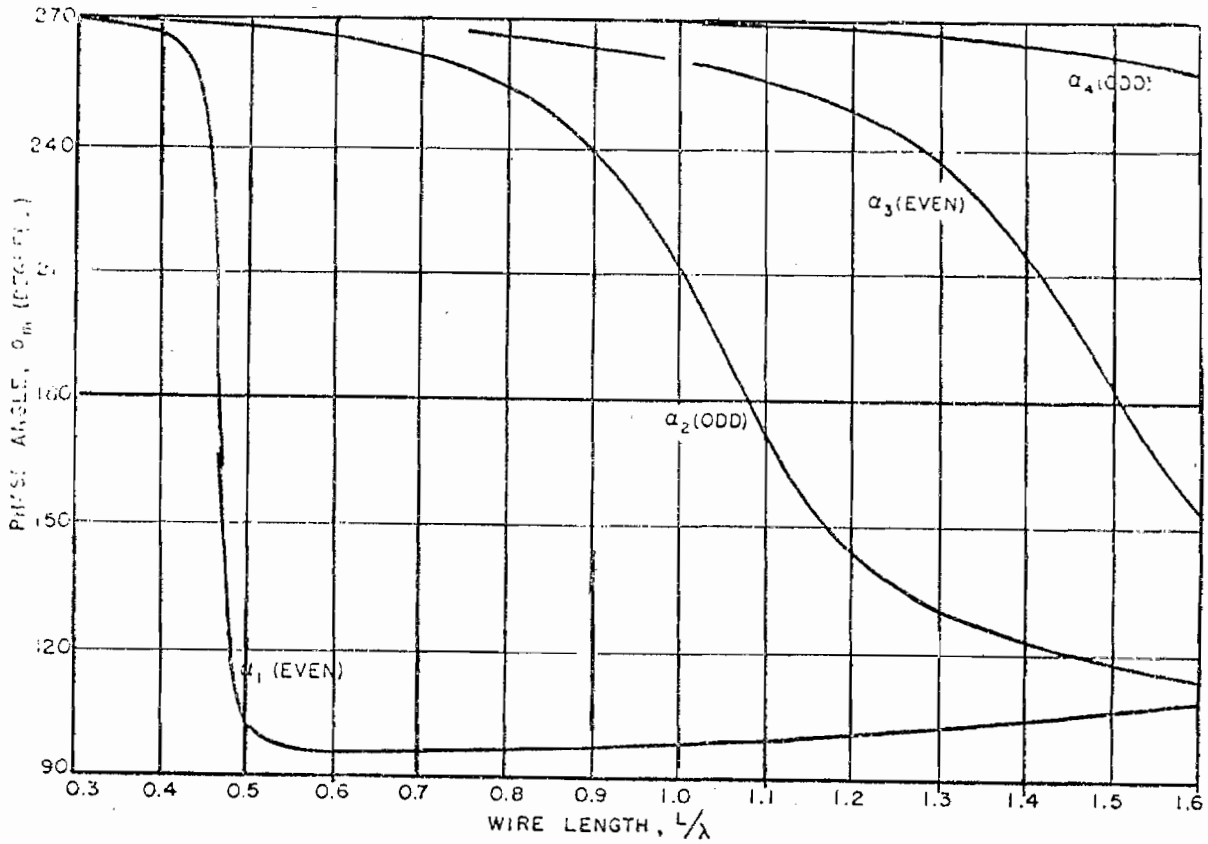

Fig. 36.--Phase angles α_m, m = 1,2,3,4, for a one-turn helix with wire length-to-diameter ratio L/2a = 100 and pitch p = 10a.

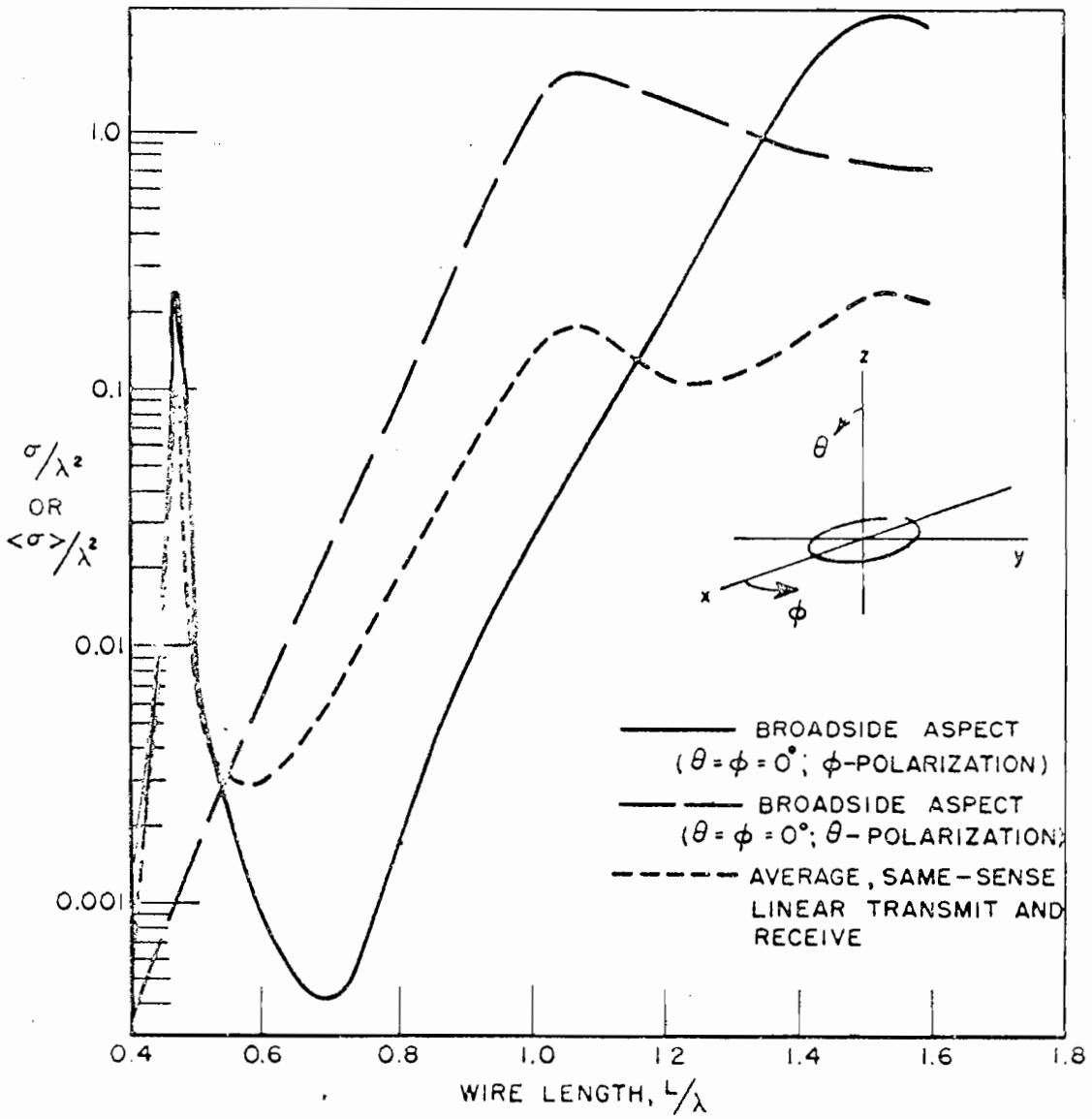

Fig. 37.--Backscattering and tumble average cross sections of a one-turn helix with L/2a = 100 and p = 10a for linear polarization.

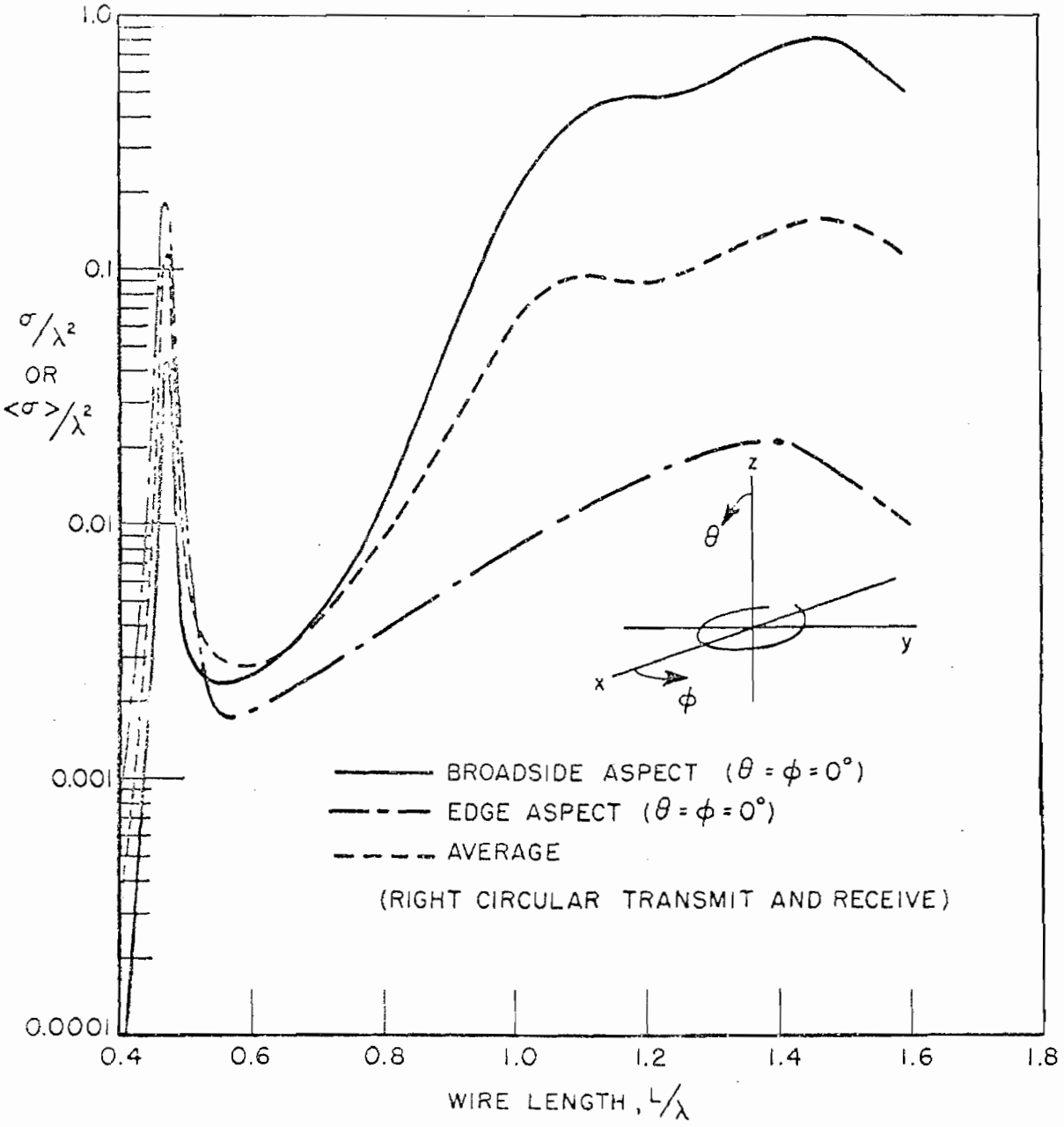

Fig. 38.--Backscattering and tumble average cross sections of a one-turn helix with L/2a = 100 and p = 10a for circular polarization.

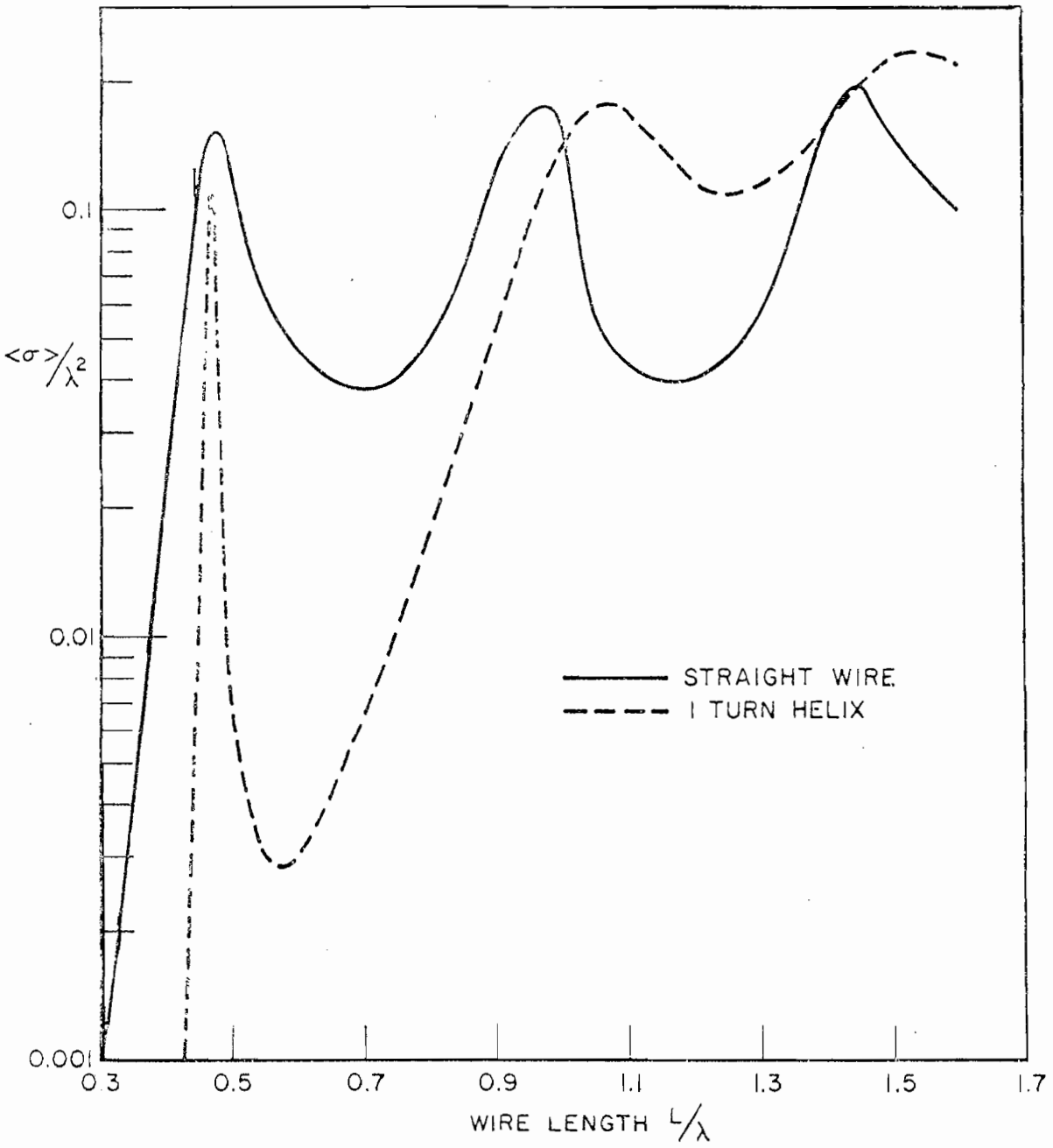

Fig. 39.--Comparison of tumble average cross sections of a straight wire and a one-turn helix, with wire length-to-diameter ratio L/2a = 100 and a helix pitch p = 10a.

CHAPTER IV
SUMMARY AND CONCLUSIONS

A numerical basis transformation is described which transforms the set of point-matching linear equations from one basis to another. It is shown that it is possible to reduce the number of linear equations needed for good accuracy and, as a result, to reduce computer solution time and storage requirements. For example, a transformation from the piecewise uniform basis to a basis of modal functions, such as cosines and sines, can reduce the number of equations, N, by a factor of 10 or more with a consequent reduction from a cubic to a square law dependence of solution time on N and at least a five-fold reduction in storage requirements. It is also shown that, following the basis transformation and the subsequent reduction from N to M equations, a least square solution is obtained. The transformation and least square techniques are applied to the solution of scattering by several thin wire objects. In particular, perfectly conducting elements in the shape of circular and elliptical loops, straight wires, and circular arcs are considered.

In the examples given here the basis transformation technique is applied only in transforming from the piecewise uniform basis to a modal basis. The technique can be employed equally well in con-

junction with other point-matching methods. It may also find application with numerical methods other than those based on point-matching. For example, the multi-segment induced emf technique,[11] a technique based on the reciprocity theorem and reaction concepts, could be combined with the basis transformation technique in the same manner as is discussed here. It should also be noted that the transformation and least square techniques are not restricted to perfectly conducting objects, although only loss-free scatterers are considered here.

Having shown the advantages afforded by a transformation of basis as applied to the solution of scattering by wires, other applications can be suggested. The point-matching technique has been applied[2,3] to bodies of revolution and to planar scatterers such as circular and rectangular plates. A basis transformation could significantly reduce the number of equations in such problems, a factor of particular importance for three-dimensional bodies. Also of interest are the application of the basis transformation and least square techniques to point-matching solutions of loaded wire scatterers and antennas and to multiple-wire scatterers such as coaxial loops.

Further application is made of the basis transformation and least square techniques to the determination of characteristic modes of loss-free, thin wires of general configuration. A method of determining characteristic mode current distributions and associated phase angles of thin wires is developed and is

applied to circular and elliptical loops, straight wires, circular arcs, and helices.

Explicit expressions are derived, in terms of the characteristic mode pattern functions, for backscattering and tumble average backscattering cross sections for arbitrary transmitter and receiver polarizations. The characteristic modes derived for the aforementioned objects are then used to compute backscattering and tumble average cross section data for the respective shapes. Also computed for heuristic purposes are input admittance data for circular loops. Where possible, the results are compared with solutions derived by independent methods.

The examples given in the preceding discussion serve to demonstrate the determination and the application of characteristic modes for the solution of scattering by wire objects. Of particular interest is the usefulness of the characteristic mode approach in calculating the tumble average cross section. Application of the method to other single-wire configurations would be of interest. The method could also be extended to multiple-wire scatterers, such as coaxial wire loops, and to wires with sharp bends and/or lumped loads. At the present time, however, the characteristic mode method is limited in a practical sense to objects for which a small number of modes, say, less than four or five, accurately describe the scattering properties.

APPENDIX A

THE LEAST SQUARE SOLUTION OF A SET OF N LINEAR COMPLEX EQUATIONS IN M UNKNOWNS, WITH $M \leq N$

The least square solution of a set of N equations,

$$(83) \qquad \sum_{j=1}^{M} Z_{ij} I_j = E_i, \quad i = 1,2,\cdots,N; \quad M \leq N,$$

is one which minimizes the quantity

$$(84) \qquad S = \sum_{i=1}^{N} [E_i - \sum_{j=1}^{M} Z_{ij} I_j] [E_i - \sum_{j=1}^{M} Z_{ij} I_j]^c,$$

where c denotes the complex conjugate. To find a minimum in S consider its first derivative with respect to each I_k, $k = 1,2,\cdots,M$, i.e.,

$$(85) \qquad \frac{\partial S}{\partial I_k} = - \sum_{i=1}^{N} \{Z_{ik}[E_i - \sum_{j=1}^{M} Z_{ij} I_j]^c + Z_{ik}^c [E_i - \sum_{j=1}^{M} Z_{ij} I_j]\} ,$$

$$k = 1, 2, \ldots, M.$$

Setting $\partial S/\partial I_k = 0$ for a minimum in S, Eq. (85) yields

$$(86) \qquad \text{Re} \{\sum_{i=1}^{N} Z_{ik}^c [E_i - \sum_{j=1}^{M} Z_{ij} I_j]\} = 0, \quad k = 1, 2, \ldots, M.$$

The matrix equivalent to Eq. (86) is

$$(87) \qquad \text{Re}\{[Z]^*[Z](I)\} = \text{Re}\{[Z]^*(E)\} ,$$

where the superscript * denotes the complex conjugate transpose and the brackets [] and parenthesis ( ) denote matrices and column vectors, respectively.

Returning to Eq. (85), we may also satisfy the condition $\partial S/\partial I_k = 0$ by setting each of the right hand terms equal to zero, i.e.,

$$(88) \qquad \sum_{i=1}^{N} Z_{ik}\left[E_i - \sum_{j=1}^{M} Z_{ij}\, I_j\right]^c = 0, \quad k = 1,2,\cdots,M,$$

and

$$(89) \qquad \sum_{i=1}^{N} Z_{ik}^c \left[E_i - \sum_{j=1}^{M} Z_{ij} I_j\right] = 0, \quad k = 1,2,\ldots,M.$$

Equation (88) is merely the complex conjugate of Eq. (89). The matrix equivalent to these equations is seen to be

$$(90) \qquad [Z]^*[Z]\ (I) = [Z]^*\ (E).$$

The solution of either Eq. (87) or Eq. (90) is a least square solution of the set of equations given in Eq. (83).

APPENDIX B
PIECEWISE UNIFORM IMPEDANCE MATRIX ELEMENTS[1-3]

The thin-wire scatterers considered in this treatise are approximated in each case by a number (N) of short, straight-wire segments. The elementary scatterer to be considered under the piecewise uniform approximation is then a short slender wire with a uniform current density on its surface.

Consider a perfectly conducting wire segment of length s and radius a to have a harmonic electric current induced uniformly over its surface. Let the axis of the wire coincide with the z axis and let the center of the wire be the coordinate origin. If the current density is $\underline{J} = \hat{z}\, J$, where J is a constant and $\hat{z}$ denotes a unit vector parallel with the z-axis, the current in amperes is given by

$$I = 2\pi a J. \tag{91}$$

In general, the free-space field of this source is expressed as a surface integral over the surface of the wire. In our application, however, the general expressions simplify as follows

$$E_\rho(\rho,\phi,z) = \frac{\rho I\sqrt{\mu/\varepsilon}}{4\pi jk}\,(1 + jkr)\,\frac{e^{-jkr}}{r}\Bigg|_{r_1}^{r_2}, \tag{92}$$

$$E_\phi(\rho,\phi,z) = 0, \tag{93}$$

and

$$(94) \qquad E_z(\rho,\phi,z) = \frac{I\sqrt{\mu/\varepsilon}}{4\pi jk} \int_{-s/2}^{s/2} [2r^2(1+jkr) - (\rho^2 + a^2)(3 + 3jkr - k^2r^2)] \frac{e^{-jkr}}{r^5} \, dt,$$

where ρ, ϕ, and z are the cylindrical coordinates of the observation point,

$$(95) \qquad k = \omega\sqrt{\mu\varepsilon} \quad ,$$

$$(96) \qquad r = \sqrt{\rho^2 + a^2 + (z - t)^2} \quad ,$$

$$(97) \qquad r_1 = \sqrt{\rho^2 + a^2 + (z + s/2)^2},$$

and

$$(98) \qquad r_2 = \sqrt{\rho^2 + a^2 + (z - s/2)^2}.$$

These expressions for the field are accurate if $\rho = 0$ or if r_1^2 and r_2^2 are large in comparison with the quantity $a\rho$. Equations (92) through (98) may be used to calculate the impedance matrix elements

$$(99) \qquad Z_{ij} = \frac{E_{ij}^T}{I_j}$$

where E_{ij}^T is the component of the field at the center of and tangential to wire segment i due to a unit current $I_j = 1$ on segment j.

APPENDIX C
COMPUTER PROGRAMS

The data given in the body of this treatise and in Appendix D were computed by means of the main programs and subprograms listed in Table 4. Statement listings are given in Figs. 43 through 58. All programming was done in the Fortran IV language, Version 13, for the Ohio State University IBM 7094 IBSYS Operating System. A brief discussion of each program and subprogram is given here.

A. Main Programs

(1) MAIN1

The main program MAIN1 derives the backscattering cross section by application of the basis transformation technique. The program receives the transformed impedance matrix $[Z_a']$ from the subroutine SUB2(b) and performs the multiplication $[Z_a']^*$ $[Z_a']$ of Eq. (11). The Crout reduction procedure which follows is interrupted following statement 118 in order to specify the desired angles of incidence and the polarization state of the incident plane wave. The tangential components of the incident electric field are calculated and are multiplied by $[Z_a']^*$. The Crout routine is then completed yielding a least square solution for the current on the scatterer in the form of coefficients of a series expansion in terms of the new basis functions. Finally,

TABLE 4

COMPUTER PROGRAMS AND SUBPROGRAMS

Program or Subprogram	Description	Figure
MAIN1	Backscattering cross section by the basis transformation technique	43
MAIN2	Backscattering cross section by the piecewise uniform method	44
MAIN3	Determination of characteristic modes of wires	45
MAIN4	Backscattering and tumble average cross sections of wires using characteristic modes	46
SUB1	Wire geometry subroutines	
	(a) circular and elliptical loops	47
	(b) straight wires, circular arcs and helices	48
SUB2	Impedance matrix subroutines	
	(a) piecewise uniform; circular loops, circular arcs, straight wires, and helices	49
	(b) piecewise uniform with basis transformations; circular loops, circular arcs, straight wires, and helices	50
	(c) piecewise uniform with basis transformation; elliptical loops	51
SUB3	Basis function subroutines	
	(a) sine and cosine functions for closed loops	52
	(b) sine and cosine functions for wires of open configuration	53
	(c) Chebyshev polynomials of the second kind	54
SUB4	Subroutine for locating $\varepsilon_{min}(\alpha_m)$	55
SUB5	Subroutine for computing $[B(\alpha)]$	56
SUB6	Subroutine for computing eigenvalues and eigenvectors of $[B(\alpha)]$	57
SUB7	Subroutine for averaging $\sigma(\theta,\phi)$ over θ and ϕ	58

the theta- and phi-polarized and total backscattering cross sections, EAT, EAP, and EA, respectively, are computed.

(2) MAIN2

The second main program, MAIN2, is similar to MAIN1 with the exception that a piecewise uniform impedance matrix is returned by SUB2(a), multiplication by the complex transpose of the impedance matrix is deleted, and the Crout reduction yields a piecewise uniform approximation to the induced current.

(3) MAIN3

The main program, MAIN3, for determining the characteristic modes of wires follows the steps outlined here. The number of separate cases is specified by the parameter NRUNS. The wire geometry for each case is calculated by the appropriate subroutine SUB1(a) or (b). Having established the wire geometry, the impedance matrix [Z] of Eq. (22) is obtained by a call to SUB2(b) or (c). The main program next proceeds to determine the phase angles α_m and the associated characteristic current distributions, finding first the even and then the odd modes. The P, Q, and R matrices of Eqs. (35)-(37) are derived from [Z]. Data cards then specify the number (NMODES) of modes to be found, the maximum number (NTRY) of "tries" to be made in seeking α_m, an estimate (ALP) of α_m (ALP = α_m - 180^o), the initial step size (ASTEP) to be used in searching for α_m and a lower limit (ERROR) in the step size. The parameters ALP, ASTEP, and ERROR are in degrees. A new estimate for α_m is computed by the subroutines SUB4 (ANULL),

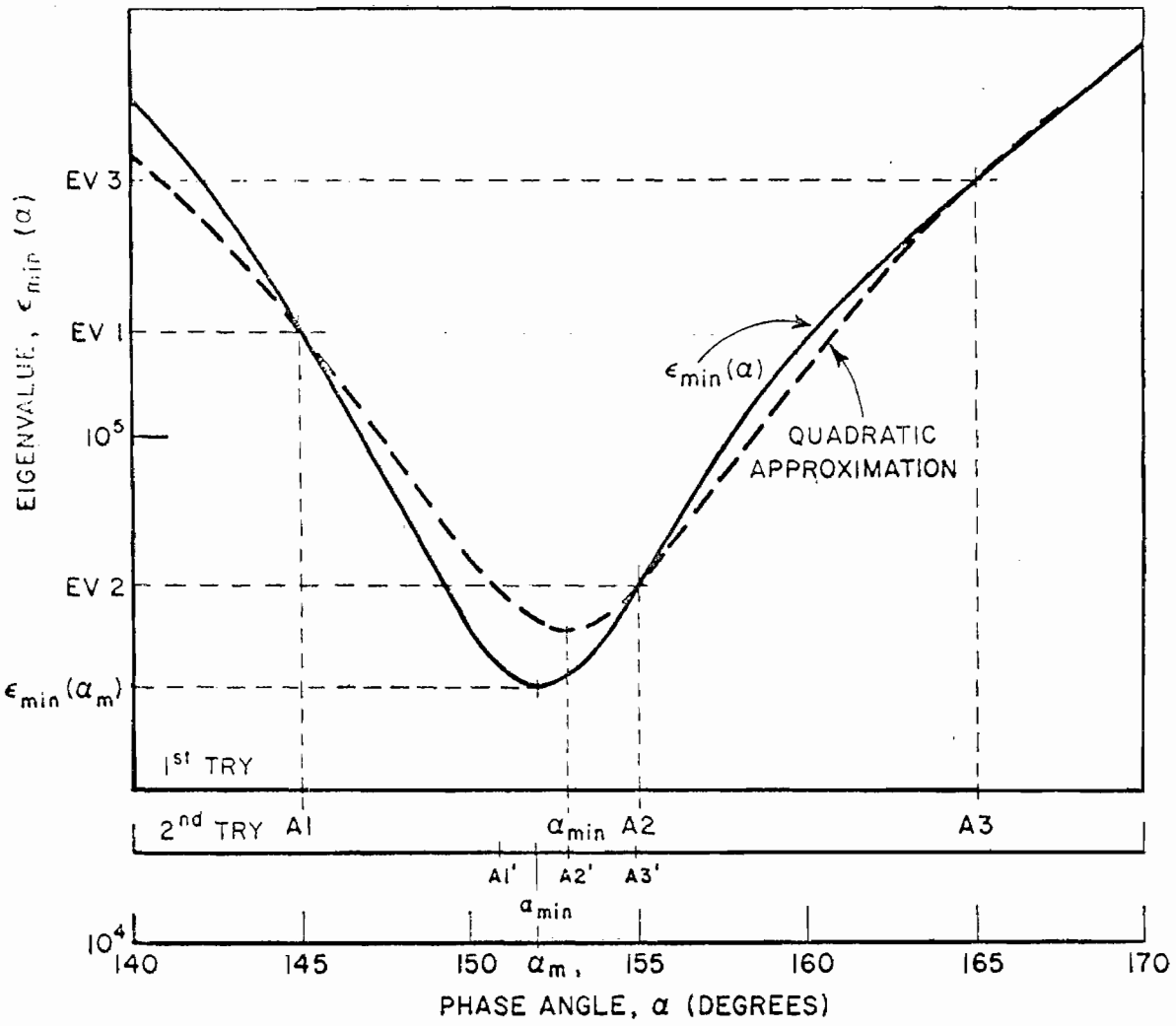

Fig. 40.--Computer method for locating α_m corresponding to the relative minimum $\varepsilon_{min}(\alpha) = \varepsilon_{min}(\alpha_m)$.

SUB5 (EGNVLU), and SUB6 (MATEIG). To do this the minimum eigenvalue $\varepsilon_{min}(\alpha)$ is computed for each of three values of α, i.e., for A1=A2-ASTEP, A2, and A3=A2+ASTEP. SUB4 calculates the angle α_{min} corresponding to the minimum of the quadratic curve defined by the three points (see Fig. 40). If no minimum is found for A1 < α < A3,

i.e., if the first derivative is non-zero or if the second derivative is negative in this region, either A1 or A3, whichever corresponds to the smaller minimum eigenvalue $\varepsilon_{min}(\alpha)$ (denoted by EV1 and EV3, respectively), becomes the new estimate of α_m and is assigned to "A2". If a minimum in $\varepsilon_{min}(\alpha)$ is found within the limits A1 < α < A3, the step size ASTEP is reduced and the process is repeated (up to NTRY times or until ASTEP $\leq$ ERROR), taking as the new "A2" the angle α_{min}. In this manner the relative minima $\varepsilon_{min}(\alpha_m)$ are located, thereby specifying the phase angles α_m and allowing the determination of the corresponding eigenvalues (I_m).

When either NTRY attempts have been made to locate α_m or the specified error limit (ERROR) has been achieved, the eigenvector (I_m) associated with the last estimate of α_m is obtained by a final call to SUB5 and thence to SUB6. The current distribution CUR (I_m), represented by the eigenvector coefficients EF ((I_m)), is then normalized to radiate unit power and the resultant normalized vector (I_m), along with the angle α_m, specify the m^{th} characteristic mode for the given obstacle.

An example set of input data is shown in Fig. 41 for a straight wire of length 1.0λ and radius 0.005λ.

(4) MAIN4

The main program MAIN4, which calculates the backscattering cross sections of an object using its characteristic modes, assumes that a significant number of characteristic mode current distributions are known for the given obstacle; that each mode is specified by the

coefficients of a Fourier series expansion in terms of predetermined basis functions and has been normalized to radiate unit power; and that the characteristic value $a_m = |\cos \alpha_m| e^{j\alpha_m}$ corresponding to each current distribution is known and is specified by the phase angle α_m, $\pi/2 < \alpha_m < 3\pi/2$.

```
$DATA
    1
  150
       1.0          1.0          0.0
     0.005
    6     5
    1
        3.0
    0     1
    2
   10
     -65.0          2.0          0.01
   10
      89.0          0.2          0.01
    1
   10
     -30.0          5.0          0.01
```

Fig. 41.--Example data for determining characteristic modes (two even and one odd) of a straight wire with length SL = 1.0λ and radius AL = 0.005λ.

After establishing the wire geometry by a call to SUB1(a) or (b) and the appropriate basis functions by a call to SUB3(a), (b), or (c), the main program reads the parameters PH and TH, which determine the limits on the integrations over phi and theta, and IPH and ITH, which specify the number of points in phi and theta in the integrations as well as the angles of incidence for which

backscattering cross section data are calculated. For wires such as straight wires and circular loops, whose scattering is independent of phi and is symmetric in theta, PH=0^{o} and TH=90^{o} are sufficient. Ellipses require PH=90^{o} and TH=90^{o}, circular arcs, PH=180^{o} and TH=90^{o}, and helices PH=180^{o} and TH=180^{o} or PH=360^{o} and TH=90^{o}.

The matrix [F], corresponding to the dyadic pattern function $\underline{\underline{F}}$ of Eq. (20), is derived in the steps through statement 500. The backscattering cross sections for the various linear and circular polarizations are then computed. In calculating the average backscattering cross section, the expressions $|F_{\theta\theta}|^2$, $|F_{\phi\phi}|^2$, $|F_{\theta\phi}|^2$, $\mathrm{Re}\{F_{\theta\theta}F_{\phi\phi}^{c}\}$, and $\mathrm{Im}\{(F_{\theta\theta}-F_{\phi\phi})F_{\theta\phi}^{c}\}$ are averaged separately. The tumble average cross sections are then formed by taking weighted combinations of these terms. The averaging over theta and phi is accomplished through a call to SUB7 (DBLINT).

An example set of input data is shown in Fig. 42 for a straight wire of length 1.0λ and radius 0.005λ.

B. Subprograms

(1) SUB1

The geometries of the various wire configurations were computed by one of two subroutines (WGRID) given in Figs. 47 and 48. The wires were represented by N straight-wire segments. The subroutines derive the x, y, and z coordinates of the center of each wire segment along with orientation angles β, the angle of rotation from the positive x-axis, and α, the angle out of the xy plane (α is

```
$DATA
    1
ST. WIRE     L/2R=100, L=1.0, N=150, MC=6, MS=5
  150
       1.0         1.0         0.0
    6    5
       0.0        90.0
    1   19
    2 EVEN     1  ODD
 .47249991E-01-0.19534167E-01 0.29270693E-02-0.24203868E-03
-0.70622786E-06-0.88828724E-05
   -113.71
 0.86228860E-03 0.13700993E 00-0.81425030E-01 0.69759121E-02
-0.81651063E-03-0.31331514E-03
   -91.57
 0.63192100E-01-0.34586068E-01 0.40849968E-02-0.36569813E-03
-0.76321271E-04
    147.70
```

Fig. 42.--Example data set for computing backscattering and tumble average cross section data for a straight wire with length SL = 1.0λ and radius AL = 0.005λ using two even and one odd characteristic modes.

considered positive if the segment is tilted toward the negative z-axis).

The subroutine of Fig. 47 generates circular and elliptical loops according to the expression

$$R(\phi) = \sqrt{\frac{A_1^2 \cdot A_2^2}{A_1^2 \sin^2 \phi + A_2^2 \cos^2 \phi}} \qquad (100)$$

In the subroutine, α = CAB and β = SAB.

Helices, straight wires, and circular arcs are generated by the subroutines of Fig. 48. The wire length is SL, the helix pitch (distance between turns) is S, and R is the helix radius. The helix is symmetric in ϕ about the positive x-axis and symmetric in z about z = 0. For a straight wire SL = S and R = 0. For

circular arcs S = 0 and R is the arc radius with SL being the arc length.

(3) SUB2

Each of the impedance matrix subroutines (ZMAT), Figs. 49, 50, and 51, are based on the piecewise uniform method formulated and programmed by Richmond.[1-3]

The program given in Fig. 49 computes the elements C(I,J) of an N x N piecewise uniform impedance matrix. Due to the symmetric geometry of the wires considered it was necessary to calculate only the first row of the matrix. The portion of the matrix on and above the main diagonal is completed by noting that $C_{i+1,j+1} = C_{ij}$, i.e., all elements on a given diagonal are equal. Finally, the elements below the main diagonal are set equal to their transpose since the matrix is symmetric.

The program shown in Fig. 50 is identical to that of Fig. 49 except that the impedance matrix is transformed from the piecewise uniform basis to the basis derived by a subroutine call to SUB3 (a) or (b). The piecewise uniform impedance matrix elements C are computed one at a time while forming the new impedance matrix elements CC(I,J). The resulting matrix is N x M in dimension ($M \leq N$), where N is the number of match points and M is the number of modes retained in the new basis.

For the elliptical geometries the symmetries assumed in SUB2 (a) and (b) are not valid. The impedance matrix subroutine SUB2 (c) written for elliptical wires takes into account the more limited

symmetries of the ellipse. In all other respects SUB2 (c) is identical to SUB2 (b).

(3) SUB3

The programs given in Figs. 52, 53, and 54 generate basis functions and form the transformation matrix [T] of Eq. (3) when called by SUB2 (b) or (c). The first, Fig. 52, computes sine and cosine functions suitable as a basis for the Fourier expansion of the current induced on closed wire loops. The modes are defined by

$$\left.\begin{aligned} (101)\qquad AJ(J,K) &= \cos\frac{2\pi(K-1)SLJ}{SL}\ ,\ K = 1,2,\cdots,MC \\ (102)\qquad AJ(J,MC+K) &= \sin\frac{2\pi K\, SLJ}{SL}\ ,\ K = 1,2,\cdots,MS \end{aligned}\right\}\quad J=1,2,\cdots,N.$$

where AJ(J,K) is an element of the transformation matrix, SL is the wire length in wavelengths, MC is the number of cosine modes, MS is the number of sine modes, and SLJ is the location of the J^{th} match point along the center-line of the wire.

The subroutine shown in Fig. 53 derives a transformation matrix similar to that just described but for wires of open configuration. The matrix elements are, in this case,

$$\left.\begin{aligned} (103)\quad AJ(J,K) &= \cos\frac{\pi(K-1)SLJ}{SL}\ ,\ K=1,2,\cdots,MC \\ (104)\quad AJ(J,MC+K) &= \sin\frac{\pi K\, SLJ}{SL}\ ,\ K=1,2,\cdots,MS \end{aligned}\right\}\quad J = 1,2,\cdots,N.$$

The Chebyshev polynomial basis functions are computed by the subroutine given in Fig. 54. The elements of the transformation matrix are

$$\left.\begin{aligned}(105)\quad AJ(J,K) &= \frac{\sin((2K-1)\cos^{-1}(2SLJ/SL))}{\sin(\cos^{-1}(2SLJ/SL))}, \quad K=1,2,\ldots,MC \\ (106)\quad AJ(J,MC+K) &= \frac{\sin((2K\cos^{-1}(2SLJ/SL))}{\sin(\cos^{-1}(2SLJ/SL))}, \quad K=1,2,\ldots,MS\end{aligned}\right\} J=1,2,\ldots,N.$$

(4) SUB4

The subroutine SUB4 (ANULL) receives three values for α (A1, A2, and A3) from MAIN3, obtains the corresponding minimum eigenvalues $\varepsilon_{min}(\alpha)$ (EV1, EV2, and EV3) from SUB5, then fits a quadratic equation to these three points (see Fig. 40) to estimate α_m, the phase angle associated with a relative minimum $\varepsilon_{min}(\alpha) = \varepsilon_{min}(\alpha_m)$.

(5) SUB 5

Given an angle α (ALP) and the matrices [P], [Q], and [R], the subroutine SUB5 derives the matrix $[B(\alpha)]$ according to Eq. (38).

(6) SUB6

The subroutine SUB6 computes the eigenvalues and eigenvectors of $[B(\alpha)]$.

(7) SUB7

The subroutine SUB7 uses Simpson's rule integration in performing a double integration of the function S over theta and phi. The limits of integration are 0 to PH on phi and 0 to TH on theta using NP points in phi and NT points in theta. If PH = 0, a single integration on theta is performed.

```
$EXECUTE        IBJOB
$IBJOB          GO
$IBFTC MAIN1    NODECK
      COMMON X(250),Y(250),Z(250),CAB(250),SAB(250)/SIZE/SI(250)
      COMMON /COEF/CC(250,20),SALP(250)/CURR/AJ(250,20)
      COMPLEX QU,PNN,EINC
      COMPLEX EXPA(250),EI(250),A(20),CC,PN,EP,ET,F
      DIMENSION P(250),Q(250)
      DOUBLE PRECISION AR(20,21),AI(20,21),R1,R2,R3,AI1,AI2,AI3
    1 FORMAT (1H ,12X,4HREAL,14X,5HIMAG,,13X,4HMAG,,13X,5HPHASE/4X,
     2     1P4E18.7)
    2 FORMAT (10H0ECHO AREA//,5X,10HTHETA POL,,E16.8,5X,8HPHI POL,,
     2     E16.8,8X,5HTOTAL,E16.8//)
    3 FORMAT (21H1CURRENT COEFFICIENTS,/(1P2E15.7))
    4 FORMAT (8H0CURRENT,/8H ELEMENT,8X,4HREAL,16X,5HIMAG,,15X,
     2     4HMAG,,13X,5HPHASE,/)
    5 FORMAT (10H0FAR FIELD//, 5X,10HTHETA POL,)
    6 FORMAT (I5,3E20.8,F13.5)
    7 FORMAT(7F10.5)
    8 FORMAT(14I5)
    9 FORMAT (1H0, 5X,8HPHI POL,)
   10 FORMAT (//,36H0ERROR IN E-FIELD AT MATCHING POINTS  //,12X,
     2     10HINC, FIELD,24X,11HSCAT, FIELD,31X,11HTOTAL FIELD)
   11 FORMAT (1H0,3E15.8)
   12 FORMAT (1H ,8E15.6)
   13 FORMAT(16H1FIRST AND LAST ,I2,3H OF,I4,79H EQUATIONS IGNORED TO RE
     2DUCE EFFECT OF WIRE ENDS ON LEAST SQUARES SOLUTION FOR ,I2,10H UNK
     2NOWNS.//34H WIRE SEGMENT LENGTH (WIRE RADII)=,F7.4//)
   70 FORMAT (30H1ANGLE OF INCIDENCE      THETA=,F7.3,7H   PHI=,F7.3,
     2     10X,12HPOLARIZATION,5X,4HETH=,F5.2,5X,4HEPH=,F5.2/)
      ZZ=376.72727
      TD=57.29578
      TA=.01745329
      PI=3.1415926
      TP=6.2831853
      CNSNT=4.*PI
      READ (5,8) NRUNS
      DO 1000 NRUN=1,NRUNS
      CALL WGRID (N)
      CALL ZMAT(B,MC,MS,N)
      M=MC+MS
      SIWL=SI(1)/B
      MM=M+1
C     FORM SQUARE, COMPLEX SYMMETRIC MATRIX BY MULTIPLYING
C          ((CC)COMPLEX TRANSPOSE)*(CC)
      READ (5,8) NTEST
      DO 1000 NT=1,NTEST
      READ (5,7) RADII
      NIGNOR=RADII/SIWL+.5
      WRITE (6,13) NIGNOR,N,M,SIWL
      N1=NIGNOR+1
      N2=N-NIGNOR
      DO 50 I=1,M
      DO 50 J=I,M
      R3=0.
      AI3=0.
      DO 40 K=N1,N2
      R1=REAL(CC(K,I))
      AI1=AIMAG(CC(K,I))
      R2=REAL(CC(K,J))
      AI2=AIMAG(CC(K,J))
      R3=R3+R1*R2+AI1*AI2
   40 AI3=AI3+R1*AI2-AI1*R2
      AR(I,J)=R3
```

Fig. 43.--Main program for the basis transformation method.

```
      AI(I,J)=AI3
      AR(J,I)=R3
   50 AI(J,I)=-AI3
C     START CROUT REDUCTION
C     CROUT METHOD FOR COMPLEX SYMMETRIC MATRIX
      DO 118 L=1,M
      LL=L-1
      DO 118 I=L,M
      IF(LLL.EQ.0) GO TO 1171
      DO 117 K=1,LLL
      R1=AR(L,K)
      R2=AR(K,I)
      AI1=AI(L,K)
      AI2=AI(K,I)
      AR(L,I)=AR(L,I)-R1*R2+AI1*AI2
  117 AI(L,I)=AI(L,I)-R1*AI2-AI1*R2
 1171 CONTINUE
      LMI=L-I
      IF(LMI) 105,118,105
  105 AR(I,L)=AR(L,I)
      AI(I,L)=-AI(L,I)
      R2=AR(L,L)
      AR(L,I)=AR(L,I)/R2
      AI(L,I)=AI(L,I)/R2
  118 CONTINUE
C     COMPUTE INCIDENT E-FIELD AND MULTIPLY BY ((CC)COMPLEX TRANSPOSE)
C          TO OBTAIN EQUALS COLUMN.
      READ (5,7) THETI,THETF,DTHETA,PHII,PHIF,DPHI,ETH,EPH
      ITH=(THETF-THETI)/DTHETA+1.1
      IPH=(PHIF-PHII)/DPHI+1.1
      PHI=PHII
      DO 300 IP=1,IPH
      PH=TA*PHI
      CPHI=COS(PH)
      SPHI=SIN(PH)
      THETA=THETI
      DO 250 IT=1,ITH
      TTA=TA*THETA
      CTHET=COS(TTA)
      STHET=SIN(TTA)
      STCP=STHET*CPHI
      STSP=STHET*SPHI
      CTCP=CTHET*CPHI
      CTSP=CTHET*SPHI
      DO 850 I=1,N
      ARG=X(I)*STCP+Y(I)*STSP+Z(I)*CTHET
      EXPA(I)=CEXP(CMPLX(0.,TP*ARG))
      P(I)=CPHI*SAB(I)-SPHI*CAB(I)
      Q(I)=CTCP*CAB(I)+CTSP*SAB(I)+STHET*SALP(I)
  850 EI(I)= (ETH*Q(I)+EPH*P(I))*EXPA(I)
      DO 220 K=1,M
      AR(K,MM)=0.
  220 AI(K,MM)=0.
      DO 1001 I=N1,N2
      R2=-REAL(EI(I))
      AI2=-AIMAG(EI(I))
      DO 1001 K=1,M
      R1=REAL(CC(I,K))
      AI1=AIMAG(CC(I,K))
      AR(K,MM)=AR(K,MM)+R1*R2+AI1*AI2
 1001 AI(K,MM)=AI(K,MM)+R1*AI2-R2*AI1
C     RESUME CROUT REDUCTION
      DO 120 L=1,M
      LL=L-1
```

Fig. 43.

```
      IF(LLL.EQ.0) GO TO 1191
      DO 119 K=1,LLL
      R1=AR(L,K)
      AI1=AI(L,K)
      R2=AR(K,MM)
      AI2=AI(K,MM)
      AR(L,MM)=AR(L,MM)-R1*R2+AI1*AI2
  119 AI(L,MM)=AI(L,MM)-R1*AI2-R2*AI1
 1191 CONTINUE
      R2=AR(L,L)
      AR(L,MM)=AR(L,MM)/R2
  120 AI(L,MM)=AI(L,MM)/R2
      DO 122 L=2,M
      I=MM-L
      II=I+1
      DO 122 K=II,M
      R1=AR(I,K)
      R2=AR(K,MM)
      AI1=AI(I,K)
      AI2=AI(K,MM)
      AR(I,MM)=AR(I,MM)-R1*R2+AI1*AI2
  122 AI(I,MM)=AI(I,MM)-R1*AI2-R2*AI1
C     END CROUT REDUCTION
C     SOLUTION IS IN MM COLUMN
C
C     CHECK ON FIELD MATCHING
      WRITE (6,10)
      DO 231 J=1,M
      CR=AR(J,MM)
      CI=AI(J,MM)
  231 A(J)=CMPLX(CR,CI)
      PNN=(0.,0.)
      PN=(0.,0.)
      DO 240 I=1,N
      EP =(0.,0.)
      DO 230 J=1,M
  230 EP=EP+C(I,J)*A(J)
      ET=EI(I)+EP
      ETM=CABS(ET)
      WRITE (6,12) EI(I),EP,ET,ETM
      EI(I)=(0.,0.)
      DO 150 J=1,M
  150 EI(I)=EI(I)+AJ(I,J)*A(J)
  240 PN=PN+CONJG(EI(I))*ET
      PNMAG=CABS(PN)
      WRITE (6,11) PN,PNMAG
      WRITE (6,3) (A(I),I=1,M)
      WRITE (6,4)
      DO 160 I=1,N
      CMAG=CABS(EI(I))
      CR=REAL(EI(I))
      CI=AIMAG(EI(I))
      PH=TD*ATAN2(CI,CR)
  160 WRITE (6,6 ) I,CR,CI,CMAG,PH
C     COMPUTE FAR FIELD AND ECHO AREA
      ET=(0.,0.)
      EP=(0.,0.)
      DO 400 I=1,N
      S=SI(I)*ZZ/2.
      F= EI(I)*EXPA(I)*CMPLX(0.,-S)
      ET=F*Q(I)+ET
  400 EP=EP+F*P(I)
      ETM=CABS(ET)
      EPM=CABS(EP)
```

Fig. 43.

```
      TB=ETM**2
      TC=EPM**2
      EAT=CNSNT*TB
      EAP=CNSNT*TC
      EA=EAT+EAP
      WRITE (6,70) THETA,PHI,ETH,EPH
      WRITE (6,2 ) EAT,EAP,EA
      ETR=REAL(ET)
      ETI=AIMAG(ET)
      EPR=REAL(EP)
      EPI=AIMAG(EP)
      PHT=TD*ATAN2(ETI,ETR)
      PHP=TD*ATAN2(EPI,EPR)
      WRITE (6,5)
      WRITE (6,1 ) ETR,ETI,ETM,PHT
      WRITE (6,9)
      WRITE (6,1 ) EPR,EPI,EPM,PHP
  250 THETA=THETA+DTHETA
  300 PHI=PHI+DPHI
 1000 CONTINUE
      STOP
      END
```

Fig. 43.

```
$(XECUTE        IBJOB
$IBJOB          GO
$IBFTC MAIN2    NODECK
      COMMON X(100),Y(100),Z(100),CAB(100),SAB(100)/SIZE/SI(100)
      COMMON /COEF/C(100,101),SALP(100)
      COMPLEX EXPA(100),ET,EP,C,CUR(100),F
      DIMENSION P(100),Q(100)
    1 FORMAT (1H ,12X,4HREAL,14X,5HIMAG.,13X,4HMAG.,13X,5HPHASE/4X,
     2     1P4E18.7)
    2 FORMAT (10HOECHO AREA//,5X,10HTHETA POL.,E16.8,5X,8HPHI POL.,
     2     E16.8,8X,5HTOTAL,E16.8//)
    4 FORMAT (8HOCURRENT,/8H ELEMENT,8X,4HREAL,16X,5HIMAG.,15X,
     2     4HMAG.,13X,5HPHASE,/)
    5 FORMAT (10HOFAR FIELD//, 5X,10HTHETA POL.)
    6 FORMAT (I5,3E20.8,F13.5)
    7 FORMAT(7F10.5)
    8 FORMAT(14I5)
    9 FORMAT (1H0, 5X,8HPHI POL.)
   70 FORMAT (30H1ANGLE OF INCIDENCE      THETA=,F7.3,7H   PHI=,F7.3,
     2     10X,12HPOLARIZATION,5X,4HETH=,F5.2,5X,4HEPH=,F5.2/)
      ZZ=376.72727
      TD=57.29578
      TA=.01745329
      PI=3.1415926
      TP=6.2831853
      CNSNT=4.*PI
      READ (5,8) NRUNS
      DO 1000 NRUN=1,NRUNS
      CALL WGRID (N)
      CALL ZMAT(B,N)
      NN=N+1
C     START CROUT REDUCTION
C     CROUT METHOD FOR SYMMETRIC MATRIX
      DO 118 L=1,N
      LLL=L-1
      DO 118 I=L,N
      IF(LLL.EQ.0) GO TO 1171
      DO 117 K=1,LLL
  117 C(L,I)=C(L,I)-C(L,K)*C(K,I)
 1171 CONTINUE
      LMI=L-I
      IF(LMI) 105,118,105
  105 C(I,L)=C(L,I)
      C(L,I)=C(L,I)/C(L,L)
  118 CONTINUE
      READ (5,7) THETI,THETF,DTHETA,PHII,PHIF,DPHI,ETH,EPH
      ITH=(THETF-THETI)/DTHETA+1.1
      IPH=(PHIF-PHII)/DPHI+1.1
      PHI=PHII
      DO 300 IP=1,IPH
      PH=TA*PHI
      CPHI=COS(PH)
      SPHI=SIN(PH)
      THETA=THETI
      DO 250 IT=1,ITH
      TTA=TA*THETA
      CTHET=COS(TTA)
      STHET=SIN(TTA)
      STCP=STHET*CPHI
      STSP=STHET*SPHI
      CTCP=CTHET*CPHI
      CTSP=CTHET*SPHI
      DO 850 I=1,N
      ARG=X(I)*STCP+Y(I)*STSP+Z(I)*CTHET
```

Fig. 44.--Main program for the piecewise uniform method.

```
      EXPA(I)=CEXP(CMPLX(0.,TP*ARG))
      P(I)=CPHI*SAB(I)-SPHI*CAB(I)
      Q(I)=CTHP*CAB(I)+CTSP*SAB(I)+STHET*SALP(I)
  850 C(I,NN)=-(ETH*Q(I)+EPH*P(I))*EXPA(I)
      DO 120 L=1,N
      LLL=L-1
      IF(LLL.EQ.0) GO TO 1191
      DO 119 K=1,LLL
  119 C(L,NN)=C(L,NN)-C(L,K)*C(K,NN)
 1191 CONTINUE
  120 C(L,NN)=C(L,NN)/C(L,L)
      DO 122 L=2,N
      I=NN-L
      II=I+1
      DO 122 K=II,N
  122 C(I,NN)=C(I,NN)-C(I,K)*C(K,NN)
      WRITE (6,4)
      DO 160 I=1,N
      CUR(I)=C(I,NN)
      CMAG=CABS(CUR(I))
      CR=REAL(CUR(I))
      CI=AIMAG(CUR(I))
      PH=TD*ATAN2(CI,CR)
  160 WRITE (6,6 ) I,CR,CI,CMAG,PH
C     COMPUTE FAR FIELD AND ECHO AREA
      ET=(0.,0.)
      EP=(0.,0.)
      DO 400 I=1,N
      S=SI(I)*ZZ/2.
      F=CUR(I)*EXPA(I)*CMPLX(0.,-S)
      ET=F*Q(I)+ET
  400 EP=EP+F*P(I)
      ETM=CABS(ET)
      EPM=CABS(EP)
      TB=ETM**2
      TC=EPM**2
      EAT=CNSNT*TB
      EAP=CNSNT*TC
      EA=EAT+EAP
      WRITE (6,70) THETA,PHI,ETH,EPH
      WRITE (6,2 ) EAT,EAP,EA
      ETR=REAL(ET)
      ETI=AIMAG(ET)
      EPR=REAL(EP)
      EPI=AIMAG(EP)
      PHT=TD*ATAN2(ETI,ETR)
      PHP=TD*ATAN2(EPI,EPR)
      WRITE (6,5)
      WRITE (6,1 ) ETR,ETI,ETM,PHT
      WRITE (6,9)
      WRITE (6,1 ) EPR,EPI,EPM,PHP
  250 THETA=THETA+DTHETA
  300 PHI=PHI+DPHI
 1000 CONTINUE
      STOP
      END
```

Fig. 44.

```
$IBFTC MAIN3   DECK
    2 FORMAT (1H ,F15.8)
    3 FORMAT (7H1ALPHA=,F13.8,8H DEGREES ,5X,11HTAN(ALPHA)=,F13.8  //)
    4 FORMAT (23H0EIGENVECTOR, EVEN MODE  //(1H ,E15.8))
    5 FORMAT (104H1CURRENT DISTRIBUTION (NORMALIZED TO MAX. AND TO RAD.
     2UNIT POWER, RESP.) AND TANGENT OF E-FIELD PHASE              )
    6 FORMAT (1H ,I5,2E17.8,10X,F15.6)
    7 FORMAT (7F10.5)
    8 FORMAT (14I5)
    9 FORMAT (1H0,///)
   10 FORMAT (5H0AAA=,F4.1)
   11 FORMAT (17H0FIGURE OF MERIT=,E16.8  )
   12 FORMAT (22H0EIGENVECTOR, ODD MODE   //(1H ,E15.8))
   13 FORMAT (16H1FIRST AND LAST ,I2,3H OF,I4,79H EQUATIONS IGNORED TO R
     2EDUCE EFFECT OF WIRE ENDS ON LEAST SQUARES SOLUTION FOR ,I2,10H UN
     2KNOWNS, //34H WIRE SEGMENT LENGTH (WIRE RADII)=,F7.4 //)
   14 FORMAT (4E15.8)
   15 FORMAT (1H1)
  120 FORMAT (9H0P MATRIX /)
  130 FORMAT (9H0Q MATRIX /)
  140 FORMAT (9H0R MATRIX /)
  150 FORMAT (1H ,6D20.12)
  160 FORMAT (3D24.15)
      DIMENSION TANPH(250),CUR(250),EF(20)
      COMMON X(250),Y(250),Z(250),CAB(250),SAB(250)/SIZE/SI(250)
      COMMON /COEF/CC(250,20),SALP(250)/CURR/AJ(250,20)
      DOUBLE PRECISION PIJ,QIJ,RIJ,P,Q,R
      COMPLEX CC,EALP,EI ,PT
      COMMON /PQR/P(20,20),Q(20,20),R(20,20)
      EQUIVALENCE (TANPH(1),SALP(1)),(CUR(1), X(1))
      XTIME=1./60.
      TD=57.29578
      TA=.01745329
      READ (5,8) NRUNS
      DO 500 NRUN=1,NRUNS
      YTIME=CLOCK(XTIME)
      WRITE (6,7) YTIME
      CALL WGRID(N)
      CALL ZMAT(8,MC,MS,N)
      YTIME=CLOCK(XTIME)
      WRITE (6,7) YTIME
      M=MC+MS
      SIWL=SI(1)/8
      READ (5,8) NTEST
      DO 500 NTT=1,NTEST
      READ (5,7) RADII
      NIGNOR=RADII/SIWL+.5
      WRITE (6,13) NIGNOR,N,M,SIWL
      N1=NIGNOR+1
      N2=N-NIGNOR
      READ (5,8) NPUNCH ,MPUNCH
C     COMPUTE P, Q AND R MATRICES
      MORDER=0
      MN=0
      MD=MC
      IF(MC) 28,28,30
   28 MD=MS
```

Fig. 45.--Main program for the determination of characteristic modes of wires.

```
      MN=MC
      MORDER=1
   30 DO 50 I=1,MD
      IC=I+MN
      DO 50 J=1,MD
      JC=J+MN
      PIJ=0.
      QIJ=0.
      RIJ=0.
      DO 40 K=N1,N2
      RKI=REAL(CC(K,IC))
      RKJ=REAL(CC(K,JC))
      AIKI=AIMAG(CC(K,IC))
      AIKJ=AIMAG(CC(K,JC))
      PIJ=PIJ+AIKI*AIKJ
      QIJ=QIJ+RKI*AIKJ+RKJ*AIKI
   40 RIJ=RIJ+RKI*RKJ
      P(I,J)=PIJ
      Q(I,J)=QIJ
      R(I,J)=RIJ
      P(J,I)=PIJ
      Q(J,I)=QIJ
   50 R(J,I)=RIJ
      WRITE (6,120)
      DO 60 I=1,MD
   60 WRITE (6,150) (P(I,J),J=1,MD)
      WRITE (6,130)
      DO 70 I=1,MD
   70 WRITE (6,150) (Q(I,J),J=1,MD)
      WRITE (6,140)
      DO 80 I=1,MD
   80 WRITE (6,150) (R(I,J),J=1,MD)
      WRITE (6,9)
      IF(NPUNCH.EQ.0) GO TO 90
      PUNCH 160, ((P(I,J),J=1,MD),I=1,MD)
      PUNCH 160, ((Q(I,J),J=1,MD),I=1,MD)
      PUNCH 160, ((R(I,J),J=1,MD),I=1,MD)
   90 READ (5,8) NMODES
      DO 425 NM=1,NMODES
      WRITE (6,15)
C     FIND ALPHA CORRESPONDING TO MINIMUM EIGENVALUE
      AAA=0.
      READ (5,8) NTRY
      READ (5,7) ALP,ASTEP,ERROR
      A2=TA*ALP
      ERROR=TA*ERROR
      ASTEP=TA*ASTEP
      DO 100 NT=1,NTRY
   92 A1=A2-ASTEP
      A3=A2+ASTEP
      IF(A1+1.5707963) 96,96,94
   94 IF(A3-1.5707963) 98,96,96
   96 ASTEP=ASTEP/2.
      GO TO 92
   98 CALL ANULL(MD,A1,A2,A3,ASTEP,ERROR)
      IF(AAA.EQ.1.) GO TO 200
      ALPHA=TD*A2
      WRITE (6,2) ALPHA
      ASTEP=ASTEP/5.0
      IF(ASTEP.LT.ERROR) ASTEP=ERROR
      IF(ASTEP.EQ.ERROR) AAA=1.
  100 CONTINUE
```

Fig. 45.

```
  200 ALPHA=TD*A2
      WRITE (6,10) AAA
      TANALP=SIN(A2)/COS(A2)
      WRITE (6,3) ALPHA,TANALP
      YTIME=CLOCK(XTIME)
      WRITE (6,7) YTIME
C     COMPUTE EIGENVECTOR CORRESPONDING TO ALPHA
      MM=0.
      CALL EGNVLU(MD,A2,EV,EF,MM)
C     COMPUTE CURRENT DISTRIBUTION AND E-FIELD PHASE
      CMAX=0.
      ERROR=0.
      PT=(0.,0.)
      EALP=CEXP(CMPLX(0.,A2))
      DO 300 I=1,N
      EI=(0.,0.)
      CUR(I)=0.
      DO 250 J=1,MD
      JC=J+MN
      EI=EI+CONJG(I,JC)*EF(J)
  250 CUR(I)=CUR(I)+AJ(I,JC)*EF(J)
      PT=PT+EI*CUR(I)*SI(I)
      IF(ABS(CUR(I)).GT.CMAX) CMAX=ABS(CUR(I))
      EI=EALP*EI
      ER=-REAL(EI)
      EAI=AIMAG(EI)
      PH=ATAN2(EAI,ER)
  300 TANPH(I)=SIN(PH)/COS(PH)
      PTOTAL=-REAL(PT)
      PNORM=SQRT(PTOTAL)
      DO 350 I=1,MD
  350 EF(I)=EF(I)/PNORM
      IF(MPUNCH.EQ.0) GO TO 375
      PUNCH 14, (EF(I),I=1,MD)
  375 IF(MORDER) 390,380,390
  380 WRITE (6,4) (EF(I),I=1,MD)
      GO TO 395
  390 WRITE (6,12) (EF(I),I=1,MD)
  395 WRITE (6,5)
      DO 400 I=1,N
      CU=CUR(I)/PNORM
      CUR(I)=CUR(I)/CMAX
      ERROR=ERROR+ABS(TANPH(I) *CUR(I))
  400 WRITE (6,6) I,CUR(I),CU,TANPH(I)
      FN=N
      ERROR=ERROR/FN
      WRITE (6,11) ERROR
      YTIME=CLOCK(XTIME)
      WRITE (6,7) YTIME
  425 CONTINUE
      IF(MS.EQ.0) GO TO 500
      IF (MORDER) 28,28,500
  500 CONTINUE
      STOP
      END
```

Fig. 45.

```
$IBFTC MAIN4   DECK
    1 FORMAT (1H1)
    2 FORMAT (6HOMODE ,I1,2X,A6//5X,6HALPHA=,F8.2//5X,
     2    22HEXPANSION COEFFICIENTS /(10X,5E20.8))
    3 FORMAT (60HOMODE CURRENT DISTRIBUTIONS (EACH NORMALIZED TO RADIATE
     2 UNIT POWER)    )
    4 FORMAT (I5,8E14.4)
    5 FORMAT (2(I5,A5))
    7 FORMAT (7F10.5)
    8 FORMAT (14I5)
   11 FORMAT(42H1AVERAGE BACKSCATTERING CROSS SECTION FOR ,12A6 ///5X,
     2  16HLINEAR TO LINEAR,15X,E20.8 // 5X, 15HLINEAR TO CROSS,16X,
     3    E20.8 //5X,26HRIGHT CIRC. TO RIGHT CIRC.,5X,E20.8 //5X,
     4    24HLEFT CIRC. TO LEFT CIRC.,7X,E20.8 //5X,
     5    25HRIGHT CIRC. TO LEFT CIRC.,6X,E20.8 //)
   12 FORMAT(22HOTOTAL RADIATED POWER=  ,F10.7,19H (SHOULD BE UNITY.) /)
   13 FORMAT (12A6)
   14 FORMAT (4E15.8)
   15 FORMAT (25H1BACKSCATTERING ECHO AREA///4X,66H(V=VERTICAL, H=HORIZ.
     2, RC=RIGHT CIRC., LC=LEFT CIRC. POLARIZATION)    // 4X,3HPHI,
     34X,5HTHETA,9X,3HV-V,12X,3HH-H,12X,3HV-H,11X,5HRC-RC,10X,5HLC-LC,
     4 10X,5HRC-LC    /)
   16 FORMAT (2F8.2,E17.5,5E15.5)
      COMMON /CURR/ AJ(250,20)
      COMMON X(250),Y(250),Z(250),CAB(250),SAB(250)/SIZE/SI(250)
      COMPLEX  FF,FTT(20,40),FPP(20,40),FTP(20,40),ALPX,FTFT,FPFP,FTFP
      COMPLEX ET(20,40),EP(20,40),EXPA,ETTP,EPTP,CEXALP
      DIMENSION SALP(250),A(20),C(8,250),F(20,40),G(20,40),H(20,40),
     2        R(20,40),SPECS(12)
      ZZ=376.72727
      TA=.01745329
      PI=3.1415926
      TP=2.*PI
      FP=4.*PI
      P2=PI/2.
      ZZ2=ZZ**2
      CCST=PI*ZZ2
      TD=57.29578
      READ (5,8) NRUNS
      DO 1000 NRUN=1,NRUNS
      READ (5,13) (SPECS(I),I=1,12)
      CALL WGRID(N)
      CALL CBASIS(MC,MS,N)
      M=MC+MS
      DO 40 K=1,N
      ALP=TA*CAB(K)
      BET=TA*SAB(K)
      CALP=COS(ALP)
      SALP(K)=SIN(ALP)
      CAB(K)=CALP*COS(BET)
   40 SAB(K)=CALP*SIN(BET)
      READ (5,7) PH,TH
      PH=TA*PH
      TH=TA*TH
      READ (5,8) IPH,ITH
      IPH=IPH/2
      IPH=2*IPH+1
      ITH=ITH/2
      ITH=2*ITH+1
      FN=ITH-1
      DTH=TH/FN
      FN=IPH-1
      DPH=PH/FN
      DO 100 IT=1,ITH
```

Fig. 46.--Main program for computing backscattering and tumble average cross sections of wires using characteristic modes.

```
      DO 100 IP=1,IPH
      FTT(IT,IP)=(0.,0.)
      FPP(IT,IP)=(0.,0.)
  100 FTP(IT,IP)=(0.,0.)
      WRITE (6,1)
      READ (5,5) ME,EVEN,MO,ODD
      NMODES=ME+MO
      MCMS=MC
      FMODE=EVEN
      DO 500 NM=1,NMODES
      IF(NM.LE.ME) GO TO 110
      MCMS=MS
      FMODE=ODD
  110 READ(5,14) (A(I),I=1,MCMS)
      READ (5,7) ALPHA
      WRITE (6,2) NM,FMODE,ALPHA,(A(I),I=1,MCMS)
      ARG=TA*ALPHA
      AMAG=ABS(COS(ARG))
      CEXALP=CEXP(CMPLX(0.,ARG))
      ALPX=AMAG*CEXALP
      DO 160 I=1,N
      CI=0.
      DO 150 J=1,MCMS
      JJ=J
      IF(NM.GT.ME) JJ=J+MC
  150 CI=CI+A(J)*AJ(I,JJ)
  160 C(NM,I)=CI
      PHI=0.
      DO 450 IP=1,IPH
      CPHI=COS(PHI)
      SPHI=SIN(PHI)
      THETA=0.
      DO 400 IT=1,ITH
      ETTP=(0.,0.)
      EPTP=(0.,0.)
      CTHET=COS(THETA)
      STHET=SIN(THETA)
      STCP=STHET*CPHI
      STSP=STHET*SPHI
      CTCP=CTHET*CPHI
      CTSP=CTHET*SPHI
      DO 1001 I=1,N
      ARG=X(I)*STCP+Y(I)*STSP+Z(I)*CTHET
      EXPA=CEXP(CMPLX(0.,TP*ARG))
      P=CPHI*SAB(I)-SPHI*CAB(I)
      Q=CTCP*CAB(I)+CTSP*SAB(I)+STHET*SALP(I)
      FF=C(NM,I)*EXPA*SI(I)
      ETTP=ETTP+FF*Q
 1001 EPTP=EPTP+FF*P
      ET(IT,IP)=ETTP
      EP(IT,IP)=EPTP
      F(IT,IP)=CABS(ETTP)**2+CABS(EPTP)**2
  400 THETA=THETA+DTH
  450 PHI=PHI+DPH
      PTOTAL=ZZ*DBLINT(F,PH,TH,IPH,ITH)/4.
      WRITE (6,12) PTOTAL
      DO 500 IT=1,ITH
      DO 500 IP=1,IPH
      FTT(IT,IP)=FTT(IT,IP)+ET(IT,IP)**2*ALPX
      FPP(IT,IP)=FPP(IT,IP)+EP(IT,IP)**2*ALPX
  500 FTP(IT,IP)=FTP(IT,IP)+ET(IT,IP)*EP(IT,IP)*ALPX
      WRITE (6,3)
      DO 501 I=1,N
  501 WRITE (6,4) I,(C(NM,I),NM=1,NMODES)
```

Fig. 46.

```
      WRITE (6,15)
      PHI=0.
      DO 610 IP=1,IPH
      PP=TD*PHI
      THETA=0.
      DO 600 IT=1,ITH
      TT=TD*THETA
      FTFT=FTT(IT,IP)
      FPFP=FPP(IT,IP)
      FTFP=FTP(IT,IP)
      FTFT2=CABS(FTFT)**2
      FPFP2=CABS(FPFP)**2
      FTFP2=CABS(FTFP)**2
      RFF=REAL(CONJG(FTFT)*FPFP)
      AIFF=AIMAG((FTFT-FPFP)*CONJG(FTFP))
      EAVV=CCST*FTFT2
      EAVH=CCST*FTFP2
      EAHH=CCST*FPFP2
      EARL=CCST*(FTFT2+FPFP2+2.*RFF)/4.
      EARR=CCST*((FTFT2+FPFP2)/4.-RFF/2.+FTFP2+AIFF)
      EALL=EARR-2.*CCST*AIFF
      WRITE (6,16) PP,TT,EAVV,EAHH,EAVH,EARR,EALL,EARL
      F(IT,IP)=FTFT2+FPFP2
      G(IT,IP)=FTFP2
      H(IT,IP)=RFF
      R(IT,IP)=AIFF
  600 THETA=THETA+DTH
  610 PHI=PHI+DPH
      AVGF=DBLINT(F,PH,TH,IPH,ITH)/FP
      AVGG=DBLINT(G,PH,TH,IPH,ITH)/FP
      AVGH=DBLINT(H,PH,TH,IPH,ITH)/FP
      AVGR=DBLINT(R,PH,TH,IPH,ITH)/FP
      AEAII=CCST*(3.*AVGF/8.+AVGG/2.+AVGH/4.)
      AEAIX=CCST*(    AVGF/8.+AVGG/2.-AVGH/4.)
      AEARL=CCST*(AVGF/4.+AVGH/2.)
      AEARR=CCST*(AVGF/4.+AVGG-AVGH/2.+AVGR)
      AEALL=AEARR-2.*CCST*AVGR
      WRITE (6,11) (SPECS(I),I=1,12),AEAII,AEAIX,AEARR,AEALL,AEARL
 1000 CONTINUE
      STOP
      END
```

Fig. 46.

```
$IBFTC SUB1     DECK
      SUBROUTINE WGRID(N)
      COMMON X(250),Y(250),Z(250),CAB(250),SAB(250)/SIZE/SI(250)
    6 FORMAT (10HOWIRE GRID  //)
    7 FORMAT (7F10.5)
    8 FORMAT (1415)
    9 FORMAT (1H0,12X,1HX,14X,1HY,14X,1HZ,13X,2HSI,12X,5HALPHA,10X,
     2        4HBETA/(I5,6F15.8))
   10 FORMAT (1H ,5X,3HA1=,F10.6,5X,3HA2=,F10.6 /)
      TP=6.2831853
      TD=57.29578
      WRITE (6,6)
      READ (5,8) N
      FN=N
      READ (5,7) A1,A2
      WRITE (6,10) A1,A2
      A1=A1**2
      A2=A2**2
      A3=A1*A2
      DPHI=TP/FN
      PHI=0.
      X1=SQRT(A3/A2)
      Y1=0.
      DO 100 I=1,N
      PHI=PHI+DPHI
      SP=SIN(PHI)
      CP=COS(PHI)
      R2=SQRT(A3/(A1*SP*SP+A2*CP*CP))
      X2=R2*CP
      Y2=R2*SP
      X(I)=(X1+X2)/2.
      Y(I)=(Y1+Y2)/2.
      Z(I)=0.
      X21=X2-X1
      Y21=Y2-Y1
      XY=X21**2+Y21**2
      SI(I)=SQRT(XY)
      CAB(I)=0.
      SAB(I)=TD*ATAN2(Y21,X21)
      X1=X2
  100 Y1=Y2
      WRITE (6,9) (I,X(I),Y(I),Z(I),SI(I),CAB(I),SAB(I),I=1,N)
      RETURN
      END
```

Fig. 47.--Wire geometry subprogram for circular and elliptical loops.

```
$IBFTC SUBI     DECK
       SUBROUTINE WGRID(N)
       COMMON X(250),Y(250),Z(250),CAB(250),SAB(250)/SIZE/SI(250)
     6 FORMAT (10H1WIRE GRID  //)
     7 FORMAT (7F10.5)
     8 FORMAT (1415)
     9 FORMAT (1H0,12X,1HX,14X,1HY,14X,1HZ,13X,2HSI,12X,5HALPHA,10X,
      2            4HBETA /(IS,6F15.8))
    10 FORMAT (1H ,5X,12HWIRE LENGTH=,F10.6,5X,12HHELIX PITCH=,F10.6,5X,
      2    13HHELIX RADIUS=,F10.6,5X,5HPHII=,F10.5,5X,5HPHIF=,F10.5/)
       TP=6.28318853
       TD=57.29578
       WRITE (6,6)
       READ (5,8) N
       FN=N
       READ (5,7) SL,S,R
       HL=SQRT(S**2+(TP*R)**2)
       FNT=SL/HL
       A=FNT*S
       Z0=-A/2.
       PHIT=FNT*360.
       PHII=-PHIT/2.
       PHIF=PHII+PHIT
       WRITE (6,10) SL,S,R,PHII,PHIF
       H1=Z0-S*PHII/360.
       PHII=PHII/TD
       PHIF=PHIF/TD
       DPHI=(PHIF-PHII)/FN
       PHI=PHII
       DO 200 I=1,N
       IF(I.GT.1) GO TO 100
       Z1=S*PHI/TP+H1
       X1=R*COS(PHI)
       Y1=R*SIN(PHI)
   100 Z2=S*(PHI+DPHI)/TP+H1
       X2=R*COS(PHI+DPHI)
       Y2=R*SIN(PHI+DPHI)
       X(I)=(X1+X2)/2.
       Y(I)=(Y1+Y2)/2.
       Z(I)=(Z1+Z2)/2.
       X21=X2-X1
       Y21=Y2-Y1
       Z21=Z2-Z1
       XY=X21**2+Y21**2
       SI(I)=SQRT(XY+Z21**2)
       XY=SQRT(XY)
       CAB(I)=-TD*ATAN2(Z21,XY)
       IF(Y21.EQ.0..AND.X21.EQ.0.) GO TO 21
       SAB(I)=TD*ATAN2(Y21,X21)
       GO TO 22
    21 SAB(I)=0.
    22 X1=X2
       Y1=Y2
       Z1=Z2
   200 PHI=PHI+DPHI
       WRITE (6,9) (I,X(I),Y(I),Z(I),SI(I),CAB(I),SAB(I),I=1,N)
       RETURN
       END
```

Fig. 48.--Wire geometry subprogram for helical and straight wires and circular arcs.

```
$IBFTC SUB2     DECK
       SUBROUTINE ZMAT(AL,N)
       COMMON X(100),Y(100),Z(100),CAB(100),SAB(100)/SIZE/SI(100)
       COMMON /COEF/C(100,101),SALP(100)
       COMPLEX C,CC
       DIMENSION D(11)
     7 FORMAT (7F10.5)
    13 FORMAT (13H1WIRE RADIUS=,F7.5,14H (WAVELENGTHS))
       TA=.01745329
       ZZ=376.72727
       PI=3.1415926
       P2=PI/2.
       TP=2.*PI
       FPP=TP*TP
       PSQ=PI*PI
       CRY=ZZ/8./PSQ
       CCST=ZZ/180./PSQ
       READ (5,7) AL
       WRITE (6,13) AL
       B2=AL**2
       BK=TP*AL
       BK2=BK*BK
       BK4=BK2*BK2
       D(1)=7.
       D(2)=32.
       D(3)=12.
       D(4)=32.
       D(5)=14.
       D(6)=32.
       D(7)=12.
       D(8)=32.
       D(9)=7.
       DO 40 K=1,N
       ALP=TA*CAB(K)
       BET=TA*SAB(K)
       CALP=COS(ALP)
       SALP(K)=SIN(ALP)
       CBET=COS(BET)
       SBET=SIN(BET)
       CAB(K)=CALP*CBET
    40 SAB(K)=CALP*SBET
       DO 300 I=1,1
       S=SI(I)
       IF(I-1) 101,42,101
   101 II=I-1
       C(I,I)=C(II,II)
       IF(S-SI(II)) 42,45,42
    42 ST=S/2.
       RR=SQRT(B2+ST*ST)
       SINB=ST/RR
       COSB=AL/RR
       TANB=(1.+SINB+COSB)/(1.-SINB+COSB)
       RK=TP*RR
       RK2=RK*RK
       ER=-PI/3.*S*(2.-BK2/3.+BK4/60.+RK2*(BK2-8.)/120.)
       EI=SINB*(1./RK2+.5+RK2*(1.-7./60.*BK2)/8.-RK2*RK2/240.)
      2-(1.-BK2/4.+7./480.*BK4)*ALOG (TANB)
       C(I,I)=ZZ*CMPLX(ER,EI)
    45 CONTINUE
       XI=X(I)
       YI=Y(I)
       ZI=Z(I)
       CABI=CAB(I)
       SABI=SAB(I)
```

Fig. 49.--Subprogram for the piecewise uniform impedance matrix of symmetric wire geometries.

```
      DO 280 J=1,N
      IF(I-J) 103,280,103
  103 S=SI(J)
      ST=S/2.
      SS=S*S
      CABJ=CAB(J)
      SABJ=SAB(J)
      XIJ=XI-X(J)
      YIJ=YI-Y(J)
      ZIJ=ZI-Z(J)
      ZP=XIJ*CABJ+YIJ*SABJ-ZIJ*SALP(J)
      RS=XIJ*XIJ+YIJ*YIJ+ZIJ*ZIJ
      RH2=RS-ZP*ZP
      RB=RH2+B2
      RBK=FPP*RB
      KK=8
      EZR=0.
      EZI=0.
      ERR=0.
      ERI=0.
      W=-1.
      T=-ST
      SSS=25.*SS
      IF(RS.GT.SSS) KK=4
      KKK=KK+1
      D(5)=(7*KK)/4
      FKK=KK
      DEL=S/FKK
      DO 50 K=1,KKK
      R2=RB+(ZP-T)*(ZP-T)
      RR=SQRT(R2)
      RK=TP*RR
      COSB=COS(RK)/RR/R2
      SINB=SIN(RK)/RR/R2
      RKCS=RK*COSB-SINB
      CRKS=COSB+RK*SINB
      TRBR=2.-3.*RB/R2
      IF(D(K)-7.) 104,104,49
  104 ERR=ERR+W*CRY*RKCS
      ERI=ERI-W*CRY*CRKS
      W=1.
   49 EZR=EZR+D(K)*(TRBR*RKCS-RBK*SINB)
      EZI=EZI-D(K)*(RBK*COSB+TRBR*CRKS)
   50 T=T+DEL
      EZR=EZR*CCST*DEL
      EZI=EZI*CCST*DEL
      Q1=CABI*CABJ+SABI*SABJ+SALP(I)*SALP(J)
      Q2=XIJ*CABI+YIJ*SABI-ZIJ*SALP(I)
      EIC=EZI-ZP*ERI
      ERC=EZR-ZP*ERR
      C(I,J)=Q1*CMPLX(ERC,EIC)+Q2*CMPLX(ERR,ERI)
  280 CONTINUE
  300 CONTINUE
      DO 400 I=2,N
      C(I,1) =C(1,I)
      DO 400 J=I,N
      J1=J-I+1
      CC=C(1,J1)
      C(I,J)=CC
  400 C(J,I)=CC
      RETURN
      END
```

Fig. 49.

```
$IBFTC SUB2     DECK
       SUBROUTINE ZMAT(AL,MC,MS,N)
       COMMON X(250),Y(250),Z(250),CAB(250),SAB(250)/SIZE/SI(250)
       COMMON /COEF/CC(250,20),SALP(250)/CURR/AJ(250,20)
       COMPLEX C,CII,CC
       DIMENSION D(11)
     7 FORMAT (7F10.5)
    13 FORMAT (13HWIRE RADIUS=,F7.5,14H (WAVELENGTHS))
       TA=.01745329
       ZZ=376.72727
       PI=3.1415926
       P2=PI/2.
       TP=2.*PI
       FPP=TP*TP
       PSQ=PI*PI
       CRY=ZZ/8./PSQ
       CCST=ZZ/180./PSQ
       READ (5,7) AL
       WRITE (6,13) AL
       B2=AL**2
       BK=TP*AL
       BK2=BK*BK
       BK4=BK2*BK2
       D(1)=7.
       D(2)=32.
       D(3)=12.
       D(4)=32.
       D(5)=14.
       D(6)=32.
       D(7)=12.
       D(8)=32.
       D(9)=7.
       CALL CBASIS (MC,MS,N)
       M=MC+MS
       DO 12 J=1,M
       DO 12 I=1,N
    12 CC(I,J)=(0.,0.)
       DO 40 K=1,N
       ALP=TA*CAB(K)
       BET=TA*SAB(K)
       CALP=COS(ALP)
       SALP(K)=SIN(ALP)
       CBET=COS(BET)
       SBET=SIN(BET)
       CAB(K)=CALP*CBET
    40 SAB(K)=CALP*SBET
```

Fig. 50.--Subprogram for the modal impedance matrix derived as a transformation of a piecewise uniform impedance matrix for symmetric wire geometries.

```
C      CO. JTE POINT-TO-POINT IMPEDANCE MATRIX COMPONENTS
C         AND CONVERT TO MODE-TO-POINT IMPEDANCE MATRIX
       S=SI(1)
    42 ST=S/2.
       RR=SQRT(B2+ST*ST)
       SINB=ST/RR
       COSB=AL/RR
       TANB=(1.+SINB+COSB)/(1.-SINB+COSB)
       RK=TP*RR
       RK2=RK*RK
       ER=-PI/3.*S*(2.-BK2/3.+BK4/60.+RK2*(BK2-8.)/120.)
       EI=SINB*(1./RK2+.5+RK2*(1.-7./60.*BK2)/8.-RK2*RK2/240.)
      2-(1.-BK2/4.+7./480.*BK4)*ALOG (TANB)
       CII =ZZ*CMPLX(ER,EI)
    45 XI=X(1)
       YI=Y(1)
       ZI=Z(1)
       CABI=CAB(1)
       SABI=SAB(1)
       DO 280 JN=1,N
       J=N-JN+1
       IF(J.EQ.1) GO TO 240
   103 S=SI(J)
       ST=S/2.
       SS=S*S
       CABJ=CAB(J)
       SABJ=SAB(J)
       XIJ=XI-X(J)
       YIJ=YI-Y(J)
       ZIJ=ZI-Z(J)
       ZP=XIJ*CABJ+YIJ*SABJ-ZIJ*SALP(J)
       RS=XIJ*XIJ+YIJ*YIJ+ZIJ*ZIJ
       RH2=RS-ZP*ZP
       RB=RH2+B2
       RBK=FPP*RB
       KK=8
       EZR=0.
       EZI=0.
       ERR=0.
       ERI=0.
       W=-1.
       T=-ST
       SSS=25.*SS
       IF(RS.GT.SSS) KK=4
       KKK=KK+1
       D(5)=(7*KK)/4
       FKK=KK
       DEL=S/FKK
       DO 50 K=1,KKK
       R2=RB+(ZP-T)*(ZP-T)
       RR=SQRT(R2)
       RK=TP*RR
       COSB=COS(RK)/RR/R2
       SINB=SIN(RK)/RR/R2
       RKCS=RK*COSB-SINB
       CRKS=COSB+RK*SINB
       TRBR=2.-3.*RB/R2
       IF(D(K)-7.) 104,104,49
```

Fig. 50.

```
104 ERR=ERR+W*CRY*RKCS
    ERI=ERI-W*CRY*CRKS
    W=1.
 49 EZR=EZR+D(K)*(TRBR*RKCS-RBK*SINB)
    EZI=EZI-D(K)*(RBK*COSB+TRBR*CRKS)
 50 T=T+DEL
    EZR=EZR*CCST*DEL
    EZI=EZI*CCST*DEL
    Q1=CABI*CABJ+SABI*SABJ+SALP(I)*SALP(J)
    Q2=XIJ*CABI+YIJ*SABI-ZIJ*SALP(I)
    EIC=EZI-ZP*ERI
    ERC=EZR-ZP*ERR
    C      =Q1*CMPLX(ERC,EIC)+Q2*CMPLX(ERR,ERI)
240 IF(J.EQ.1) C=CII/2.
    DO 250 L=1,M
    CC(I,L)=CC(I,L)+C*AJ(J,L)
250 CC(J,L)=CC(J,L)+C*AJ(I,L)
    IF(J.EQ.N) GO TO 280
    K=1
    JP=J+1
    DO 270 I=JP,N
    K=K+1
    DO 260 L=1,M
    CC(K,L)=CC(K,L)+C*AJ(I,L)
    CC(I,L)=CC(I,L)+C*AJ(K,L)
260 CONTINUE
270 CONTINUE
280 CONTINUE
    RETURN
    END
```

Fig. 50.

```
$IBFTC SUB2     DECK
      SUBROUTINE ZMAT(AL,MC,MS,N)
      COMMON X(250),Y(250),Z(250),CAB(250),SAB(250)/SIZE/SI(250)
      COMMON /COEF/CC(250,20),SALP(250)/CURR/AJ(250,20)
      COMPLEX C,CC,C1
      DIMENSION D(11)
    7 FORMAT (7F10.5)
   13 FORMAT (13H1WIRE RADIUS=,F7.5,14H (WAVELENGTHS))
      TA=.01745329
      ZZ=376.72727
      PI=3.1415926
      P2=PI/2.
      TP=2.*PI
      FPP=TP*TP
      PSQ=PI*PI
      CRY=ZZ/8./PSQ
      CCST=ZZ/180./PSQ
      READ(5,7) AL
      WRITE (6,13) AL
      B2=AL**2
      BK=TP*AL
      BK2=BK*BK
      BK4=BK2*BK2
      D(1)=7.
      D(2)=32.
      D(3)=12.
      D(4)=32.
      D(5)=14.
      D(6)=32.
      D(7)=12.
      D(8)=32.
      D(9)=7.
      CALL CBASIS(MC,MS,N)
      M=MC+MS
      DO 12 J=1,M
      DO 12 I=1,N
   12 CC(I,J)=(0.,0.)
      DO 40 K=1,N
      ALP=TA*CAB(K)
      BET=TA*SAB(K)
      CALP=COS(ALP)
      SALP(K)=SIN(ALP)
      CBET=COS(BET)
      SBET=SIN(BET)
      CAB(K)=CALP*CBET
   40 SAB(K)=CALP*SBET
```

Fig. 51.--Subprogram for the modal impedance matrix derived as a transformation of a piecewise uniform impedance matrix for elliptical wire geometries.

```
      N2=N/2
      N4=N/4
      DO 300 I=1,N4
      S=SI(I)
      ST=S/2.
      RR=SQRT(B2+ST*ST)
      SINB=ST/RR
      COSB=AL/RR
      TANB=(1.+SINB+COSB)/(1.-SINB+COSB)
      RK=TP*RR
      RK2=RK*RK
      ER=-PI/3.*S*(2.-BK2/3.+BK4/60.+RK2*(BK2-8.)/120.)
      EI=SINB*(1./RK2+.5+RK2*(1.-7./60.*BK2)/8.-RK2*RK2/240.)
     2-(1.-BK2/4.+7./480.*BK4)*ALOG (TANB)
      C1=ZZ*CMPLX(ER,EI)
   45 CONTINUE
      XI=X(I)
      YI=Y(I)
      ZI=Z(I)
      CABI=CAB(I)
      SABI=SAB(I)
      I1=N2-I+1
      I2=N2+I
      I3=N-I+1
      DO 280 J=1,N
      IF(I-J) 47,46,47
   46 C=C1
      GO TO 52
   47 S=SI(J)
      ST=S/2.
      SS=S*S
      CABJ=CAB(J)
      SABJ=SAB(J)
      XIJ=XI-X(J)
      YIJ=YI-Y(J)
      ZIJ=ZI-Z(J)
      ZP=XIJ*CABJ+YIJ*SABJ-ZIJ*SALP(J)
      RS=XIJ*XIJ+YIJ*YIJ+ZIJ*ZIJ
      RH2=RS-ZP*ZP
      RB=RH2+B2
      RBK=FPP*RB
      KK=6
      EZR=0.
      EZI=0.
      ERR=0.
      ERI=0.
      W=-1.
      T=-ST
      SSS=25.*SS
      IF(RS.GT.SSS) KK=4
      KKK=KK+1
      D(5)=(7*KK)/4
      FKK=KK
      DEL=S/FKK
```

Fig. 51

```
      DO 50 K=1,KK
      R2=RB+(ZP-T)*(ZP-T)
      RR=SQRT(R2)
      RK=TP*RR
      COSB=COS(RK)/RR/R2
      SINB=SIN(RK)/RR/R2
      RKCS=RK*COSB-SINB
      CRKS=COSB+RK*SINB
      TRBR=2.-3.*RB/R2
      IF(D(K)-7.) 104,104,49
  104 ERR=ERR+W*CRY*RKCS
      ERI=ERI-W*CRY*CRKS
      W=1.
   49 EZR=EZR+D(K)*(TRBR*RKCS-RBK*SINB)
      EZI=EZI-D(K)*(RBK*COSB+TRBR*CRKS)
   50 T=T+DEL
      EZR=EZR*CCST*DEL
      EZI=EZI*CCST*DEL
      Q1=CABI*CABJ+SABI*SABJ+SALP(I)*SALP(J)
      Q2=XIJ*CABI+YIJ*SABI-ZIJ*SALP(I)
      EIC=EZI-ZP*ERI
      ERC=EZR-ZP*ERR
      C=Q1*CMPLX(ERC,EIC)+Q2*CMPLX(ERR,ERI)
      IF(J.GT.N2) GO TO 55
   52 J1=N2-J+1
      J2=N2+J
      J3=N-J+1
      GO TO 60
   55 J1=N-J+N2+1
      J2=J-N2
      J3=N-J+1
   60 DO 280 L=1,M
      CC(I,L)=CC(I,L)+C*AJ(J,L)
      CC(I1,L)=CC(I1,L)+C*AJ(J1,L)
      CC(I2,L)=CC(I2,L)+C*AJ(J2,L)
  280 CC(I3,L)=CC(I3,L)+C*AJ(J3,L)
  300 CONTINUE
      RETURN
      END
```

Fig. 51.

```
$IBFTC SUB3     DECK
       SUBROUTINE CBASIS(MC,MS,N)
       COMMON /CURR/AJ(250,20)/SIZE/SI(250)
     8 FORMAT (14I5)
     9 FORMAT (15H1BASIS CURRENTS,//(1H ,12F10.6))
       PI=3.1415926
       SL=0.
       DO 40 I=1,N
    40 SL=SL+SI(I)
       N21=N/2+1
       READ (5,8) MC,MS
       M=MC+MS
       PS=2.*PI/SL
       SLJ=.5*SI(N21)
       DO 500 J=N21,N
       JJ=N-J+1
       IF(MC.EQ.0) GO TO 350
       DO 300 K=1,MC
       FK=K
       FKC=(FK-1.)*PS
       AJ(J,K)=COS(FKC*SLJ)
   300 AJ(JJ,K)=AJ(J,K)
       IF(MS.EQ.0) GO TO 450
   350 DO 400 K=1,MS
       KK=K+MC
       FK=K
       FKS=FK*PS
       AJ(J,KK)=SIN(FKS*SLJ)
   400 AJ(JJ,KK)=-AJ(J,KK)
   450 J1=J+1
   500 SLJ=SLJ+.5*(SI(J)+SI(J1))
       WRITE (6,9) ((AJ(J,K),J=1,N),K=1,M)
       RETURN
       END
```

Fig. 52.--Sine and cosine basis functions for wire loops.

```
$IBFTC SUB3     DECK
       SUBROUTINE CBASIS(MC,MS,N)
       COMMON /CURR/AJ(250,20)/SIZE/SI(250)
     8 FORMAT (14I5)
     9 FORMAT (15H1BASIS CURRENTS,//(1H ,12F10.6))
       PI=3.1415926
       SL=0.
       DO 40 I=1,N
    40 SL=SL+SI(I)
       N21=N/2+1
       READ (5,8) MC,MS
       M=MC+MS
       PS=PI/SL
       SLJ=.5*SI(N21)
       DO 500 J=N21,N
       JJ=N-J+1
       IF(MC.EQ.0) GO TO 350
       DO 300 K=1,MC
       FK=K
       FKC=(FK-1.)*PS
       AJ(J,K)=COS(FKC*SLJ)
   300 AJ(JJ,K)=AJ(J,K)
       IF(MS.EQ.0) GO TO 450
   350 DO 400 K=1,MS
       KK=K+MC
       FK=K
       FKS=FK*PS
       AJ(J,KK)=SIN(FKS*SLJ)
   400 AJ(JJ,KK)=-AJ(J,KK)
   450 J1=J+1
   500 SLJ=SLJ+.5*(SI(J)+SI(J1))
       WRITE (6,9) ((AJ(J,K),J=1,N),K=1,M)
       RETURN
       END
```

Fig. 53.--Sine and cosine basis functions for wires of open configuration.

```
$IBFTC SUB3     DECK
       SUBROUTINE CBASIS(MC,MS,N)
       COMMON /CURR/AJ(250,20)/SIZE/SI(250)
     2 FORMAT (15H1BASIS CURRENTS //)
     8 FORMAT (14I5)
     9 FORMAT (1H ,12F10.6)
       ARCCOS(X)=SQRT(1.-X)*(1.5707288-.2121144*X+.074261*X*X
      2          -.0187293*X*X*X)
       SL=0.
       DO 40 I=1,N
    40 SL=SL+SI(I)
       N21=N/2+1
       READ (5,8) MC,MS
       M=MC+MS
       SL2=SL/2.
       SLJ=.5*SI(N21)
       DO 500 J=N21,N
       JJ=N-J+1
       EL=SLJ/SL2
       ACOS=ARCCOS(EL)
       IF(MC) 200,350,200
   200 DO 300 K=1,MC
       FK=2*(K-1)
       AJ(J,K)=SIN((FK+1.)*ACOS)/SIN(ACOS)
   300 AJ(JJ,K)=AJ(J,K)
       IF(MS) 350,450,350
   350 DO 400 K=1,MS
       KK=K+MC
       FK=2*K-1
       AJ(J,KK)=SIN((FK+1.)*ACOS)/SIN(ACOS)
   400 AJ(JJ,KK)=-AJ(J,KK)
   450 J1=J+1
   500 SLJ=SLJ+.5*(SI(J)+SI(J1))
       WRITE (6,2)
       DO 600 K=1,M
   600 WRITE (6,9) (AJ(J,K),J=1,N)
       RETURN
       END
```

Fig. 54.--Chebyshev polynomial basis functions.

```
$IBFTC SUB4     DECK
       SUBROUTINE ANULL(M,A1,A2,A3,ASTEP,ERROR)
     5 FORMAT (1H ,3(F15.6,E18.8))
       COMMON /PQR/P(20,20),Q(20,20),R(20,20)
       DIMENSION EF(20)
       DOUBLE PRECISION P,Q,R
       MM=1
       CALL EGNVLU(M,A1,EV1,EF,MM)
       CALL EGNVLU(M,A2,EV2,EF,MM)
       CALL EGNVLU(M,A3,EV3,EF,MM)
       WRITE (6,5) A1,EV1,A2,EV2,A3,EV3
       A12=A1**2
       A22=A2**2
       A32=A3**2
       D=A22*A3-A32*A2-A12*A3+A32*A1+A12*A2-A22*A1
       IF(D) 8,6,8
     6 S=0.
       GO TO 10
     8 A= EV1*A2-EV2*A1-EV1*A3+EV3*A1+EV2*A3-EV3*A2
       S=A/D
       IF(S.LE.0.) GO TO 10
       B= A12*EV2-A22*EV1-A12*EV3+A32*EV1+A22*EV3-A32*EV2
       A0=-B/(2.*A)
       WRITE (6,5) A0
       IF(A0.LT.A1.OR.A0.GT.A3) GO TO 10
       A2=A0
       RETURN
    10 IF(EV3-EV1) 20,30,30
    20 A0=A3
       GO TO 40
    30 A0=A1
    40 ASTEP=5.0*ASTEP
       A2=A0
       RETURN
       END
```

Fig. 55.--Subroutine for locating $\epsilon_{min}(\alpha_m)$.

```
$IBFTC SUB5     DECK
       SUBROUTINE EGNVLU(M,ALP,EV,EF,MM)
       COMMON /PQR/P(20,20),Q(20,20),R(20,20)
       DIMENSION EF(20)
       DOUBLE PRECISION P,Q,R,B,D,TALP,TALP2
       COMMON /BDAR/B(20,20),D(20,20)
       TALP=SIN(ALP)/COS(ALP)
       TALP2=TALP**2
       DO 20 J=1,M
       DO 20 I=J,M
       B(I,J)=P(I,J)+TALP*Q(I,J)+TALP2*R(I,J)
    20 B(J,I)=B(I,J)
       CALL MATEIG(M,MM)
       EV=B(1,1)
       DO 30 I=1,M
    30 EF(I)=D(I,1)
       RETURN
       END
```

Fig. 56.--Subroutine for computing [B(α)].

```
$IBFTC SUB6     DECK
       SUBROUTINE MATEIG(N,MV)
       DOUBLE PRECISION A,R,ANORM,ANRMX,THR,X,Y,Z
      2       SINX,SINX2,COSX,COSX2,SINCS,AA
       COMMON /BDAR/A(20,20),R(20,20)
       FN=N
       IF(MV-1) 10,25,10
    10 DO 20 J=1,N
       DO 20 I=1,N
       R(I,J) =0.
    20 R(I,I)=1.
    25 ANORM=0.
       DO 35 I=1,N
       DO 35 J=1,N
       IF(I-J) 30,35,30
    30 ANORM=ANORM+A(I,J)*A(I,J)
    35 CONTINUE
       IF(ANORM) 165,165,40
    40 ANORM=1.414*DSQRT(ANORM)
       ANRMX=ANORM*1.0E-6/FN
       IND=0
       THR=ANORM
    45 THR=THR/FN
       NM1=N-1
    50 DO 149 L=1,NM1
       L1=L+1
       DO 149 M=L1,N
       AA=A(L,M)**2
       AA=DSQRT(AA)
    62 IF(AA-THR) 149,65,65
    65 IND=1
       X=.5*( A(L,L)-A(M,M))
    68 Y=A(L,M)
       Z=DSQRT(Y*Y+X*X)
       Y=-A(L,M)/Z
       IF(X) 70,75,75
    70 Y=-Y
    75 SINX=Y/DSQRT(2.*(1.+(DSQRT(1.-Y*Y))))
       SINX2=SINX**2
    78 COSX=DSQRT(1.-SINX2)
       COSX2=COSX**2
       SINCS=SINX*COSX
       DO 90 I=1,N
       IF(I-L) 80,90,80
    80 IF(I-M) 85,90,85
    85 X=A(I,L)*COSX-A(I,M)*SINX
       A(I,M)=A(I,L)*SINX+A(I,M)*COSX
       A(I,L)=X
    90 CONTINUE
```

Fig. 57.--Subroutine for computing the eigenvalues and eigenvectors of [B(α)].

```
      X=2.*A(L,M)*SINCS
      Y=A(L,L)*COSX2+A(M,M)*SINX2-X
      X=A(L,L)*SINX2+A(M,M)*COSX2+X
      A(L,M)=(A(L,L)-A(M,M))*SINCS+A(L,M)*(COSX2-SINX2)
      A(L,L)=Y
      A(M,M)=X
      DO 100 I=1,N
      A(L,I)=A(I,L)
      A(M,I)=A(I,M)
      IF(MV-1) 95,100,95
   95 X=R(I,L)*COSX-R(I,M)*SINX
      R(I,M)=R(I,L)*SINX+R(I,M)*COSX
      R(I,L)=X
  100 CONTINUE
  149 CONTINUE
  150 IF(IND-1) 160,155,160
  155 IND=0
      GO TO 50
  160 IF(THR-ANRMX) 165,165,45
  165 DO 185 I=1,N
      DO 185 J=1,N
      IF(A(I,I)-A(J,J)) 170,185,185
  170 X=A(I,I)
      A(I,I)=A(J,J)
      A(J,J)=X
      DO 180 K=1,N
      X=R(K,I)
      R(K,I) =R(K,J)
  180 R(K,J)=X
  185 CONTINUE
      RETURN
      END
```

Fig. 57.

```
$IBFTC SUB7     DECK
       FUNCTION DBLINT(S,PH,TH,NP,NT)
       DIMENSION S(20,40),G(40),F(20)
       PI=3.1415926
       TP=2.*PI
       PHI=PH
       IF(PH) 50,50,60
    50 PHI=1.
       NP=1
    60 PTM=PI/TH*TP/PHI
       FNP=NP
       DPH=PH/(FNP-1.)
       FNT=NT
       DTH=TH/(FNT-1.)
       NT1=NT-1
       NT2=NT-2
       NP1=NP-1
       NP2=NP-2
       DO 200 I=1,NP
       DO 100 J=1,NT
       FJ=J
       THETA=(FJ-1.)*DTH
   100 F(J)=S(J,I)*SIN(THETA)
       GG=0.
       DO 120 JJ=2,NT1,2
   120 GG=GG+F(JJ)
       G(I)=F(1)+4.*GG
       GG=0.
       DO 140 JJ=3,NT2,2
   140 GG=GG+F(JJ)
   200 G(I)=(G(I)+2.*GG+F(NT))*DTH/3.
       IF(PH) 300,300,210
   210 GG=0.
       DO 220 JJ=2,NP1,2
   220 GG=GG+G(JJ)
       DBLINT=G(1)+4.*GG
       GG=0.
       DO 240 JJ=3,NP2,2
   240 GG=GG+G(JJ)
       DBLINT=(DBLINT+2.*GG+G(NP))*DPH/3.*PTM
       RETURN
   300 DBLINT=G(1)*PTM
       RETURN
       END
```

Fig. 58.--Subroutine for averaging $\sigma(\theta,\phi)$ over θ and ϕ.

APPENDIX D
CHARACTERISTIC MODE DATA

The coefficients of the series approximations to the characteristic current distributions and the associated phase angles, α_m, are given in Tables 5 through 8 for the circular and elliptical loops, straight wires, and one-turn helices. The modes of all but the circular loops are ordered such that the magnitudes $|\cos \alpha_m|$ form a non-increasing sequence of numbers with increasing integer m. The modes of the circular loops are ordered on m in the conventional manner, beginning with m = 0. In each case, the modes are normalized to radiate unit power. The tables are as follows:

Table 5--Circular Loops

The left-most column of Table 5 is the loop radius in wavelengths. Each row to the right of a given radius contains the coefficients of the m^{th} order cosine or sine function for the m^{th} even or odd characteristic current distribution, respectively, for m = 0,1,2,3. (Recall that in the case of the circular loop the characteristic current distributions are simply cosine and sine functions.) The corresponding phase angles, α_m, are given in parenthesis following each coefficient.

As an example, the $\binom{\text{even}}{\text{odd}}$ characteristic current, I_m, of a loop of radius R = 0.35 λ for, say, m = 2, is

(107) $$I_2(\ell) \approx 0.069158 \begin{pmatrix} \cos \\ \sin \end{pmatrix} \frac{4\pi\ell}{L}$$

where L is the loop diameter. The corresponding phase angle is $\alpha_2 = 161.59^0$.

Table 6--Elliptical Loops

The first column in Table 6 gives the axial ratios of the elliptical loops in descending order, starting with a ratio of unity (a circular loop). For a given axial ratio, the next column to the right specifies the mode number m and the mode character, i.e., even or odd. The associated phase angles, α_m, are found in the next column and to the right of that, the coefficients of the cosine (for even modes) or sine (for odd modes) series approximations to the characteristic currents. The basis functions are the cosine and sine functions $\cos \frac{2\pi n\ell}{L}$, n=0,1,2,..., and $\sin \frac{2\pi n\ell}{L}$, n=1,2,..., where L is the ellipse circumference (L=1.1λ) and ℓ is measured from ℓ = 0 on the positive x axis. (See the ellipse geometry in Fig. 19, Section D of Chapter III.)

For example, the characteristic current for the dominant mode (m = 1) of an ellipse with axial ratio 0.890 is approximated by the series

(108) $$I_1(\ell) \approx (7.7450 \times 10^{-2}) \sin \frac{2\pi\ell}{L} - (7.3738 \times 10^{-11}) \sin \frac{4\pi\ell}{L}$$
$$- (6.4297 \times 10^{-5}) \sin \frac{6\pi\ell}{L} + (8.8768 \times 10^{-9}) \sin \frac{8\pi\ell}{L}$$
$$+ (6.0340 \times 10^{-6}) \sin \frac{10\pi\ell}{L} .$$

Table 7--Straight Wires

These data are similar to the data given in Table 6, except that the basis functions are the even and odd Chebyshev polynomials of the second kind, and the first column, as noted, gives the wire length. The polynomials are denoted by U_n, even modes having even subscripts and odd modes having odd subscripts. For example, the characteristic current I_m of a straight wire of length $L = 1.5\lambda$, with $m = 2$ (an odd mode, as noted in the second column), is approximated by

$$(109) \qquad I_2(\ell) \quad 3.7329 \times 10^{-2} U_1 - 2.6274 \times 10^{-2} U_3 + 6.5850 \times 10^{-3} U_5 - 8.5873 \times 10^{-4} U_7, + 3.6305 \times 10^{-5} U_9.$$

Table 8--One-Turn Helix

These data are similar to the data given in Table 7.

TABLE 5

CHARACTERISTIC MODES OF CIRCULAR LOOPS WITH A LOOP RADIUS-TO-WIRE RADIUS RATIO R/a = 100.

RADIUS	I	$\cos\frac{2\pi\ell}{L}$ $\sin\frac{2\pi\ell}{L}$	$\cos\frac{4\pi\ell}{L}$ $\sin\frac{4\pi\ell}{L}$	$\cos\frac{6\pi\ell}{L}$ $\sin\frac{6\pi\ell}{L}$
0.100	0.187730 (91.37)	0.122641 (265.92)		
0.125	0.122874 (92.51)	0.102554 (259.70)	0.321039 (269.84)	
0.150	0.087714 (94.08)	0.090180 (240.74)	0.230386 (269.60)	
0.162	0.075924 (94.99)	0.085800 (210.00)	0.200019 (269.41)	
0.175	0.066591 (95.98)	0.082291 (170.81)	0.176003 (269.12)	
0.187	0.059085 (97.05)	0.079485 (140.47)	0.158000 (268.80)	
0.200	0.052965 (98.21)	0.077250 (126.05)	0.141005 (268.24)	
0.210	0.048800 (99.20)	0.075800 (119.70)	0.130500 (268.00)	
0.220	0.045500 (100.00)	0.074700 (115.50)	0.121000 (266.80)	
0.230	0.042226 (101.20)	0.073609 (112.30)	0.113541 (266.22)	
0.240	0.039700 (102.10)	0.072800 (110.00)	0.106000 (264.50)	
0.250	0.037191 (103.32)	0.072083 (108.12)	0.100738 (263.83)	0.269318 (269.75)
0.275	0.032471 (106.07)	0.070617 (104.84)	0.088825 (258.46)	0.210891 (269.52)
0.300	0.028995 (108.84)	0.069040 (102.78)	0.080148 (246.94)	0.170737 (269.13)
0.325	0.026415 (111.56)	0.066745 (101.56)	0.073795 (216.81)	0.141830 (268.50)
0.340	0.025200 (113.00)	0.064800 (101.50)	0.071000 (178.40)	0.127500 (268.00)
0.350	0.024505 (114.11)	0.063361 (101.06)	0.069158 (161.59)	0.120527 (267.47)
0.360	0.024000 (115.00)	0.061600 (101.50)	0.067900 (146.20)	0.112800 (267.20)
0.375	0.023115 (116.40)	0.058929 (101.18)	0.065809 (131.48)	0.104531 (265.83)
0.400	0.022142 (118.33)	0.053869 (101.90)	0.063413 (119.36)	0.092350 (263.15)

TABLE 6

CHARACTERISTIC MODES OF ELLIPTICAL LOOPS WITH 1.1λ
CIRCUMFERENCE AND WIRE RADIUS a = 0.00175λ
AS A FUNCTION OF AXIAL RATIO

AXIAL RATIO	MODE	ALPHA	$\frac{1}{\sin\frac{2\pi\ell}{L}}$	$\frac{\cos\frac{2\pi\ell}{L}}{\sin\frac{4\pi\ell}{L}}$	$\frac{\cos\frac{4\pi\ell}{L}}{\sin\frac{6\pi\ell}{L}}$	$\frac{\cos\frac{6\pi\ell}{L}}{\sin\frac{8\pi\ell}{L}}$	$\frac{\cos\frac{8\pi\ell}{L}}{\sin\frac{10\pi\ell}{L}}$	$\frac{\cos\frac{10\pi\ell}{L}}{\sin\frac{12\pi\ell}{L}}$
1.000								
	1 (EVEN)	170.81	-0.	8.2291E-02	-0.	-0.	-0.	-0.
	2 (ODD)	170.81	-0.	8.2291E-02	-0.	-0.	-0.	
	3 (EVEN)	95.98	6.6591E-02	-0.	-0.	-0.	-0.	-0.
	4 (EVEN)	269.12	-0.	-0.	1.7600E-01	-0.	-0.	-0.
	5 (ODD)	269.12	-0.	-0.	1.7600E-01	-0.	-0.	
0.943								
	1 (ODD)	174.01	7.9804E-02	1.0295E-08	-4.3569E-05	9.2380E-09	1.4024E-06	
	2 (EVEN)	167.24	5.5281E-14	8.4988E-02	-1.2531E-11	-9.6613E-05	3.2887E-09	-9.3901E-06
	3 (EVEN)	95.98	6.6690E-02	0.	-5.6382E-04	0.	-1.9330E-05	0.
	4 (ODD)	269.13	2.8778E-08	1.7585E-01	1.5627E-08	9.7779E-04	4.1388E-08	
	5 (EVEN)	269.14	-1.7178E-03	-2.9820E-08	1.7624E-01	-1.8405E-08	9.4782E-04	1.4948E-08
0.890								
	1 (ODD)	177.42	7.7450E-02	-7.3738E-11	-6.4297E-05	8.8768E-09	6.0340E-06	
	2 (EVEN)	163.09	-2.3465E-12	8.8022E-02	-4.1651E-11	-1.9620E-04	5.1995E-09	-6.4427E-06
	3 (EVEN)	95.93	6.7031E-02	0.	-1.0948E-03	0.	-4.0770E-05	0.
	4 (ODD)	269.12	7.3742E-08	1.7546E-01	-2.9342E-08	1.9735E-03	3.7929E-08	
	5 (EVEN)	269.14	-3.5353E-03	1.1720E-08	1.7706E-01	-5.6453E-08	1.9585E-03	1.6462E-08
0.838								
	1 (ODD)	179.93	7.5264E-02	-1.2011E-10	-6.3918E-05	9.5299E-09	1.4370E-05	
	2 (EVEN)	157.88	-2.5689E-09	9.1255E-02	-2.2191E-08	-3.2819E-04	4.3295E-09	-2.5474E-06
	3 (EVEN)	95.98	6.7477E-02	-5.2641E-17	-1.6231E-03	-7.2948E-15	-7.6478E-05	1.6210E-15
	4 (ODD)	269.10	8.4482E-08	1.7451E-01	-2.9164E-08	2.9286E-03	4.3482E-08	
	5 (EVEN)	269.15	-5.3523E-03	1.2671E-08	1.7811E-01	-6.7459E-08	2.9518E-03	1.9696E-08
0.788								
	1 (ODD)	182.35	7.3192E-02	-2.3134E-10	-4.2621E-05	1.3464E-08	2.7359E-05	
	2 (EVEN)	152.38	-3.7420E-09	9.4910E-02	-2.5653E-08	-5.0202E-04	7.0754E-09	1.5872E-06
	3 (EVEN)	95.79	6.8191E-02	-2.3148E-16	-2.1701E-03	-2.3594E-14	-1.2832E-04	1.0759E-14
	4 (ODD)	269.10	9.3301E-08	1.7331E-01	-2.4453E-08	3.8752E-03	5.5734E-08	
	5 (EVEN)	269.17	-7.2752E-03	-9.5848E-09	1.7981E-01	-6.7584E-08	3.9711E-03	3.5118E-08
0.758								
	1 (ODD)	183.89	7.1993E-02	-2.5986E-10	-1.8506E-05	1.2901E-08	3.7935E-05	
	2 (EVEN)	149.00	-3.3368E-11	9.7388E-02	-2.1323E-10	-6.3132E-04	1.1016E-08	3.8268E-06
	3 (EVEN)	95.69	6.8799E-02	-7.4687E-13	-2.5043E-03	1.7672E-11	-1.6959E-04	-4.8391E-10
	4 (ODD)	269.09	1.0855E-07	1.7253E-01	-3.6827E-08	4.4439E-03	5.7544E-08	
	5 (EVEN)	269.18	-8.5383E-03	1.1647E-09	1.8128E-01	-8.5333E-08	4.6074E-03	3.9900E-08

TABLE 6--Continued

0.739								
	1 (ODD)	184.18	7.1254E-02	-8.5435E-08	-3.4808E-06	-2.0587E-08	4.5009E-05	
	2 (EVEN)	145.85	6.9071E-02	5.9706E-05	-2.6989E-03	9.3772E-06	-1.8975E-04	3.6606E-06
	3 (EVEN)	95.68	-4.4656E-05	9.8888E-02	3.9612E-05	-7.0727E-04	8.3549E-06	1.0061E-05
	4 (ODD)	269.08	2.5340E-07	1.7168E-01	-3.5686E-07	4.7589E-03	-1.1975E-07	
	5 (EVEN)	269.20	-9.2442E-03	-2.3868E-05	1.8191E-01	2.6481E-05	4.9874E-03	9.7368E-06
0.720								
	1 (ODD)	185.30	7.0485E-02	-4.1138E-10	2.1229E-05	1.7071E-08	5.4461E-05	
	2 (EVEN)	143.89	-5.2731E-11	1.0079E-01	-2.9103E-10	-8.3044E-04	1.2636E-08	5.6701E-06
	3 (EVEN)	95.60	6.9631E-02	-1.3008E-12	-2.9544E-03	2.8986E-11	-2.3066E-04	-6.6940E-10
	4 (ODD)	269.07	1.1856E-07	1.7112E-01	-3.1965E-08	5.1368E-03	7.2726E-08	
	5 (EVEN)	269.21	-1.0155E-02	-1.8860E-08	1.8327E-01	-8.8652E-08	5.4213E-03	4.7751E-08
0.693								
	1 (ODD)	186.03	6.9409E-02	-4.3527E-10	5.6947E-05	1.6048E-08	6.8759E-05	
	2 (EVEN)	139.81	-8.0013E-09	1.0349E-01	-4.1869E-08	-1.0032E-03	1.7999E-08	5.8460E-06
	3 (EVEN)	95.53	7.0313E-02	-1.5600E-12	-3.3028E-03	3.3911E-11	-2.8078E-04	-7.0088E-10
	4 (ODD)	269.06	1.4198E-07	1.6988E-01	-6.5095E-08	5.6154E-03	6.2449E-08	
	5 (EVEN)	269.23	-1.1393E-02	2.4967E-08	1.8490E-01	-1.1277E-07	6.0124E-03	4.6212E-08
0.646								
	1 (ODD)	187.49	6.7676E-02	-6.1925E-10	1.3442E-04	1.8994E-08	9.8232E-05	
	2 (EVEN)	133.32	-1.0001E-08	1.0861E-01	-4.8375E-08	-1.3544E-03	1.6674E-08	3.6526E-06
	3 (EVEN)	95.36	7.1821E-02	-2.7903E-12	-3.9027E-03	5.9194E-11	-3.8331E-04	-1.0327E-09
	4 (ODD)	269.03	1.6405E-07	1.6776E-01	-7.1563E-08	6.3936E-03	7.2730E-08	
	5 (EVEN)	269.26	-1.3729E-02	1.3908E-08	1.8854E-01	-1.3993E-07	7.0394E-03	5.8338E-08
0.602								
	1 (ODD)	188.71	6.6036E-02	-7.5016E-10	2.3120E-04	1.9480E-08	1.3459E-04	
	2 (EVEN)	126.07	-1.2440E-08	1.1452E-01	-5.7034E-08	-1.7972E-03	2.1178E-08	-3.1511E-06
	3 (EVEN)	95.15	7.3736E-02	-4.1584E-12	-4.5390E-03	8.9037E-11	-5.0613E-04	-1.3365E-09
	4 (ODD)	268.98	1.8766E-07	1.6546E-01	-9.0562E-08	7.1080E-03	7.8136E-08	
	5 (EVEN)	269.29	-1.6309E-02	1.3586E-08	1.9321E-01	-1.5238E-07	8.0815E-03	6.9004E-08
0.515								
	1 (ODD)	190.43	6.3022E-02	-1.4116E-09	4.7713E-04	2.7392E-08	2.3068E-04	
	2 (EVEN)	115.50	-1.7608E-08	1.2943E-01	-7.6446E-08	-3.0685E-03	3.6170E-08	-3.4943E-05
	3 (EVEN)	95.63	7.9107E-02	-8.2923E-12	-5.9777E-03	2.0458E-10	-8.1986E-04	-2.3700E-09
	4 (ODD)	268.88	2.2293E-07	1.6048E-01	-1.0437E-07	8.2734E-03	1.0252E-07	
	5 (EVEN)	269.38	-2.2532E-02	-4.2416E-08	2.0643E-01	-1.9833E-07	1.0177E-02	1.0050E-07
0.306								
	1 (ODD)	186.16	5.6925E-02	-6.1282E-09	1.1505E-03	6.0404E-08	8.4044E-04	1.5508E-08
	2 (EVEN)	97.17	-4.8049E-08	2.0291E-01	-2.1290E-07	-1.1791E-02	1.4730E-07	-1.4741E-04
	3 (ODD)	268.49	3.3013E-07	1.4484E-01	-1.2412E-07	1.2542E-02	2.1442E-07	5.6492E-03
	4 (EVEN)	269.64	-5.3150E-02	-7.7679E-07	2.8259E-01	-5.4717E-07	1.4419E-02	2.8224E-07

TABLE 7

CHARACTERISTIC MODES OF STRAIGHT WIRES WITH A LENGTH-TO-DIAMETER RATIO L/2a = 100

LENGTH	MODE	ALPHA	u_0 u_1	u_2 u_3	u_4 u_5	u_6 u_7	u_8 u_9	u_{10} u_{11}
0.300								
	1 (EVEN)	265.26	1.3436E-01	-3.9998E-02	-3.1200E-04	-2.6043E-04	-7.9192E-05	-6.7434E-05
0.400								
	1 (EVEN)	248.07	1.0244E-01	-3.1555E-02	2.8345E-04	-1.8810E-04	-5.5523E-05	-4.7831E-05
0.450								
	1 (EVEN)	211.29	9.1924E-02	-2.8876E-02	5.3394E-04	-1.6606E-04	-4.7326E-05	-4.1133E-05
0.475								
	1 (EVEN)	179.10	8.7526E-02	-2.7779E-02	6.5187E-04	-1.5756E-04	-4.3803E-05	-3.8285E-05
0.500								
	1 (EVEN)	153.43	8.3584E-02	-2.6810E-02	7.6624E-04	-1.5049E-04	-4.0588E-05	-3.5696E-05
	2 (ODD)	269.40	1.9987E-01	-8.8205E-02	4.6230E-04	-6.1491E-04	-4.7598E-04	
0.550								
	1 (EVEN)	130.34	7.6819E-02	-2.5189E-02	9.8678E-04	-1.4023E-04	-3.4914E-05	-3.1139E-05
	2 (ODD)	268.98	1.6921E-01	-7.5670E-02	1.1688E-03	-5.1833E-04	-3.7208E-04	
0.600								
	1 (EVEN)	122.06	7.1229E-02	-2.3896E-02	1.1976E-03	-1.3457E-04	-3.0022E-05	-2.7314E-05
	2 (ODD)	268.34	1.4413E-01	-6.5976E-02	1.6205E-03	-4.4538E-04	-3.1046E-04	
0.750								
	1 (EVEN)	115.14	5.9114E-02	-2.1314E-02	1.8003E-03	-1.4141E-04	-1.8312E-05	-1.8590E-05
	2 (ODD)	263.15	9.8583E-02	-4.7912E-02	2.6789E-03	-3.3670E-04	-1.8459E-04	
0.850								
	1 (EVEN)	113.77	5.3507E-02	-2.0339E-02	2.2567E-03	-1.6663E-04	-1.0870E-05	-9.8731E-06
	2 (ODD)	246.18	8.0602E-02	-4.0783E-02	3.2982E-03	-3.2452E-04	-9.1602E-05	
	3 (EVEN)	269.54	-1.1513E-02	2.1230E-01	-1.1537E-01	6.4136E-03	-9.8463E-04	-2.5023E-04
0.900								
	1 (ODD)	227.26	7.3809E-02	-3.8223E-02	3.5423E-03	-3.2825E-04	-7.7500E-05	
	2 (EVEN)	113.69	5.1185E-02	-1.9958E-02	2.4551E-03	-1.8472E-04	-7.6815E-06	-8.5274E-06
	3 (EVEN)	269.30	-6.2874E-03	1.8166E-01	-1.0155E-01	6.5214E-03	-8.9055E-04	-3.1622E-04
0.950								
	1 (ODD)	186.52	6.8057E-02	-3.6087E-02	3.7782E-03	-3.3856E-04	-6.5217E-05	
	2 (EVEN)	113.72	4.9113E-02	-1.9641E-02	2.6522E-03	-2.0640E-04	-4.3893E-06	-7.4722E-06
	3 (EVEN)	268.94	-2.3384E-03	1.5682E-01	-8.9842E-02	6.8035E-03	-8.3101E-04	-2.1268E-04

TABLE 7--Continued

1.000								
	1 (ODD)	147.70	6.3192E-02	-3.4586E-02	4.0850E-03	-3.6570E-04	-7.6321E-05	
	2 (EVEN)	246.29	4.7250E-02	-1.9534E-02	2.9271E-03	-2.4204E-04	-7.0623E-07	-8.8829E-06
	3 (EVEN)	268.43	8.6229E-04	1.3701E-01	-8.1425E-02	6.9759E-03	-8.1651E-04	-3.1332E-04
1.050								
	1 (ODD)	132.63	5.8945E-02	-3.3060E-02	4.3218E-03	-3.8861E-04	-6.3385E-05	
	2 (EVEN)	113.87	4.5559E-02	-1.9332E-02	3.1403E-03	-2.7361E-04	3.3172E-06	-7.7714E-06
	3 (EVEN)	267.68	3.2406E-03	1.2045E-01	-7.3575E-02	7.1545E-03	-7.9027E-04	-2.6068E-04
1.150								
	1 (ODD)	121.62	5.2025E-02	-3.0660E-02	4.7952E-03	-4.5169E-04	-4.0039E-05	
	2 (EVEN)	114.27	4.2601E-02	-1.9045E-02	3.5806E-03	-3.5038E-04	1.2494E-05	-5.8790E-06
	3 (EVEN)	264.93	6.5933E-03	9.5215E-02	-6.1556E-02	7.4656E-03	-7.7992E-04	-1.7846E-04
1.250								
	1 (ODD)	117.98	4.6650E-02	-2.8901E-02	5.2757E-03	-5.3708E-04	-1.8519E-05	
	2 (EVEN)	114.74	4.0081E-02	-1.8899E-02	4.0554E-03	-4.4964E-04	2.4243E-05	-4.5705E-06
	3 (EVEN)	258.39	8.7461E-03	7.7250E-02	-5.2963E-02	7.7405E-03	-8.1032E-04	-1.2155E-04
1.300								
	1 (ODD)	117.12	4.4392E-02	-2.8201E-02	5.5215E-03	-5.8832E-04	-7.8376E-06	
	2 (EVEN)	114.97	3.8944E-02	-1.8885E-02	4.3200E-03	-5.1106E-04	3.1680E-05	-4.0956E-06
	3 (EVEN)	251.50	9.5461E-03	7.0162E-02	-4.9575E-02	7.8790E-03	-8.3851E-04	-9.7918E-05
1.400								
	1 (EVEN)	212.62	1.0884E-02	5.8670E-02	-4.4209E-02	8.2039E-03	-9.2380E-04	-6.3619E-05
	2 (ODD)	116.25	4.0527E-02	-2.7122E-02	6.0526E-03	-7.1250E-04	1.1693E-05	
	3 (EVEN)	115.46	3.6847E-02	-1.9026E-02	4.9600E-03	-6.7238E-04	5.2085E-05	-3.8326E-06
	4 (ODD)	268.73	8.9135E-03	1.3637E-01	-1.0007E-01	1.5205E-02	-2.0749E-03	
1.450								
	1 (EVEN)	176.30	1.1448E-02	5.3957E-02	-4.1985E-02	8.3590E-03	-9.7440E-04	-4.3573E-05
	2 (ODD)	116.09	3.8857E-02	-2.6671E-02	6.3176E-03	-7.8276E-04	2.3814E-05	
	3 (EVEN)	115.69	3.5867E-02	-1.9161E-02	5.3320E-03	-7.7432E-04	6.5689E-05	-3.8899E-06
	4 (ODD)	268.22	1.0799E-02	1.1995E-01	-9.0887E-02	1.4856E-02	-2.0264E-03	
1.500								
	1 (EVEN)	149.95	1.2002E-02	4.9766E-02	-4.0024E-02	8.5188E-03	-1.0315E-03	-2.4476E-05
	2 (ODD)	116.05	3.7329E-02	-2.6274E-02	6.5850E-03	-8.5873E-04	3.6305E-05	
	3 (EVEN)	115.93	3.4913E-02	-1.9355E-02	5.7556E-03	-8.9596E-04	8.2588E-05	-4.2478E-06
	4 (ODD)	267.50	1.2274E-02	1.0604E-01	-8.3065E-02	1.4597E-02	-1.9671E-03	
1.600								
	1 (EVEN)	129.11	1.3245E-02	4.2528E-02	-3.6699E-02	8.8495E-03	-1.1646E-03	1.2782E-05
	2 (EVEN)	116.40	3.3009E-02	-2.0034E-02	6.8865E-03	-1.2394E-03	1.3325E-04	-6.3205E-06
	3 (ODD)	116.14	3.4621E-02	-2.5645E-02	7.1555E-03	-1.0347E-03	6.4596E-05	
	4 (ODD)	265.03	-1.4311E-02	-8.4048E-02	7.0531E-02	-1.4178E-02	1.9028E-03	

$$u_n(\ell) = \frac{\sin((n+1)\cos^{-1}(2\ell/L))}{\sin(\cos^{-1}(2\ell/L))}$$

TABLE 8

CHARACTERISTIC MODES OF A ONE-TURN HELIX WITH A WIRE LENGTH-TO-DIAMETER RATIO L/2a = 100 AND A PITCH p = 10a

LENGTH	MODE	ALPHA	u_0 u_1	u_2 u_3	u_4 u_5	u_6 u_7	u_8 u_9	u_{10} u_{11}	u_{12} u_{13}
0.300									
	1 (EVEN)	269.31	3.3951E-01	-1.3988E-01	2.3234E-02	-2.8440E-03	-8.3942E-05	-7.5260E-05	
	2 (ODD)	269.52	1.5140E-01	-8.9017E-02	1.3108E-02	-7.5689E-04	5.2783E-06		
0.400									
	1 (EVEN)	266.41	2.7787E-01	-9.3308E-02	7.0837E-03	-1.4836E-03	-2.0490E-04	-9.7157E-05	
	2 (ODD)	268.81	1.1507E-01	-6.7370E-02	9.7807E-03	-5.7375E-04	-5.2004E-08		
0.450									
	1 (EVEN)	250.86	2.5379E-01	-7.6440E-02	1.4992E-03	-1.0065E-03	-2.4680E-04	-1.0352E-04	
	2 (ODD)	268.25	1.0321E-01	-6.0435E-02	8.7943E-03	-5.1144E-04	3.8338E-06		
0.460									
	1 (EVEN)	235.15	2.4677E-01	-7.3995E-02	7.9624E-04	-9.6841E-04	-2.8789E-04	-1.0548E-04	-3.5058E-05
	2 (ODD)	268.12	1.0115E-01	-5.9225E-02	8.6110E-03	-5.0112E-04	2.2165E-06		
0.470									
	1 (EVEN)	166.94	2.4279E-01	-7.1224E-02	-1.1712E-04	-8.9800E-04	-2.9686E-04	-1.0664E-04	-3.5093E-05
	2 (ODD)	267.96	9.9270E-02	-5.8036E-02	8.4898E-03	-4.8636E-04	2.4245E-05		
0.475									
	1 (EVEN)	135.86	2.4032E-01	-6.9808E-02	-5.1838E-04	-8.5832E-04	-2.9865E-04	-1.0676E-04	-3.5238E-05
	2 (ODD)	267.90	9.8281E-02	-5.7558E-02	8.4042E-03	-4.8417E-04	9.4800E-06		
0.500									
	1 (EVEN)	102.84	2.2974E-01	-6.2513E-02	-2.4712E-03	-6.2809E-04	-2.6722E-04	-1.0538E-04	
	2 (ODD)	267.51	9.3822E-02	-5.4920E-02	8.0022E-03	-4.6146E-04	7.7087E-06		
0.600									
	1 (EVEN)	95.73	1.8349E-01	-4.2533E-02	-6.3013E-03	-1.4283E-04	-2.5261E-04	-9.7776E-05	
	2 (ODD)	265.25	7.9973E-02	-4.6700E-02	6.7803E-03	-3.8740E-04	1.2269E-05		
0.750									
	1 (ODD)	258.51	6.6646E-02	-3.8772E-02	5.5537E-03	-3.1639E-04	7.0508E-06		
	2 (EVEN)	95.74	1.3015E-01	-2.6510E-02	-6.7703E-03	1.5011E-04	-1.8092E-04	-7.7214E-05	
	3 (EVEN)	267.00	4.1600E-02	6.5053E-02	-4.5546E-02	4.4018E-03	-7.9711E-04	-1.0847E-04	
0.900									
	1 (ODD)	239.75	5.8350E-02	-3.3953E-02	4.7991E-03	-2.7286E-04	-3.9212E-06		
	2 (EVEN)	96.99	9.6215E-02	-1.8788E-02	-5.7984E-03	2.3351E-04	-1.2476E-04	-7.2625E-05	
	3 (EVEN)	263.87	1.9211E-02	5.8344E-02	-3.9089E-02	4.4157E-03	-7.4218E-04	-1.0193E-04	

TABLE 8--Continued

1.000									
	1 (ODD)	211.12	5.4515E-02	-3.1732E-02	4.4340E-03	-2.6344E-04	2.8587E-06	-1.0123E-05	-5.8245E-06
	2 (EVEN)	260.73	1.1786E-02	5.4844E-02	-3.6377E-02	4.5551E-03	-7.2794E-04	-8.3723E-05	
	3 (EVEN)	98.26	8.0568E-02	-1.5997E-02	-4.8551E-03	2.4766E-04	-8.9670E-05	-6.3058E-05	
	4 (ODD)	269.19	-3.8287E-02	-8.7102E-02	1.0535E-01	-3.6204E-02	6.2290E-03	-5.9E45E-04	1.0593E-04
1.100									
	1 (ODD)	170.53	5.1659E-02	-2.9980E-02	4.1439E-03	-2.4245E-04	2.5158E-06	-9.7838E-06	-5.7948E-06
	2 (EVEN)	256.12	7.1616E-03	5.1991E-02	-3.4527E-02	4.7691E-03	-7.3339E-04	-6.7101E-05	
	3 (EVEN)	99.69	6.8780E-02	-1.4203E-02	-3.9678E-03	2.4807E-04	-6.2466E-05	-5.3971E-05	
	4 (ODD)	268.67	-3.2408E-02	-7.4102E-02	8.9281E-02	-3.0681E-02	5.2599E-03	-5.0796E-04	7.4691E-05
1.250									
	1 (ODD)	135.53	4.8695E-02	-2.7981E-02	3.7808E-03	-2.0530E-04	-5.9666E-06		
	2 (EVEN)	244.20	3.2804E-03	4.8768E-02	-3.2952E-02	5.2346E-03	-7.6512E-04	-4.9119E-05	
	3 (EVEN)	102.13	5.5853E-02	-1.2763E-02	-2.6774E-03	2.3408E-04	-3.0567E-05	-4.0636E-05	
	4 (ODD)	267.40	-2.5815E-02	-5.9835E-02	7.2501E-02	-2.4512E-02	3.8323E-03		
1.400									
	1 (EVEN)	215.97	1.6141E-03	4.6212E-02	-3.2441E-02	5.8085E-03	-8.4399E-04	-2.3136E-05	-2.6164E-05
	2 (ODD)	121.83	4.6740E-02	-2.6790E-02	3.5470E-03	-1.9550E-04	-1.4491E-05		
	3 (EVEN)	104.79	4.6905E-02	-1.2605E-02	-1.3518E-03	1.8514E-04	-1.5645E-05	-2.9551E-05	-5.7493E-06
	4 (ODD)	265.03	2.1345E-02	5.0453E-02	-6.0593E-02	2.0391E-02	-3.1543E-03		
1.500									
	1 (EVEN)	182.79	1.3544E-03	4.4710E-02	-3.2081E-02	6.0871E-03	-8.4856E-04	-2.2492E-05	-2.4332E-05
	2 (ODD)	116.95	4.5842E-02	-2.6229E-02	3.4432E-03	-1.9733E-04	-1.7757E-05		
	3 (EVEN)	106.63	4.2404E-02	-1.3199E-02	-2.1475E-04	1.1425E-04	-3.2319E-06	-2.3882E-05	-4.0639E-06
	4 (ODD)	262.47	1.9059E-02	4.5799E-02	-5.4643E-02	1.8303E-02	-2.8072E-03		
1.600									
	1 (EVEN)	153.19	1.8996E-03	4.3139E-02	-3.1634E-02	6.2270E-03	-8.1647E-04	-2.5840E-05	-2.1913E-05
	2 (ODD)	113.50	4.5146E-02	-2.5778E-02	3.3807E-03	-2.0955E-04	-1.4243E-05		
	3 (EVEN)	108.47	3.8751E-02	-1.4627E-02	1.3465E-03	-2.3614E-05	7.6881E-06	-1.6076E-05	-2.0836E-06
	4 (ODD)	258.77	1.7211E-02	4.2026E-02	-4.9880E-02	1.6631E-02	-2.5439E-03		

$$u_n(\ell) = \frac{\sin\left((n+1)\cos^{-1}\left(2\ell/L\right)\right)}{\sin\left(\cos^{-1}\left(2\ell/L\right)\right)}$$

REFERENCES

1. Richmond, J.H., "Scattering by Wire Loops and Square Plates in the Resonance Region," Report 2097-1, 28 January 1966, ElectroScience Laboratory, Department of Electrical Engineering, The Ohio State University; prepared under Contract AF 19(628)-4883 for Electronic Systems Division. (AD 804 313)
2. Richmond, J.H., "A Point-Matching Solution for Scattering by Conducting Bodies of Revolution," Report 2097-2, 15 May 1966, ElectroScience Laboratory, Department of Electrical Engineering, The Ohio State University; prepared under Contract AF 19(628)-4883 for Electronic Systems Division. (AD 804 314)
3. Richmond, J.H., "A Wire-Grid Model for Scattering by Conducting Bodies," IEEE Trans. on Antennas and Propagation, Vol. AP-14, No. 6, November 1966, pp. 782-786.
4. Thiele, G.A., "Scattering by Imperfectly Conducting Wires of Arbitrary Shape," Report 2409-6, 21 June 1968, ElectroScience Laboratory, Department of Electrical Engineering, The Ohio State University; prepared under Subcontract 359 for Massachusetts Institute of Technology.
5. Harrington, R.F., Field Computation by Moment Methods, MacMillan Company, New York, 1968.

6. Harrington, R.F., et al., "Matrix Methods for Solving Field Problems," Tech. Rept. No. RADC-TR-66-351, Vol. I, Rome Air Development Center, Griffiss Air Force Base, Rome, New York, August 1966. (AD 639 744)

7. Baghdasarian, A. and Angelakos, D., "Scattering from Conducting Loops and Solution of Circular Loop Antennas by Numerical Methods," Proc. of the IEEE, Vol. 53, No. 8, August 1965, pp. 818-822.

8. Yeh, Y.S. and Mei, K.K., "Theory of Conical Equiangular-Spiral Antennas, Part I - Numerical Technique," IEEE Trans. on Antennas and Propagation, Vol. AP-15, No. 5, September 1967, pp. 634-639.

9. Schelkunoff, S.A. and Friis, H.T., Antennas, Theory and Practice, John Wiley and Sons, Inc., New York, 1952, pp. 370, 401.

10. Otto, D.V. and Richmond, J.H., "Rigorous Field Expressions for Piecewise-Sinusoidal Line Sources," IEEE Trans. on Antennas and Propagation, Vol. AP-17, January 1969, p. 98.

11. Richmond, J.H., "Theoretical Study of V Antenna Characteristics for the ATS-E Radio Astronomy Experiment," Report 2619-1, 13 February 1969, ElectroScience Laboratory, Department of Electrical Engineering, The Ohio State University; prepared under Contract NAS5-11543 for National Aeronautics and Space Administration; (N69 19062)

12. Richmond, J.H., "Digital Computer Solution of the Rigorous Equations for Scattering Problems," Proc. of the IEEE, Vol. 53, No. 8, August 1965, pp. 796-804.

13. Thiele, G.A., "On the Application of the Point Matching Technique to Antenna and Scattering Problems," Ph.D. Dissertation, The Ohio State University, 1968.

14. Richmond, J.H., "Scattering by Imperfectly Conducting Wires," Report 2169-1, 22 November 1966, ElectroScience Laboratory, Department of Electrical Engineering, The Ohio State University. (Internal Report)

15. Neureuther, A.R., et al., "A Comparison of Numerical Methods for Thin Wire Antennas," Department of Electrical Engineering and Computer Sciences and the Electronics Research Laboratory, University of California, Berkeley. (unpublished paper)

16. Kennaugh, E.M., "Multiple Field Expansions and Their Use in Approximate Solutions of Electromagnetic Scattering Problems," Ph.D. Dissertation, The Ohio State University, 1959.

17. Fenlon, F.H., "Calculation of the Acoustic Radiation Field at the Surface of a Finite Cylinder by the Method of Weighted Residuals," Proc. of the IEEE, Vol. 57, No. 3, March 1969, pp. 291-306.

18. Hildebrand, F.B. and Crout, P.D., "A Least Square Procedure for Solving Integral Equations by Polynomial Approximation," Journal of Math. and Physics, Vol. 20, 1941, pp. 310-335.

19. Crout, P.D., "A Least Square Procedure for Solving Homogeneous Integral Equations," Journal of Math. and Physics, Vol. 40, 1961, pp. 103-115.

20. Garbacz, R.J., "A Generalized Expansion for Radiated and Scattered Fields," Ph.D. Dissertation, The Ohio State University, 1968, Interaction Note 180.

21. Garbacz, R.J., "Introduction to Characteristic Modes for Chaff Applications," Report 2584-6 (to be published), ElectroScience Laboratory, Department of Electrical Engineering, The Ohio State University; prepared under Contract F 33615-68-C-1252 for Air Force Avionics Laboratory, Wright-Patterson Air Force Base, Ohio.

22. Curtis, W.L., "Average Radar Cross Section of Arbitrarily-Shaped Wires of Finite Conductivity," The Boeing Company, Seattle, Wash., December 1967 (unpublished paper).

23. Borison, S.L., "Bistatic Scattering Cross Section of a Randomly-Oriented Dipole," IEEE Trans. on Ant. and Prop., Vol. AP-15, No. 2, March, 1967, pp. 320-321.

24. Palermo, C.J. and Bauer, L.H., "Bistatic Scattering Cross Section of Chaff Dipoles with Application to Communications," Proc. of the IEEE, Vol. 53, No. 8, August, 1965, pp. 1119-1121.

25. Hessemer, R.A., Jr., "Scatter Communications with Radar Chaff," IRE Trans. on Ant. and Prop., Vol. AP-9, No. 2, March 1961, pp. 211-217.

26. Morrow, W.E., Jr., and MacLellan, D.C., "Properties of Orbiting Dipole Belts," Astron. J., Vol. 66, April 1961, p. 109.

27. Smirnov, V.I., Linear Algebra and Group Theory, McGraw-Hill Book Co., New York, 1961, pp. 95-106.

28. Fischback, J.W., "Solution of Least Squares Problems by an N Step Gradient Method," Technical Note No. 719, Ballistic Research Laboratories, Aberdeen Proving Ground, Maryland, July 1962.

29. Berezin, I.S. and Zhidkov, N.P., Computing Methods, Pergammon Press, New York, 1965, Vol. I, pp. 442-447, Vol. II, pp. 658-661.

30. Forsythe, G.E. and Moler, C.B., Computer Solution of Linear Algebraic Systems, Prentice Hall, Inc., Englewood Cliffs, N.J., 1967, pp. 16,17.

31. Crout, P.D., "A Short Method for Evaluating Determinants and Solving Systems of Linear Equations with Real or Complex Coefficients," AIEE Transactions (Supplement), Vol. 60, December 1941, pp. 1235-1241.

32. Ott, R.H., "The Scattering by a Two-Dimensional Periodic Array of Plates," Report 2148-2, 30 June 1966, ElectroScience Laboratory, Department of Electrical Engineering, The Ohio State University; prepared under Contract AF 33(615)-3461 for Air Force Avionics Laboratory, Wright-Patterson Air Force Base, Ohio. (AD 486 777)

33. Ott. R.H., Kouyoumjian, R.G. and Peters, L., Jr., "Scattering by a Two-Dimensional Periodic-Array of Narrow Plates," Radio Science, Vol. 2 (New Series), No. 11, November 1967, pp. 1347-1359.

34. Copley, L.G., "Integral Equation Methods for Radiation from Vibrating Bodies," J. Acoust. Soc. of Am., Vol. 41, April 1967, pp. 807-816.

35. Stratton, J.A., Electromagnetic Theory, McGraw-Hill Book Co., Inc., New York, 1941, p. 458.

36. Kouyoumjian, R.G., "The Back-Scattering from a Circular Loop," Report 662-5, 30 April 1956, ElectroScience Laboratory, Department of Electrical Engineering, The Ohio State University; prepared under Contract DA 36-039-sc-70174 for Signal Corps Supply Agency. (AD 107 981)

37. Schelkunoff and Friis, loc. cit., pp. 213-237.

38. Pocklington, H.E., "Electrical Oscillations in Wires," Camb. Phil. Soc. Proc., Vol. 9, October 25, 1897, pp. 324-332.

39. Handbook of Mathematical Functions, U.S. Dept. of Commerce, National Bureau of Standards, Applied Math. Series 55, Supt. of Documents, U.S. Government Printing Office, Washington, D.C., 1964, p. 776.

40. Harrington, R.F. and Mautz, J., "Matrix Methods for Solving Field Problems," Tech. Rept. No. RADC-TR-66-351, Vol. II, Rome Air Development Center, Griffiss Air Force Base, Rome, N.Y., August 1966. (AD 639 745)

41. Thiele, G.A., "Radar Cross Section of Open Circular Loops," Report 2409-3, 9 November 1967, ElectroScience Laboratory, Department of Electrical Engineering, The Ohio State University; prepared under Subcontract 359 for Massachusetts Institute of Technology.

42. Thiele, G.A., "Radar Cross Section of Open Circular Loops," IEEE Trans. on Antennas and Propagation, Vol. AP-16, No. 3, May 1968, pp. 373-375.

43. Smirnov, loc. cit., pp. 151, 152.

44. Kennaugh, E.M., "Effects of Type of Polarization on Echo Characteristics," Report 389-12, 1 March 1952, ElectroScience Laboratory, Department of Electrical Engineering, The Ohio State University; prepared under Contract AF 28(099)-90 for Rome Air Development Center. (AD 2494)

45. Kraus, J.D., Antennas, McGraw-Hill Book Co., Inc., New York, 1950, pp. 477, 478.

46. Rumsey, V.H., "Transmission Between Elliptically Polarized Antennas," Proc. of IRE, Vol. 39, May 1951, pp. 535-540.

47. Kaler, M.L., "Elliptically Polarized Waves and Antennas," Proc. of IRE, Vol. 39, May 1951, pp. 544-549.

48. Garbacz, R.J., personal correspondence.

49. Rumsey, V.H., "Reaction Concept in Electromagnetic Theory," Phys. Rev., Vol. 94, 1954, pp. 1483-1491.

50. Richmond, J.H., Reciprocity Theorems and Plane Surface Waves, Bulletin 176, Engineering Experiment Station, The Ohio State University, 1959.

51. Cohen, M.H., "Application of the Reaction Concept to Scattering Problems," IRE Group on Antennas and Propagation, Vol. AP-3, pp. 193-199, April 1955.

52. Harrington, R.F. and Mautz, J., "Computations for Loaded Wire Loops," Tech. Rept. No. RADC-TR-67-8, Rome Air Development Center, Griffiss Air Force Base, Rome, N.Y.

53. Thiele, G.A., "Scattering by Circular Tungsten Wire Arcs," Report 2409-5, 13 March 1968, ElectroScience Laboratory, Department of Electrical Engineering, The Ohio State University; prepared under Subcontract 359 for Massachusetts Institute of Technology.

54. Thiele, G.A., "Radar Cross Section of a Small, Low-Pitch Angle Helix," Report 2409-8, 28 May 1969, ElectroScience Laboratory, Department of Electrical Engineering, The Ohio State University; prepared under Subcontract 359 for Massachusetts Institute of Technology.